NASA CR-134866

N76-27240

Quiet Clean Short-Haul Experimental Engine (QCSEE) Aerodynamic Characteristics of 30.5 cm Diameter Inlets

by

D.L. Paul

GENERAL ELECTRIC COMPANY

Prepared For

National Aeronautics and Space Administration

NASA-Lewis Research Center
NAS3-18021

1. Report No.	2. Government Accession No.	3. Recipient's Catalog No.
NASA CR-134866		

4. Title and Subtitle
QUIET, CLEAN SHORT-HAUL EXPERIMENTAL ENGINE (QCSEE)
AERODYNAMIC CHARACTERISTICS OF 30.5 CENTIMETER DIAMETER INLETS

5. Report Date
August 1975

6. Performing Organization Code

7. Author(s)
David L. Paul
Advanced Engineering & Technology Programs Department

8. Performing Organization Report No.
R75AEG494

9. Performing Organization Name and Address
General Electric Company
Aircraft Engine Group
Cincinnati, Ohio 45215

10. Work Unit No.

11. Contract or Grant No.
NAS3-18021

12. Sponsoring Agency Name and Address
National Aeronautics and Space Administration
Washington, D. C. 20546

13. Type of Report and Period Covered
Contractor Report

14. Sponsoring Agency Code

15. Supplementary Notes
Test Report, Project Manager, C.C. Ciepluch, QCSEE Project Office
Technical Advisor, H. L. Wesoky
NASA Lewis Research Center, Cleveland, Ohio 44135

16. Abstract

A low-speed test program was conducted in the NASA Lewis 9- by 15-Foot V/STOL Wind Tunnel to investigate internal performance characteristics and determine key design features required for an inlet to meet the demanding operational conditions of the QCSEE application. Four models each having a design average throat Mach number of 0.79 were tested over a range of incidence angle, throat Mach number, and freestream velocity. Diffuser exit diameter was 30.5 centimeters (12 inches), which corresponds to a 16.9% scale of the QCSEE fan. Principal design variable was internal lip diameter ratio. In addition, one model investigated the effect of forebody contour. Stable, efficient inlet performance was found to be feasible at and beyond the 50° incidence angle required by the QCSEE application at its 41.2 m/sec (80 knot) nominal takeoff velocity, through suitably designed inlet lip and diffuser components. Forebody design was found to significantly impact flow stability via nose curvature. Measured inlet wall pressures were used to select a location for the inlet throat Mach number control's static pressure port that properly balanced the conflicting demands of relative insensitivity to flow incidence and sufficiently high response to changes in engine flow demand.

17. Key Words (Suggested by Author(s))			18. Distribution Statement
QCSEE	Design	Wind Tunnel Tests	Unlimited
Inlet Design	STOL		
Subsonic	High Mach Number Inlet		
Inlet Lip Design	Distortion		
Performance	Angle of Attack		
Stability	Incidence		

19. Security Classif. (of this report)	20. Security Classif. (of this page)	21. No. of Pages	22. Price*
Unclassified	Unclassified	95	

FOREWORD

The contributions of Messrs. Donelson and Jones of McDonnell-Douglas and Messrs. Luidens, Albers, Miller, Wesoky, Steffen, and Stockman of NASA-Lewis during the design phase are appreciated. In addition, the personnel of the 9-by 15-Foot V/STOL Wind Tunnel, and especially Messrs. Miller and Wesoky, played a key role in the timely and successful completion of the test phase.

Page Intentionally Left Blank

TABLE OF CONTENTS

LIST OF ILLUSTRATIONS

LIST OF ILLUSTRATIONS (Continued)

LIST OF ILLUSTRATIONS (Concluded)

SECTION 1.0

SUMMARY

A low-speed test program was conducted in the NASA-Lewis 9-by 15-Foot V/STOL Wind Tunnel to investigate internal performance characteristics and determine key design features required for a 0.79 throat Mach number inlet to meet the demanding operational conditions of the QCSEE (Quiet, Clean Short-haul Experimental Engine) application. Four models were tested over a wide range of incidence angle and throat Mach number at nominal freestream velocities of 0, 18.0, 41.2, and 61.7 m/sec (0, 35, 80, and 120 knots). Diffuser exit diameter was 30.5 centimeters (12 inches), which corresponds to a 16.9% scale of the QCSEE fan. The principal design variable was inlet hilight diameter to throat diameter ratio. Values tested were 1.17, 1.21, and 1.25. In addition, one model investigated the effect of forebody contour. The same diffuser and centerbody were used throughout the test. Design average throat Mach number for the 41.2 m/sec (80 knot) takeoff condition was 0.79.

Results indicate that stable, efficient inlet performance is feasible at and beyond the 50° incidence angle required by the QCSEE application through suitably designed inlet lip and diffuser components. A hilight to throat diameter ratio of 1.21 was found to be the best of those tested and has been selected for future QCSEE inlet evaluation. The lowest diameter ratio tested did not fully satisfy all operational requirements, while the highest value tested did not produce performance benefits commensurate with its accompanying increased nacelle diameter. Forebody design was also demonstrated to have a significant impact on flow stability, via its effect on nose curvature. For the same internal lip, a 33.8% reduction in forebody thickness (corresponding to a 3.2% reduction in inlet maximum diameter) degraded angle of attack capability by 10° to 35°, depending on throat Mach number.

Measured inlet wall pressures were useful in selecting a location for the throat Mach number control. This is a key system for such a high design throat Mach number inlet, since relatively minor flow increases can cause inlet choking and unstable, highly distorted flow conditions. Test data were employed to select a location that properly balanced the conflicting demands of relative insensitivity to flow incidence and sufficiently high response to changes in engine flow demand.

SECTION 2.0

INTRODUCTION

Operational characteristics and acoustic performance objectives of the QCSEE program require an inlet that can operate stably in high flow incidence situations during short takeoff rolls with a relatively high average throat Mach number. In order to obtain the inlet design data required, a test program was jointly structured and conducted at the NASA-Lewis Research Center. Four 30.5 centimeter (12 inch) diameter models were evaluated in the NASA-Lewis 9-by 15-Foot V/STOL Wind Tunnel to determine inlet design parameter values that would satisfy the QCSEE operational requirements while simultaneously meeting the objective throat Mach number, length, treatment capability, and drag divergence characteristics. Internal lip contraction ratio was the primary geometric variable while forebody contour effect was also studied. Due to program scope, a single diffuser was used for all models.

Test variables included average throat Mach number, which varied from approximately ground or flight idle to choking; tunnel velocity, which ranged from zero to 61.7 m/sec (zero to 120 knots); and inlet incidence angle, which was varied from zero to beyond the separation point at takeoff velocities. Static crosswind simulations were also conducted.

Inlet aerodynamic measurements included flow rate, diffuser exit steady-state total pressure recovery and distortion, wall static pressures, and wall and stream dynamic (time-variant) pressures in the diffuser.

Performance of the four inlets is compared in terms of angle of attack capability (stable operating region), total pressure recovery, and steady-state and dynamic total pressure distortion level and selected patterns. Operating characteristics in static crosswind are also discussed. Additional performance data are presented for the 1.21 diameter contraction ratio inlet selected for further evaluation in the QCSEE program. This includes a description of the wall Mach number gradients considered in selecting the throat Mach number control's static pressure port location. The function of the Mach number control is to maintain a 0.79 average throat Mach number in the inlet for noise suppression during takeoff and landing.

SECTION 3.0

DESCRIPTION OF TEST FACILITY

The NASA-Lewis Research Center 9-by 15-Foot V/STOL Wind Tunnel is described in detail in Reference 1. Figure 1 shows the general arrangement of the test section entrance, test section, and exhaust diffuser, together with the inlet model, turntable to set desired inlet incidence angles, and discharge piping system. A schematic of the isolated inlet model attachment to a portion of the discharge ducting is given in Figure 2. Also shown are the model diffuser exit instrumentation, the 14.0 centimeter (5-1/2 inch) diameter siren used as a noise source to facilitate acoustic suppression studies, and the downstream vanes used to turn the exhaust flow into the vertical duct leading out of the test section. A photograph of one of the models installed in the wind tunnel is included as Figure 3. Three of the dynamic total pressure rakes and four of the dynamic wall static pressure transducers are visible in this view. The models were rotated in a horizontal plane by the turntable indicated in Figure 1 to effect desired flow incidence settings. Since the models were each axisymmetric, both in-flight angle of attack, as well as static crosswind operation, could be simulated without the necessity of circumferentially indexing the inlets. In the zero angle-of-attack or head-on setting, the inlets were mounted midway along the 2.74 meter (nine foot) tunnel height and 1.37 meter (4.5 feet) from the nearer tunnel side wall, to facilitate 90° rotation of the inlet and its mounting pipe toward the other side wall. In all cases, the portion of the inlet lip near "3 o'clock," looking downstream, or into the inlet, was the windward zone; the inlets were never rotated toward the nearer side wall.

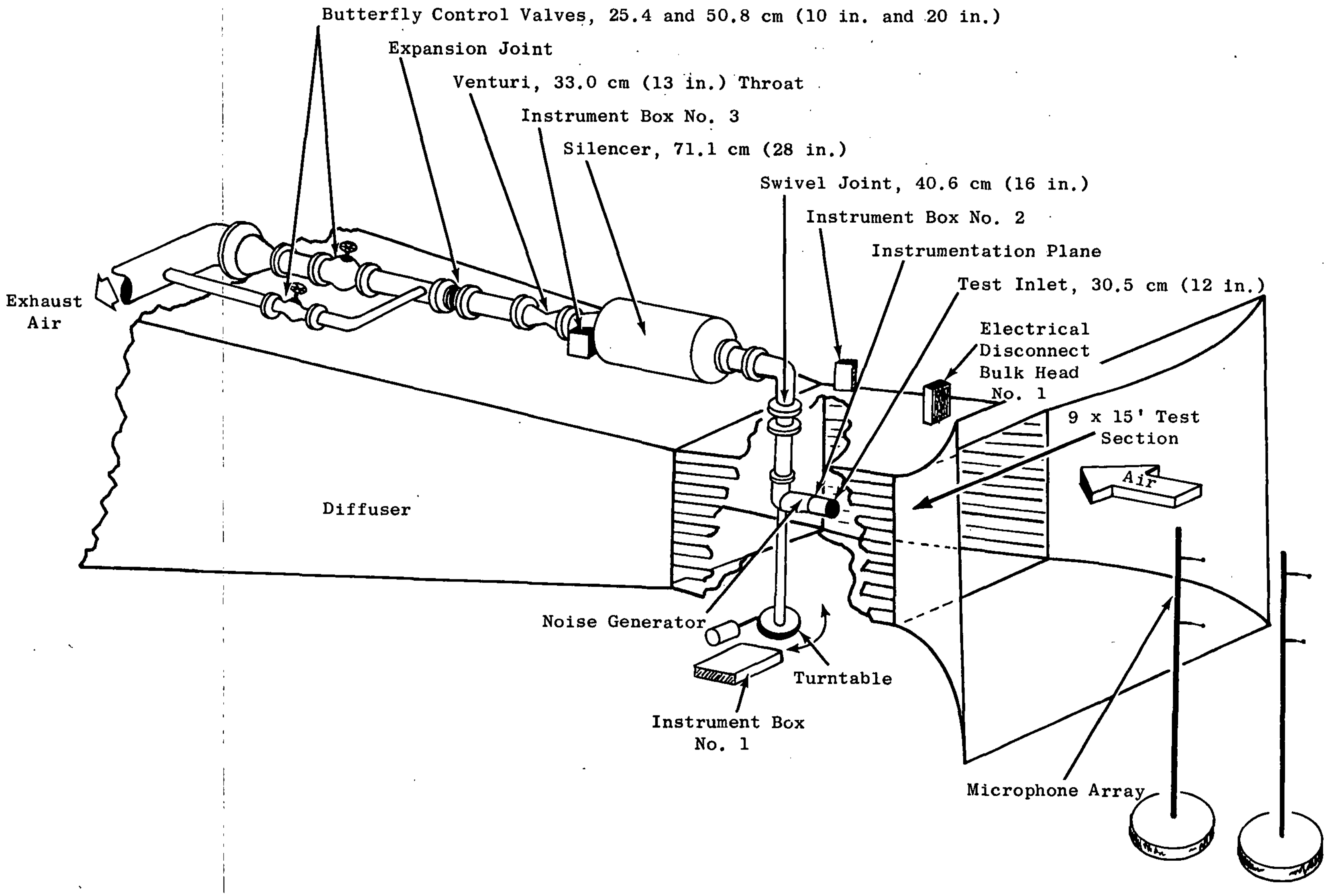

Figure 1. General Arrangement of the NASA LeRC 9- by 15-Foot V/STOL Wind Tunnel.

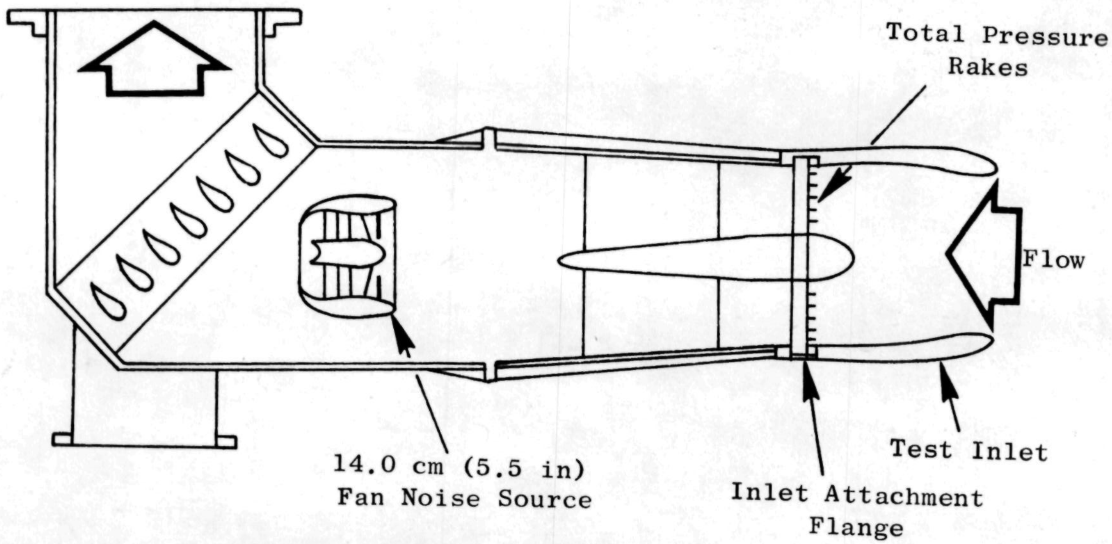

Figure 2. Schematic of the 30.5 cm (12 in.) Inlet Model Attachment.

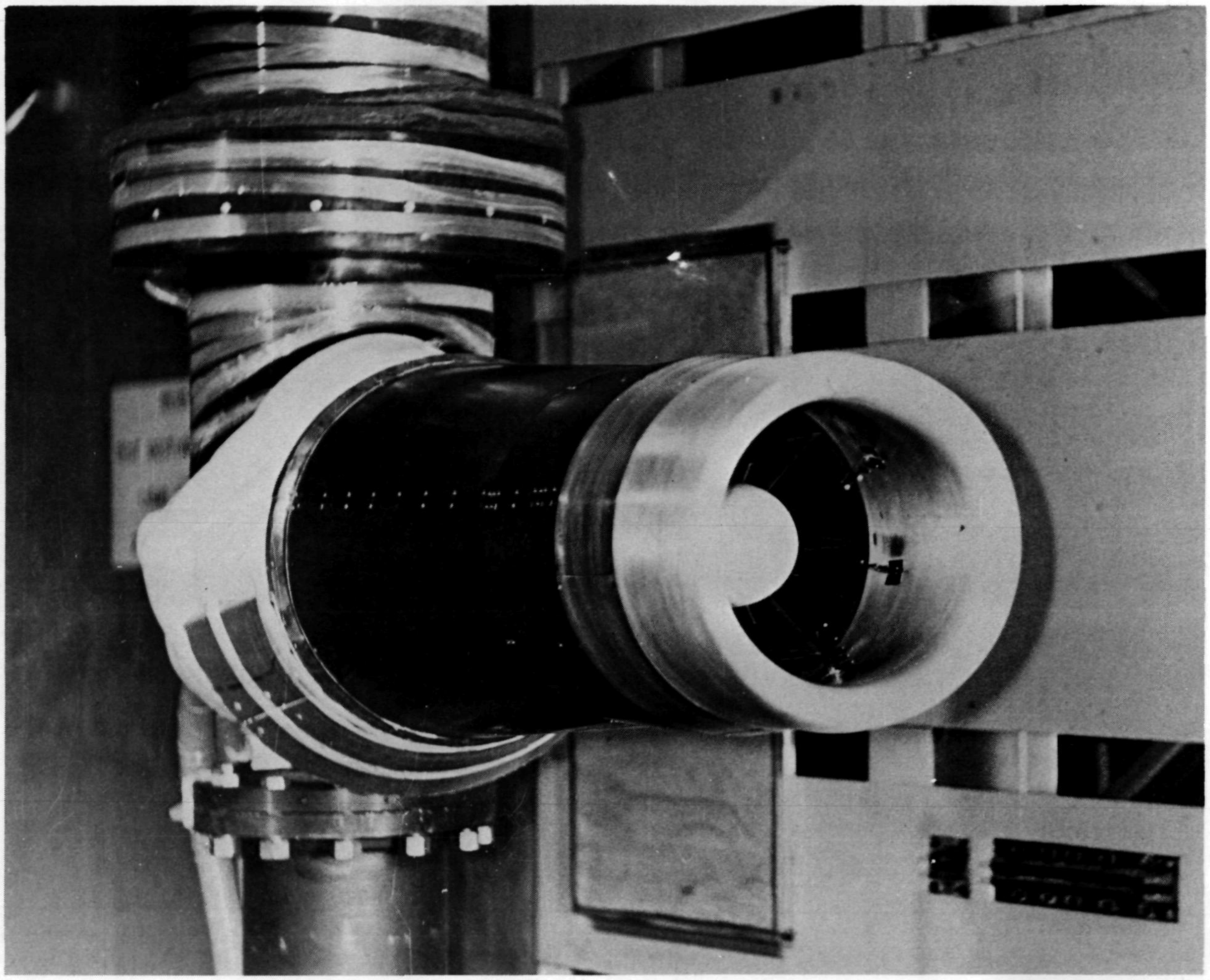

Figure 3. Photograph of a 30.5 cm (12 in.) QCSEE Inlet Model Installed in the Wind Tunnel.

SECTION 4.0

INLET DESIGN CONSIDERATIONS, DESIGN PROCEDURE, AND MODEL DESCRIPTION

4.1 INLET DESIGN CONSIDERATIONS

The model aerodynamic design was a joint product of the General Electric Company, NASA-Lewis Research Center, and McDonnell-Douglas organizations. The design phase profited greatly from this cooperative effort, especially since only a two-month period was available to design, fabricate, and instrument the models prior to the one-month tunnel occupancy. Various constraints guided the inlet design, including QCSEE program requirements, typical aircraft certification demonstration procedure, QCSEE acoustic measuring points, and some general aerodynamic and acoustic design objectives. These factors are summarized below and define requirements for an inlet suitable for both under-the-wing (UTW) and over-the-wing (OTW) engine installations.

QCSEE UTW/OTW Inlet Design Constraints

- QCSEE Program Requirements - No inlet separation from flight idle to takeoff power setting at 41.2 m/sec (80 knots) freestream velocity and up to 50° angle of attack. Also, no inlet separation up to takeoff power setting when operating in a 18.0 m/sec (35 knot) static 90° crosswind.

- STOL Aircraft Operational Input (YC-15 Zero Degree Flaps Takeoff Demonstration Point for Aircraft Certification) - No inlet separation for takeoff and approach power settings at 61.7 m/sec (120 knots) freestream velocity and up to 43° angle of attack. The YC-15 aircraft is a prototype military STOL transport being built by McDonnell-Douglas Corporation under contract to the United States Air Force.

- Design Objectives

Takeoff throat Mach Number	= 0.79
Treatment length/fan diameter	= 0.74
Inlet length/fan diameter	= 1.0
Drag divergence Mach Number	= 0.72

These constraints are largely self-explanatory. The design objectives reflect the desire for an inlet that can provide a takeoff throat Mach number that is relatively high for acoustic suppression, plus sufficient treatment for acoustic suppression in approach and reverse-thrust operating modes. In addition, the stringent angle-of-attack capability previously described must be achievable at this high design throat Mach number. Finally, inclusion of the desired acoustic treatment length, plus the required internal lip and an initial untreated diffuser segment to allow diffusion to subsonic local velocity prior to the treatment, produces a total inlet L/D_F of approximately 1.0. This is relatively short, considering the foregoing constraints, yet somewhat longer than might be required by aerodynamic considerations alone. The 0.79 M_{TH} value was selected after consideration of the likely variance from nominal that might occur (engine-to-engine flow variation, manufacturing tolerance, control accuracy, transient overshoot), in conjunction with the anticipated limiting throat Mach number, beyond which rapid degradation of inlet performance and stability would occur.

4.2 INLET DESIGN PROCEDURE

Definition of the appropriate range of inlet model design parameters was initiated at a joint meeting in which applicable analytical experience and experimental results were pooled. A tentative four-configuration matrix resulted.

Subsequent evaluation suggested that the relatively high internal lip diameter ratios planned might necessitate a reduction in the forebody diameter ratio initially selected ($D_{HL}/D_{Max.} = 0.91$), in order to avoid an excessively sharp curvature mismatch at the leading edge. A second joint meeting was held to discuss this consideration as well as other design details. Angle-of-attack flow analyses conducted by NASA and Douglas were used as a basis for selecting the forebody designs. It was concluded that, while curvature of both internal and external lips near the highlight was of paramount importance to achieving desired angle-of-attack capability, the QCSEE requirements could be satisfied by employing a Douglas-developed forebody contour, the DAC Series 1 (Reference 2) with a diameter ratio $D_{HL}/D_{Max.} = 0.905$ - only slightly less than the value initially selected. This value also allowed the inlet forebody to be about equal to or less than the 200.2 centimeter (78.8 inch) full-scale maximum diameter established by all other nacelle considerations with either the 1.21 or 1.17 D_{HL}/D_{TH} internal lips.

The remainder of the inlet components (diffuser, centerbody representation of engine spinner) and the test matrix were finalized at that meeting. Key design parameters are summarized in Table I.

A brief description of the logic involved in these selections follows:

Internal Lip - The analytical and experimental base of the initial meeting indicated that a D_{HL}/D_{TH} between 1.17 and 1.25 should suffice for both the in-flight angle-of-attack and static crosswind operating conditions. It was felt that perhaps the 1.17 value would be adequate for the crosswind requirement (i.e., side inlet contours), while the 1.21 value would probably handle the angle-of-attack condition (i.e., bottom inlet contour). Thus, an inlet with an asymmetric (circumferentially varying) internal lip might result, with an even lower contraction ratio for the top contour (e.g., 1.12 - 1.13) which is not faced with any major extreme flow incidence situation. The 1.25 D_{HL}/D_{TH} configuration (No. 3) was a "fallback" position, to be used only if the 1.21 (No. 2) model gave unsatisfactory performance. The data base showed that a

Table I. Summary of Key 30.5 cm (12 in.) QCSEE Inlet Design Parameters.

Inlet Component	Design Parameter	Configuration Number			
		1	2	3	4
Internal Lip:	D_{HL}/D_{TH}	1.17	1.21	1.25	1.21
	Contour	1/4 Ellipse	1/4 Ellipse	1/4 Ellipse	1/4 Ellipse
	a/b	2.0	2.0	2.0	2.0
Forebody:	$D_{HL}/D_{Max.}$	0.905	0.905	0.905	0.935
	$X/D_{Max.}$	0.200	0.200	0.200	0.175
	Contour	DAC Series 1	DAC Series 1	DAC Series 1	NACA 1-Series
Diffuser:	A_{EX}/A_{TH}*	1.445	1.445	1.445	1.445
	L/D_F	0.826	0.826	0.826	0.826
	Contour	Cubic	Cubic	Cubic	Cubic
	$\theta_{Max.}$	8.68°	8.68°	8.68°	8.68°
	$2\theta_{EQ}$*	11.62°	11.62°	11.62°	11.62°
Overall Inlet:	L/D_F	0.967	1.001	1.034	1.001
	Full-Scale $D_{Max.}$	193.9 cm (76.349 in.)	200.6 cm (78.964 in.)	207.2 cm (81.579 in.)	194.1 cm (76.432 in.)

* Excluding centerbody

quarter-ellipse of axes ratio a/b = 2.00 would be about the lowest value (shortest lip) consistent with the operating requirements.

Forebody - Beyond the low flight speed considerations already discussed, these designs were also selected to satisfy the required drag divergence (high speed) Mach number. The No. 4 configuration evolved from a desire to see whether satisfactory internal performance could be obtained from a higher diameter ratio (lower envelope diameter) and a correspondingly sharper external shape. It also duplicated forebody designs previously tested by NASA in 50.8 centimeter (20 inch) diameter models, Reference 3, allowing the study of Reynolds number effects to be made. (The NASA inlets had internal lip diameter ratios of D_{HL}/D_{TH} = 1.122 and 1.162, and were therefore not exactly similar to configuration No. 4 of this test.)

Diffuser - Since the scope of this program allowed only one diffuser contour, its design was obviously crucial to the success of the entire investigation. Available analytical results (Reference 4) indicated that cubic diffusers with the inflection point (location of maximum wall slope) at, or forward of, the diffuser midpoint were superior to further-aft inflection point locations in terms of boundary layer stability under high angle-of-attack operating conditions comparable to those of the QCSEE application. These results were obtained for average throat Mach numbers of 0.60. They were presumed to be valid also for the 0.79 M_{TH} QCSEE value; this was then confirmed by subsequent NASA analysis. The midpoint location (i.e., "balanced" cubic) was adopted following this effort and after coordination with GE Fan Aerodynamic Design showed that such a design was satisfactory in terms of predicted QCSEE fan rotor incidence.

The diffuser was sized for a one-dimensional average throat Mach number of 0.79 at the 41.2 m/sec (80 knot) takeoff condition. Associated design parameters were an engine face corrected flow of 408.9 kg/sec (901.5 lb/sec), and estimated inlet model recovery of 0.990. Throat flow coefficient, defined as the ratio of the actual to ideal one-dimensional choking weight flow, was estimated to be 0.990 and used for inlet sizing. It should be noted that the upcoming 50.8 centimeter (20 inch) and full-scale QCSEE inlets will be sized slightly differently, to reflect latest engine flow of 405.5 kg/sec (894 lb/sec), as well as minor changes in inlet recovery and throat flow coefficient based on 30.5 centimeter (12 inch) inlet test data and anticipated Reynolds Number effects.

Centerbody - While not part of the inlet as such, consideration was given to this component because it influences the diffuser flow characteristics. The inlet sketch shown in Figure 4 indicates that the interface with the NASA hardware dictates that the centerbody terminate with a horizontal slope, unlike the QCSEE spinner contour which is still increasing in radius at that point. Consequently, the test centerbody had to be longer than the equivalent scaled QCSEE spinner in order to avoid a nonrepresentative velocity spike near the interface that would otherwise occur due to sharp curvature. Such a velocity peak was undesirable because it might cause separation on the hub surface that would be reflected in the downstream pressure survey, and hence

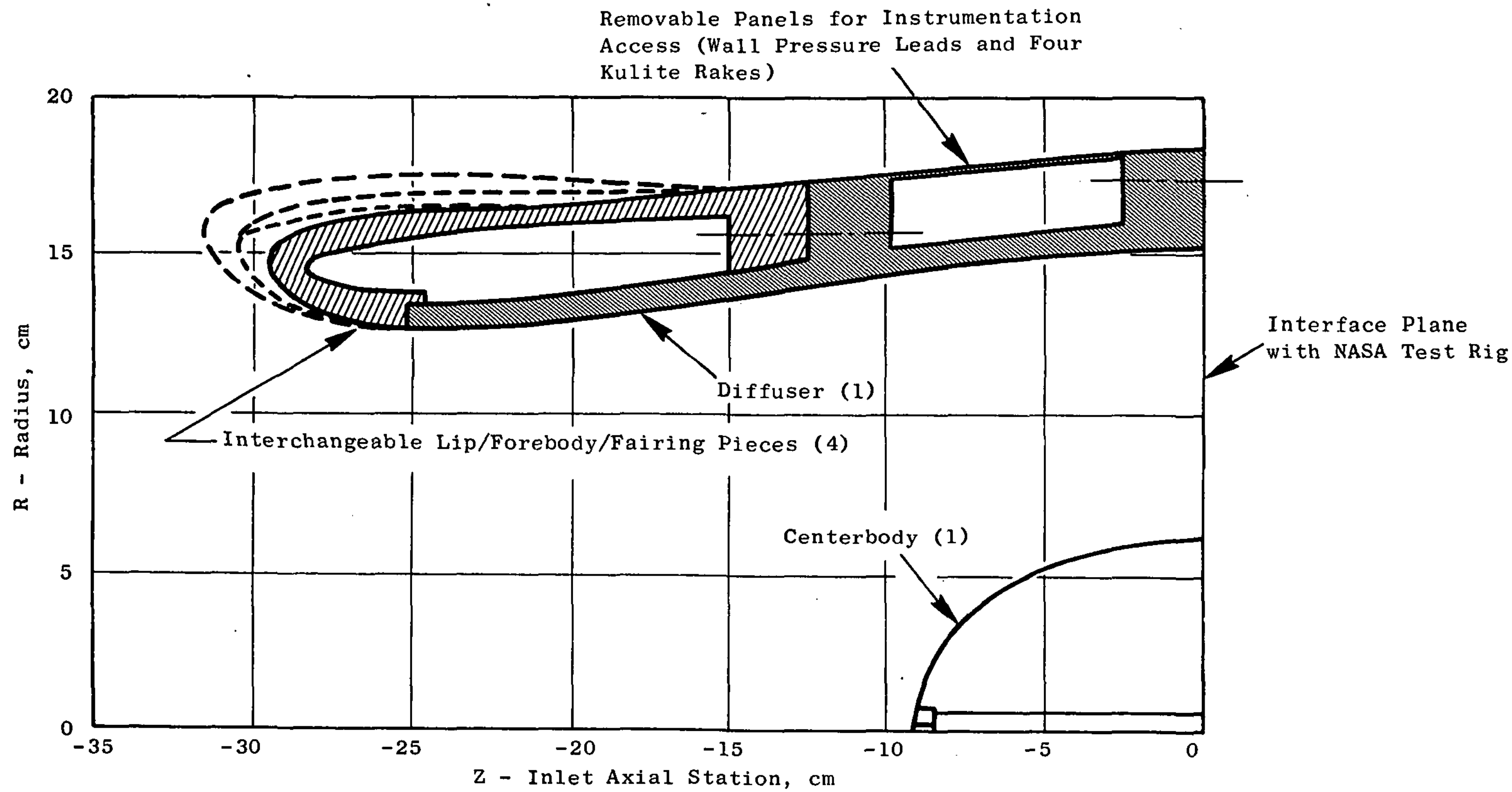

Figure 4. Schematic of 30.5 cm (12 in.) QCSEE Inlet Construction, Showing Interchangeable Lip and Instrumentation Access.

falsely degrade the measured inlet performance. After some analytical evaluation of this point, a 1.5:1 (a/b) quarter-ellipse was selected as the best compromise between simulating the QCSEE spinner length and totally eliminating the hub velocity peak. It was felt that this design allowed the inlet geometry to be meaningfully evaluated, as intended, within the limitations described.

The NASA facility hub-to-tip radius ratio, 0.400, is close to the QCSEE UTW and OTW values of 0.443 and 0.418, respectively, at the diffuser exit station.

4.3 MODEL DESCRIPTION

The foregoing inlet configurations were constructed from aluminum by making one separate diffuser and four interchangeable lips. Each of these lips was a one-piece item that combined the internal lip, forebody, and a fairing leading from the inlet $D_{Max.}$ (which occurred at a different axial station and radius for each configuration) to a common termination on the external flow surface having the same axial station, radius, and slope. This latter point was the initiation of a conical sheet metal fairing which covered an instrumentation access region housed between two flanges in the diffuser. This feature facilitated configuration changes by allowing lip static pressure tubing to be disconnected and reconnected. Dynamic pressure rakes were also installed in this region. These details are indicated schematically in Figure 4.

SECTION 5.0

AERODYNAMIC INSTRUMENTATION AND DATA ACQUISITION

5.1 INSTRUMENTATION

The following are the key items of aerodynamic instrumentation included in this test, as indicated in Figure 5:

- A comprehensive total and static pressure survey, contained in a NASA instrumentation ring, located just aft of the test diffuser exit plane. A total of 128 total and 32 wall static pressure measurements was made in this plane to enable an accurate determination of inlet total pressure recovery and distortion to be made. A detailed sketch of the locations is given in Figure 6; the sensors are equally allocated among eight circumferential sectors. Included are eight six-element, equal area-weighted rakes that span the stream, plus eight five-element boundary layer rakes on both tip (inlet) and hub (centerbody) flowpaths. The radial locations of these probes are given in Figure 7.

- A total of 52 wall static pressure taps for each of the four configurations. Thirty-six of these were located in the (common) diffuser, with the remaining 16 in each lip component. The taps were distributed into two axial rows of 20 along each of the windward and leeward circumferential locations, plus circumferential rings of eight at each of two axial stations - one in the forward portion of the diffuser and the other near the diffuser exit. Figure 8 provides a list of the physical and relative tap locations for each configuration.

- Four total pressure rakes with four stream-mounted Kulite transducers each were mounted near the diffuser midpoint (due to space limitations) to monitor dynamic distortion activity and to detect the onset of inlet separation. Steady-state pressure level was also measured for each of the probes. The rake and probe locations are given in Figure 9; three rakes were concentrated on the windward side, with the remaining one diametrically opposite, to confirm the expected relative lack of dynamic activity in that area and for dynamic distortion index computation.

- Seven Kulite transducers were flush-mounted in the diffuser wall to further assess dynamic activity. Four were aligned in an axial row spanning most of the diffuser length on the windward side. One (the most forward) of the foregoing plus three others were arranged in a circumferential ring. In this manner, both axial and circumferential variations could be evaluated with a moderate amount of instrumentation. Exact transducer locations are provided in Figure 10.

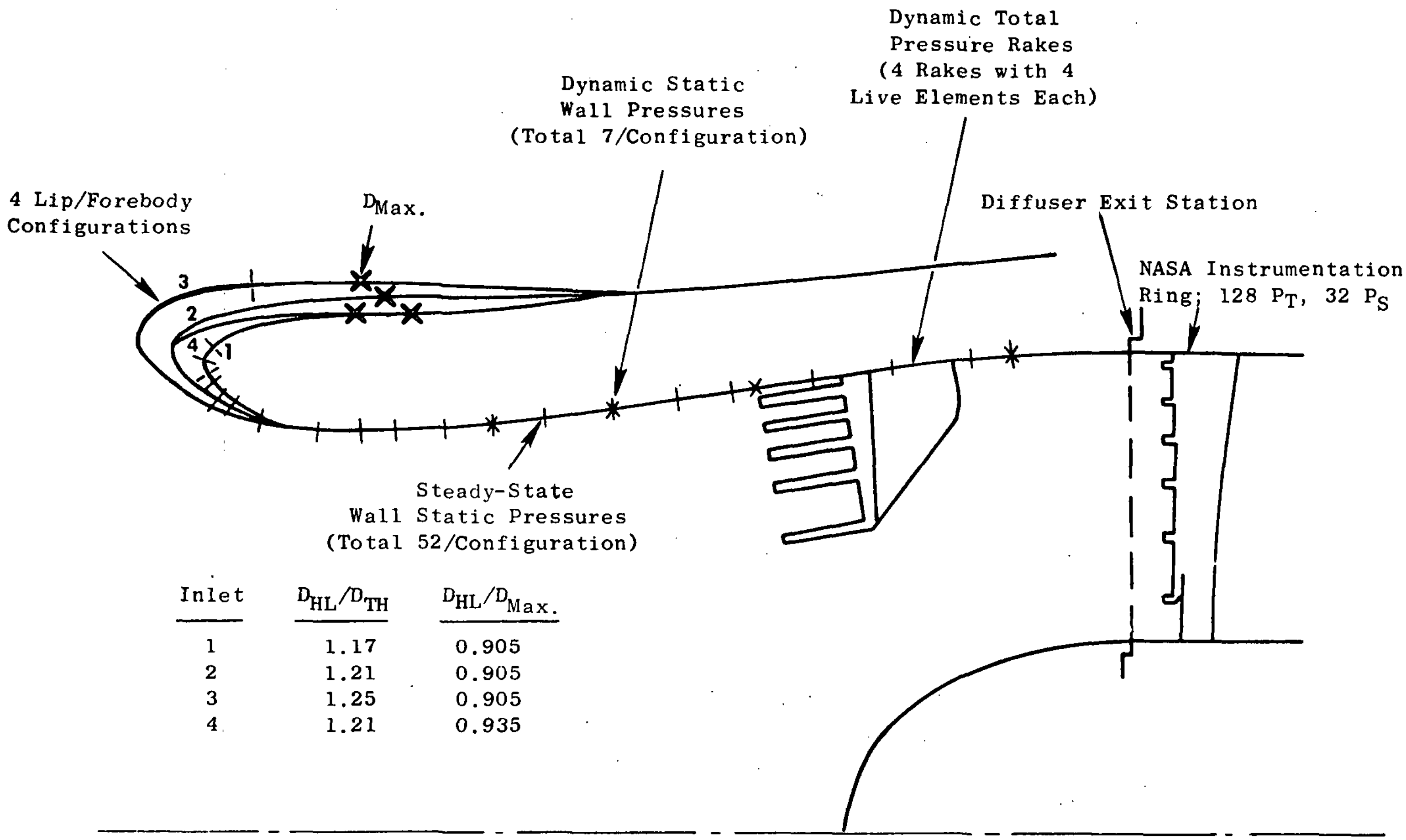

Inlet	D_{HL}/D_{TH}	$D_{HL}/D_{Max.}$
1	1.17	0.905
2	1.21	0.905
3	1.25	0.905
4	1.21	0.935

Figure 5. 30.5 cm (12 in.) QCSEE Inlet Model with Instrumentation.

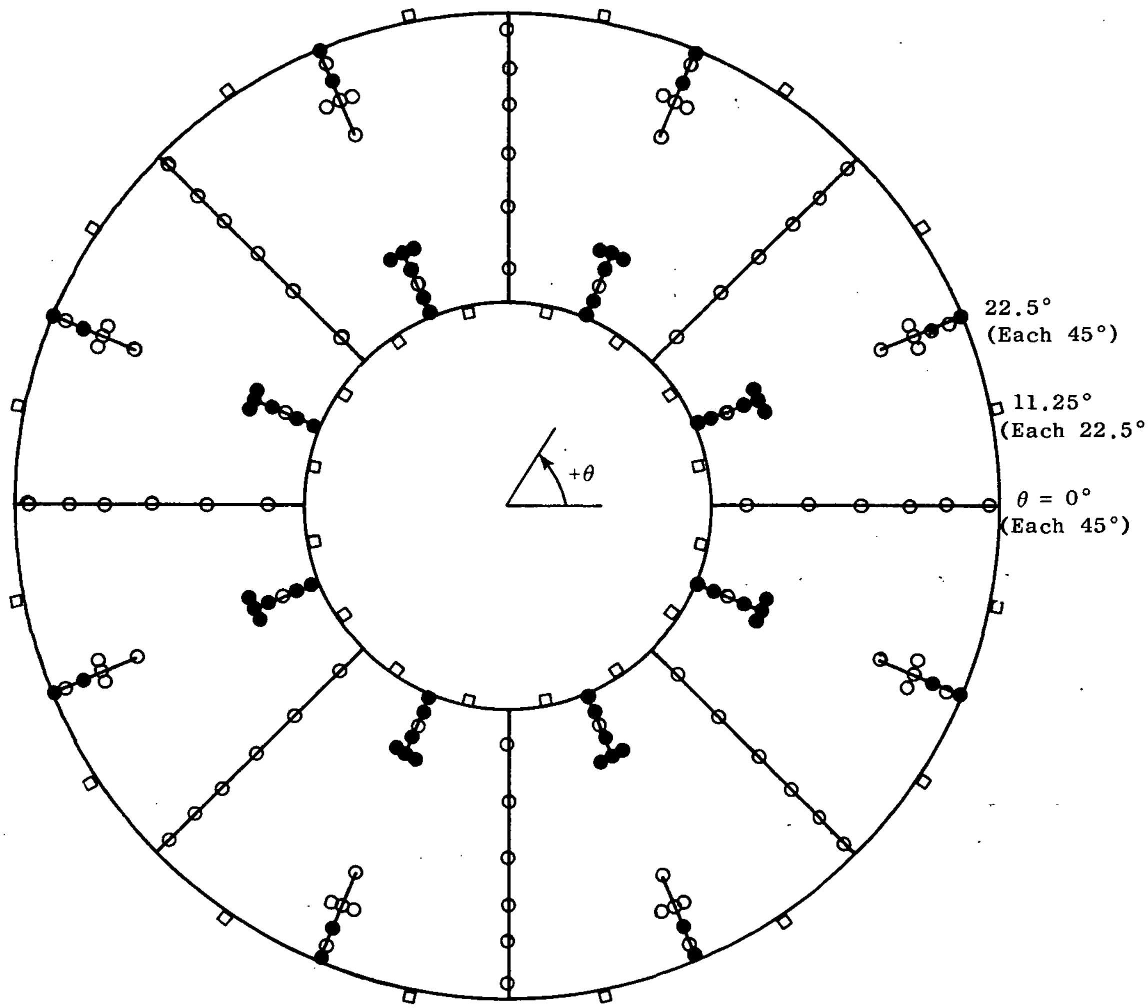

○ = Total Pressure

○ Same Radial Location for all Rakes
● B.L. Rake Radial Location
○○○ Flow Angle Probe (Not Used)

□ = Static Pressure

128 Total Pressure Measurements
32 Static Pressure Measurements

Figure 6. NASA Diffuser Exit Instrumentation Ring.

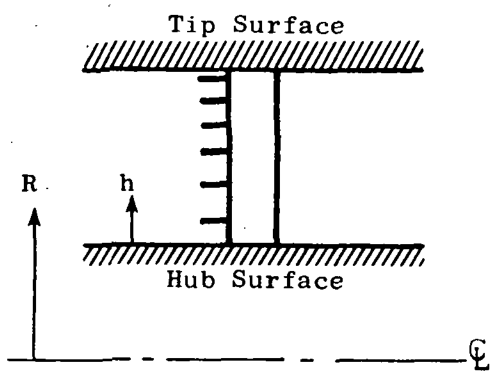

Tube	h/L*	R/L*	% Area
1 (Innermost)	0.48	2.88	8.38
2	1.25	3.65	25.01
3	1.89	4.29	41.81
4	2.44	4.84	58.42
5	2.93	5.33	74.90
6 (Outermost)	3.39	5.79	91.81

(a) Six-element stream rakes.

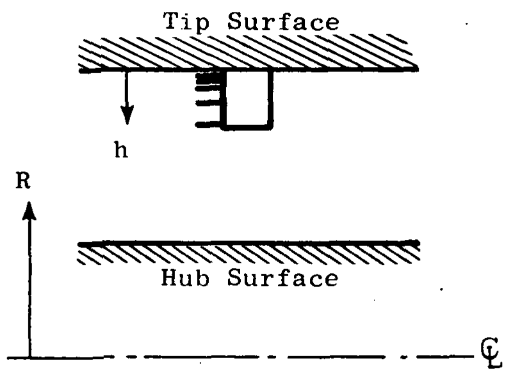

Tube	h/L*	R/L*	% Area
1 (Innermost)	0.10	5.90	96.06
2	0.21	5.79	91.81
3	0.40	5.60	84.66
4	0.67	5.33	74.90
5 (Outermost)	1.16	4.84	58.42

(b) Five-element tip surface boundary layer rakes.

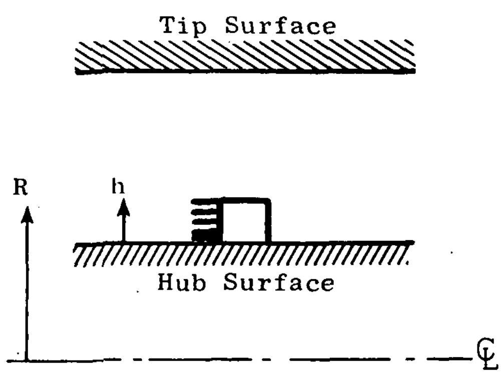

Tube	h/L*	R/L*	% Area
1 (Innermost)	0.10	2.50	1.62
2	0.26	2.66	4.35
3	0.48	2.88	8.38
4	0.68	3.08	12.32
5 (Outermost)	0.90	3.30	16.96

(c) Five-element hub surface boundary layer rakes.

$L^* \equiv 2.54$ cm.

Figure 7. Radial Locations of NASA Total Pressure Probes.

L* = 2.54 cm

Tube Number	θ Degrees	Inlet No. 1 Z/L*	Inlet No. 1 X/L	Inlet No. 2 Z/L*	Inlet No. 2 X/L	Inlet No. 3 Z/L*	Inlet No. 3 X/L	Inlet No. 4 Z/L*	Inlet No. 4 X/L
130	0	-11.45**	-.0137	-11.85**	-.0132	-12.24**	-.0136	-11.80**	-.0174
131	180	-11.45**	-.0137	-11.85**	-.0132	-12.24**	-.0136	-11.80**	-.0174
904	0	-11.58**	-.0025	-11.98**	-.0024	-12.38**	-.0023	-11.94**	-.0057
905	180	-11.58**	-.0025	-11.98**	-.0024	-12.38**	-.0023	-11.94**	-.0057
906	0	-11.57	.0034	-11.97	.0032	-12.36	.0039	-11.97	.0032
907	180	-11.57	.0034	-11.97	.0032	-12.36	.0039	-11.97	.0032
908	0	-11.51	.0085	-11.89	.0099	-12.27	.0112	-11.89	.0099
909	180	-11.51	.0085	-11.89	.0099	-12.27	.0112	-11.89	.0099
910	0	-11.41	.0171	-11.76	.0207	-12.11	.0241	-11.76	.0207
911	180	-11.41	.0171	-11.76	.0207	-12.11	.0241	-11.76	.0207
912	0	-11.26	.0301	-11.58	.0357	-11.90	.0410	-11.58	.0357
913	180	-11.26	.0301	-11.58	.0357	-11.90	.0410	-11.58	.0357
914	0	-10.86	.0645	-11.09	.0765	-11.31	.0886	-11.09	.0765
915	180	-10.86	.0645	-11.09	.0765	-11.31	.0886	-11.09	.0765
916	0	-10.19	.1222	-10.26	.1456	-10.32	.1683	-10.26	.1456
917	180	-10.19	.1222	-10.26	.1456	-10.32	.1683	-10.26	.1456
918	0	-9.65	.1687	-9.65	.1964	-9.65	.2223	-9.65	.1964
919	45	-9.65	.1687	-9.65	.1964	-9.65	.2223	-9.65	.1964
920	90	-9.65	.1687	-9.65	.1964	-9.65	.2223	-9.65	.1964
921	135	-9.65	.1687	-9.65	.1964	-9.65	.2223	-9.65	.1964
922	180	-9.65	.1687	-9.65	.1964	-9.65	.2223	-9.65	.1964
923	225	-9.65	.1687	-9.65	.1964	-9.65	.2223	-9.65	.1964
924	270	-9.65	.1687	-9.65	.1964	-9.65	.2223	-9.65	.1964
925	315	-9.65	.1687	-9.65	.1964	-9.65	.2223	-9.65	.1964
132	0	-9.20	.2075	-9.20	.2339	-9.20	.2586	-9.20	.2339
133	180	-9.20	.2075	-9.20	.2339	-9.20	.2586	-9.20	.2339
134	0	-8.60	.2592	-8.60	.2839	-8.60	.3070	-8.60	.2839
135	180	-8.60	.2592	-8.60	.2839	-8.60	.3070	-8.60	.2839
230	0	-8.00	.3109	-8.00	.3338	-8.00	.3553	-8.00	.3338
231	180	-8.00	.3109	-8.00	.3338	-8.00	.3553	-8.00	.3338
232	0	-7.35	.3669	-7.35	.3880	-7.35	.4077	-7.35	.3880
233	180	-7.35	.3669	-7.35	.3880	-7.35	.4077	-7.35	.3880
234	0	-6.50	.4401	-6.50	.4587	-6.50	.4762	-6.50	.4587
235	180	-6.50	.4401	-6.50	.4587	-6.50	.4762	-6.50	.4587
330	0	-5.70	.5090	-5.70	.5254	-5.70	.5407	-5.70	.5254
331	180	-5.70	.5090	-5.70	.5254	-5.70	.5407	-5.70	.5254
332	0	-5.00	.5693	-5.00	.5836	-5.00	.5971	-5.00	.5836
430	180	-5.00	.5693	-5.00	.5836	-5.00	.5971	-5.00	.5836
434	0	-4.00	.6554	-4.00	.6669	-4.00	.6777	-4.00	.6669
435	180	-4.00	.6554	-4.00	.6669	-4.00	.6777	-4.00	.6669
530	0	-3.00	.7416	-3.00	.7502	-3.00	.7582	-3.00	.7502
531	180	-3.00	.7416	-3.00	.7502	-3.00	.7582	-3.00	.7502
532	0	-2.00	.8277	-2.00	.8335	-2.00	.8388	-2.00	.8335
333	45	-2.00	.8277	-2.00	.8335	-2.00	.8388	-2.00	.8335
334	90	-2.00	.8277	-2.00	.8335	-2.00	.8388	-2.00	.8335
335	135	-2.00	.8277	-2.00	.8335	-2.00	.8388	-2.00	.8335
533	180	-2.00	.8277	-2.00	.8335	-2.00	.8388	-2.00	.8335
431	225	-2.00	.8277	-2.00	.8335	-2.00	.8388	-2.00	.8335
432	270	-2.00	.8277	-2.00	.8335	-2.00	.8388	-2.00	.8335
433	315	-2.00	.8277	-2.00	.8335	-2.00	.8388	-2.00	.8335
534	0	-1.00	.9139	-1.00	.9167	-1.00	.9194	-1.00	.9167
535	180	-1.00	.9139	-1.00	.9167	-1.00	.9194	-1.00	.9167

** Denotes Taps on External Portion of Lip, as does Negative X/L

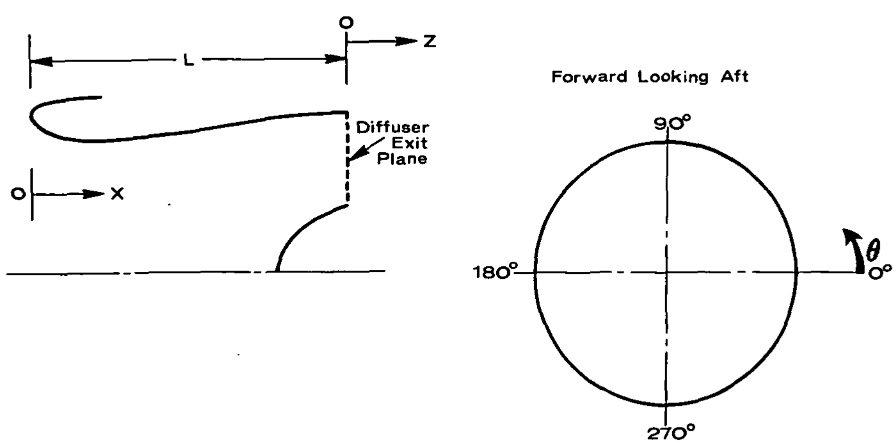

Figure 8. Summary of Wall Static Pressure Tap Locations.

(a) Rake Circumferential Locations

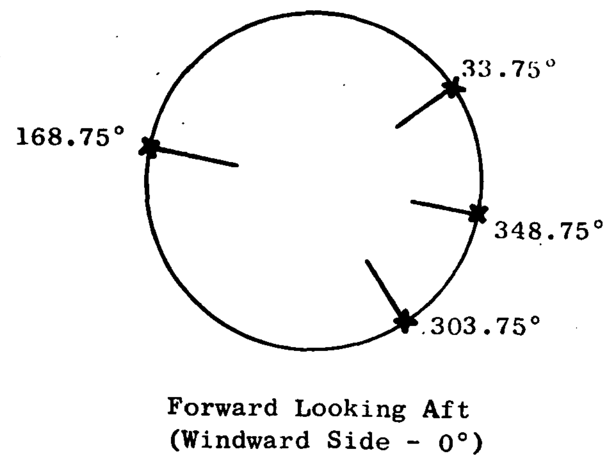

(b) Rake Axial Location and Probe Radial Locations

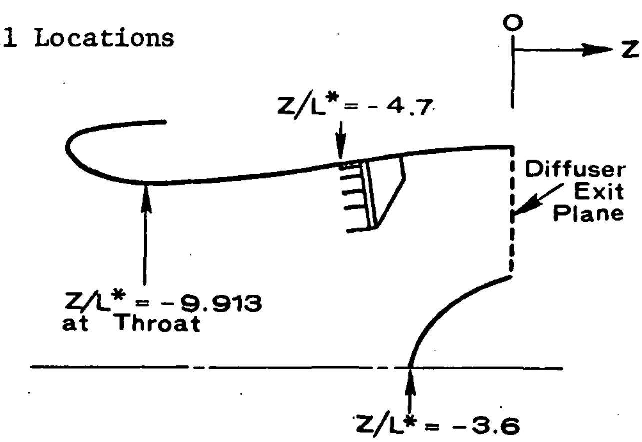

Probe	Radial Location ~R/L*	% Flow Area
A (Outermost)	5.344	93.2
B (No Kulite)	5.016	82.1
C	4.641	70.3
D	4.234	58.5
E (Innermost)	3.656	43.6

L* ≡ 2.54 cm.

Figure 9. Kulite Total Pressure Rake and Probe Locations.

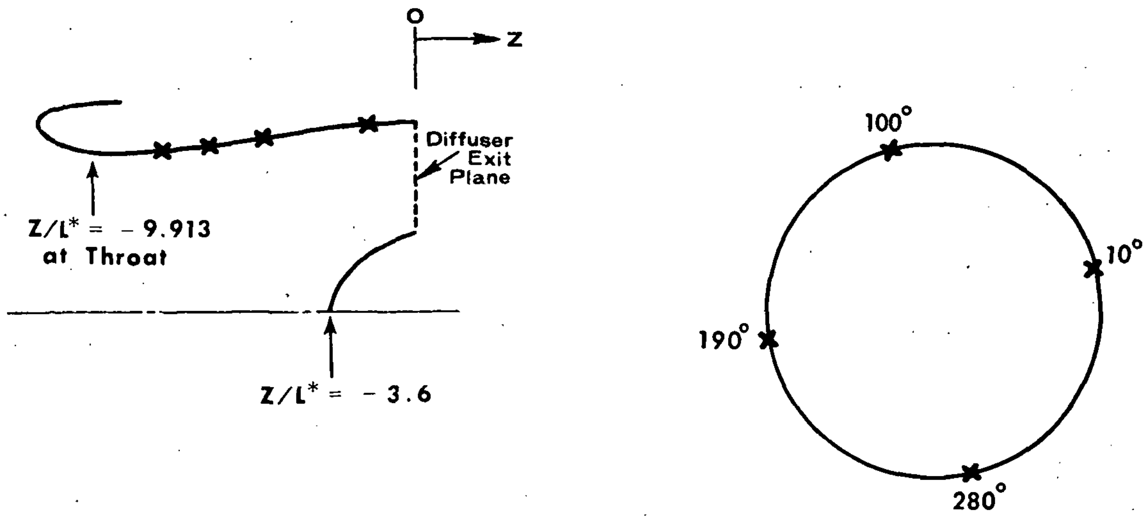

Forward Looking Aft
(Windward Side - 0°)

Kulite Number	Z/L*	θ	
1	-8.0	10°	
2	-8.0	100°	
3	-8.0	190°	
4	-8.0	280°	
5	-6.5	10°	
6	-4.7	10°	(In Plane of P_T Kulites)
7	-1.5	10°	

$L^* \equiv 2.54$ cm.

Figure 10. Diffuser Wall Kulite Locations.

In addition, various facility measurements were made, among them inlet airflow (via a venturi meter), inlet angle of attack, and tunnel velocity, pressure, and temperature, to enable calculation of key performance variables such as inlet throat Mach Number, pressure recovery, and freestream Mach Number.

5.2 DATA ACQUISITION

All steady-state pressures were acquired via NASA scanivalves which were linked to the NASA steady-state pressure acquisition system, Central Automatic Digital Data Encoder (CADDE). These measurements, plus the other facility parameters, were then converted to engineering units and also to performance parameters by a NASA computer program. All total pressure measurements, together with wall static pressures in the same plane, were integrated to determine the area-weighted total pressure recovery. Boundary layer rake pressure probes closer than 8.19% of the annular flow area to the wall (i.e., within the outermost and innermost probes of the six-element stream rakes) were excluded in determining the total pressure distortion, consistent with established GE Practices.

Various aspects of the dynamic data system and results have been reported in Reference 5, hence only a brief summary will be given here. All Kulite data were recorded on two standard, 14 channel FM analog recording systems. Electrical transducer outputs were direct-coupled to the tape recorders and also to a EAI TR-48 analog computer that was employed to process data on-line and aid test conduct, as described in the following section. Transducers were back-pressured to a common, constant reference-pressure source so that time-variant absolute pressure could be accurately measured by combining the fluctuating and constant reference components of the signal. Constant sensitivity was provided to the analog computer and recording system by NASA-supplied Preston line driving amplifiers. NASA also provided signal conditioning via PPM power supplies and bridge balance networks. A block diagram of the entire system, taken from Reference 5, is included in Figure 11.

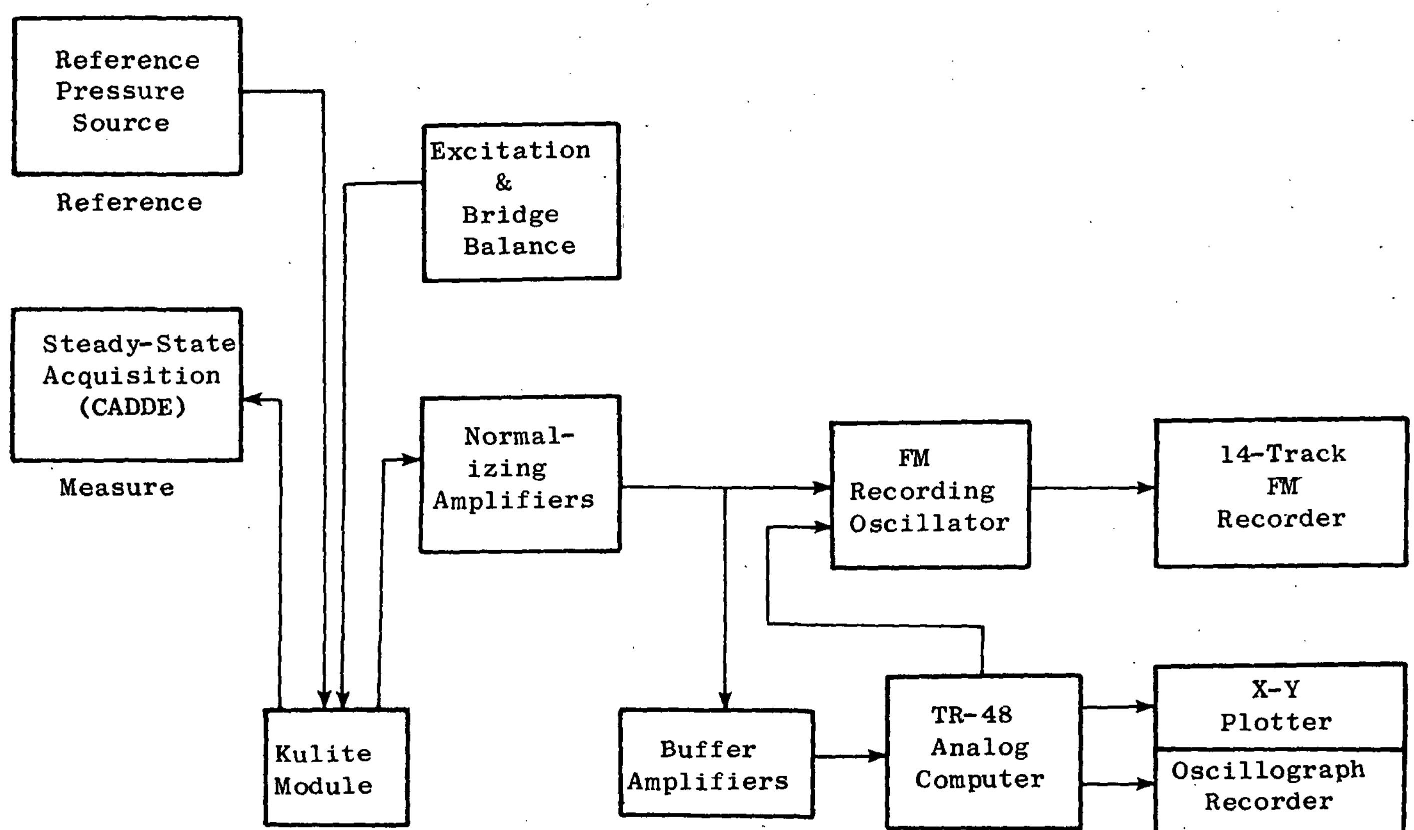

Figure 11. Dynamic Data Acquistion System, QCSEE 30.5 cm (12 in.) Inlet Test.

SECTION 6.0

TEST CONDUCT

The same general test matrix was followed for each of the four configurations, with minor additions or deletions depending on available tunnel time and on-line test results peculiar to each inlet. The general test matrix is shown below.

Tunnel Velocity	Angle of Attack	Average Throat Mach Numbers
0 m/sec (0 kts)	0°	0.10, 0.30, 0.45, 0.60, 0.70, 0.75, 0.79, 0.82, Max. Flow
18.0 m/sec (35 kts)	0,90°	Same as for 0 m/sec
41.2, 61.7 m/sec (80, 120 kts)	0,15,30,40 50°, (α_s* ± 5°)	Same as for 0 m/sec, except 0.10 deleted
*α_s = Angle of attack at which inlet separation first occurs, increasing from zero.		

This matrix was structured to provide data at and above the 0.79 M_{TH} design point, to assess available operating margin; around the flight idle power setting (estimated at 0.38-0.46 M_{TH} for two different applications at the time of the test); near the estimated ground idle power setting ($\sim$0.10 M_{TH}) in crosswind; and at objective flight angles of attack (50° at 41.2 m/sec, 80 kts, 43° at 61.7 m/sec 120 kts)and beyond, if possible, with a definition of the performance on each side of the separation point as well as the available angle-of-attack margin. (It may be noted that a comparable definition of the separation point, if above the required value, is not planned for the forthcoming 50.8 centimeter (20 inch) inlet tests with a turbofan simulator, in deference to vehicle safety.)

Desired test points were efficiently set with the aid of several on-line displays available in the tunnel control room. These included:

- Tunnel "Q" or dynamic head, which is directly relatable to velocity.
- Inlet angle of attack in degrees.
- Inlet flow rate in lbm/sec.

- A pressure parameter, termed $\Delta P/P$, that is a calibratable function of diffuser exit (rake plane) Mach number (corrected flow), if inlet pressure losses are neglected. It was obtained by dividing the difference between tunnel total pressure and diffuser exit static pressure by total pressure.

- X-Y plots of several parameters as a function of inlet angle of attack; these were used as separation indicators. They included both steady-state and dynamic (Kulite) pressure measurements, as follows.

  Steady-state pressure indicators:

  - An inlet lip wall static gage pressure. (An abrupt decrease in gage pressure, corresponding to an increase in absolute pressure, is indicative of reduced local wall Mach number caused by flow separation.)

  - The difference of two diffuser exit total pressures, located opposite each other on windward and leeward sides of the duct. (An abrupt increase from a relatively low value denotes circumferential flow nonuniformity caused by flow separation.)

  Dynamic pressure indicators, via the TR-48 analog computer:

  - Difference between hub and tip ring average pressures - a radial distortion indicator.

  - Difference in windward and leeward rake average pressures - a circumferential distortion indicator.

  - Area-weighted, face average-pressure recovery.

  - Inlet distortion, $(P_{T_{Max.}} - P_{T_{Min.}})/P_{T_{Avg}}$

- Additional parameters recorded on a strip chart included three Kulite pressures, $(P_{T_{Avg}} - P_{T_{Min.}})/P_{T_{Avg}}$, $(P_{T_{Max.}} - P_{T_{Min.}})/P_{T_{Avg}}$ and inlet angle of attack. Relatively little use was made of these signals in conducting the test.

- A reverberant noise frequency spectrum display was used, together with other indicators, in determining the maximum flow, or choking, point. A selected spectrum, such as the tunnel floor noise level, could be "locked" into the display for comparison with a "live" test signal to define the point of maximum meaningful noise suppression.

The basic manner in which these on-line displays were used to set test points is as follows. The desired tunnel velocity was set and, with the inlet at zero angle of attack, the corrected flows corresponding to the desired throat Mach numbers were set to define the corresponding flow parameters, $\Delta P/P$. These values were then used to set all other angle-of-attack points for a given inlet and tunnel velocity. This procedure, setting an approximately constant corrected flow (Mach number), closely simulates actual engine operation. After taking the zero angle-of-attack point, the model was slowly rotated until the separation point was noted. The model was then swept back into the attached flow region, to zero, to define the hysteresis pattern that exists for different directions of angle-of-attack variation. Desired data points on either side of the separation boundary were then taken (after the hysteresis had been cleared), after which the remaining angle-of-attack points (15, 30, 40, 50°) were obtained.

In the crosswind portion of the test, data were taken for some of the inlets with flow parameter set with the inlet in the zero position and in the 90° position. This was done because it is conceivable that power (flow) might be set in either fashion in the eventual installation, i.e., with the inlet either aligned with, or normal to, a runway with prevailing crosswind.

For some of the inlets, more than one blade-passing frequency on the 14.0 centimeter (5.5 inch) inch siren was tested statically, to obtain acoustic data pertinent to both OTW and UTW versions of the QCSEE engine.

After desired test conditions were set for a given point, data were taken for a period of approximately 30 seconds, following which steps to set the next point were immediately initiated. Data taken, in addition to the aerodynamic parameters already described, included several acoustic signals as well as some of the wall Kulites which were acquired by a remotely located NASA recorder that was operated from the control room.

Copies of the test logs are included in Appendix A; the CADDE (Reading) numbers for all test matrix points taken are shown in the appropriate location. A total of 584 data points was taken.

SECTION 7.0

DISCUSSION OF RESULTS

Rather than attempt to provide an inclusive summary, selective test results will be presented from a pragmatic viewpoint of selecting "the" QCSEE inlet geometry, i.e., the requisite lip design for bottom, side and top contours. A tabulation of key test parameters is provided in Appendix B which, together with the test logs of Appendix A, can be used in data-bank fashion to further examine any steady-state performance aspect not discussed in this report. Reference 5, and its companion data bank, provide a more detailed guide to the dynamic data.

7.1 SELECTION OF BOTTOM INLET CONTOUR

The initial screening parameter to assess in making this selection is inlet angle-of-attack capability, relative to the design constraints enumerated in Section 4.1. Figures 12-15 provide this evaluation, in the form of separation angle of attack versus average throat Mach number, for all four inlets tested. Data for both 41.2 and 61.7 m/sec (80 and 120 kts) tunnel velocities are shown, together with the appropriate required operating envelope. Both steady-state and dynamic pressure indications of separation are presented.

Inspection of these figures shows that inlets No. 1 and No. 4 (Figures 12 and 15, respectively) are clearly deficient, the latter inlet by a wide margin (10-15°). Inlet No. 2 and No. 3 (Figures 13 and 14, respectively) each satisfy the operating envelope requirement. The increased lip contraction ratio (greater nacelle maximum diameter required) of inlet No. 3 provides some additional angle-of-attack margin, but very little where inlet No. 2 is most marginal - at 41.2 m/sec (80 kts) and flight-idle power setting.

These data confirm the preliminary selection of 1.21 D_{HL}/D_{TH} for the bottom lip contraction ratio, providing evidence of its acceptability as well as identifying other designs that are over- and underdesigned. They also point out the importance of external lip design, in that the operating range of inlet No. 4 was inferior not only to that of inlet No. 2 (with the same internal lip) but also to No. 1, which had a significantly lower internal lip diameter ratio (1.17 vs 1.21).

It should be noted that both steady-state lip and diffuser separation indicators were triggered simultaneously, within the accuracy of the X-Y plotters. This is interpreted to indicate that the lip separated initially, followed closely by the diffuser. If the separation had originated in the diffuser, only the diffuser separation indicator would have been triggered.

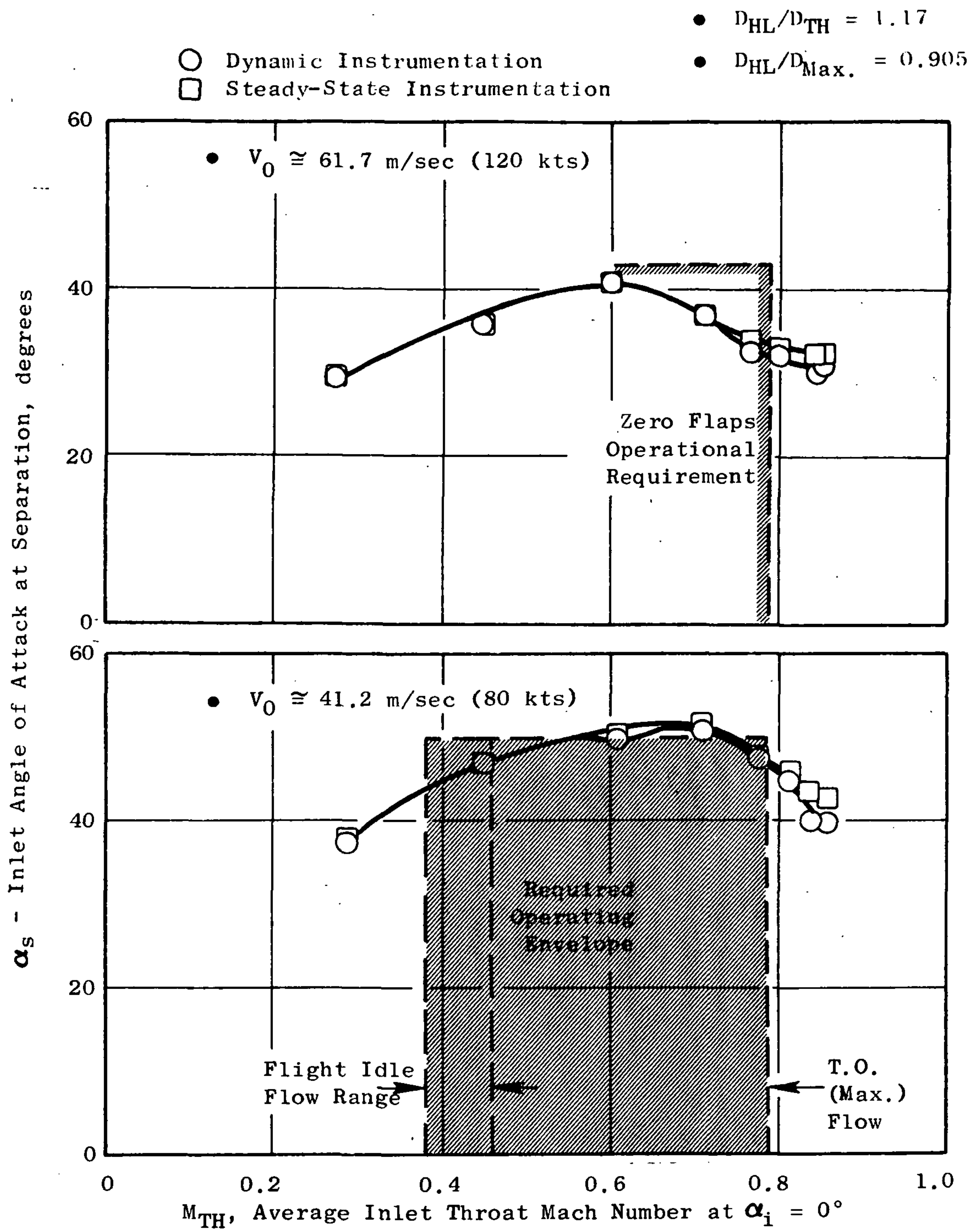

Figure 12. Inlet Separation Boundaries at Angle of Attack, Inlet No. 1.

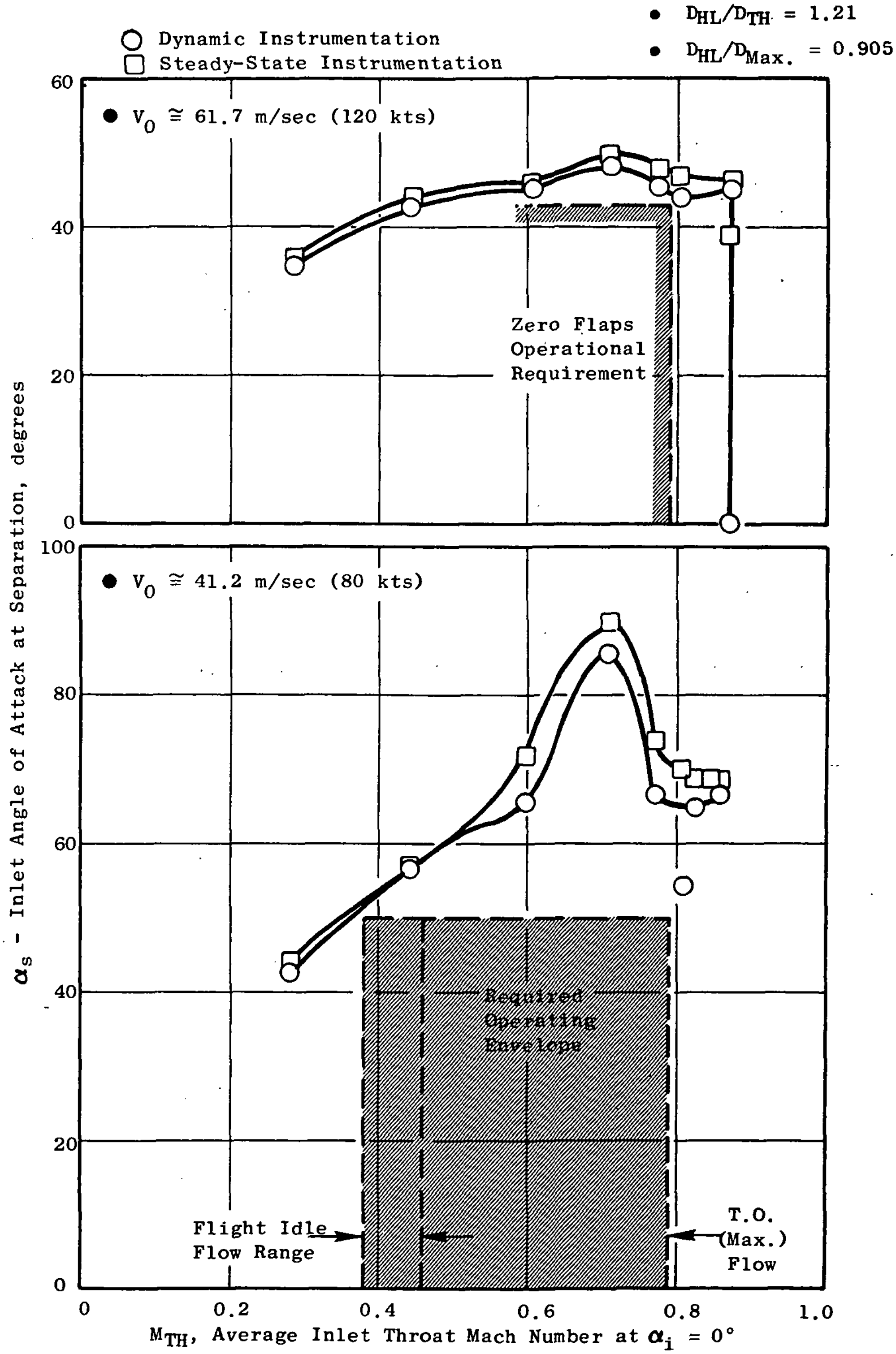

Figure 13. Inlet Separation Boundaries at Angle of Attack, Inlet No. 2.

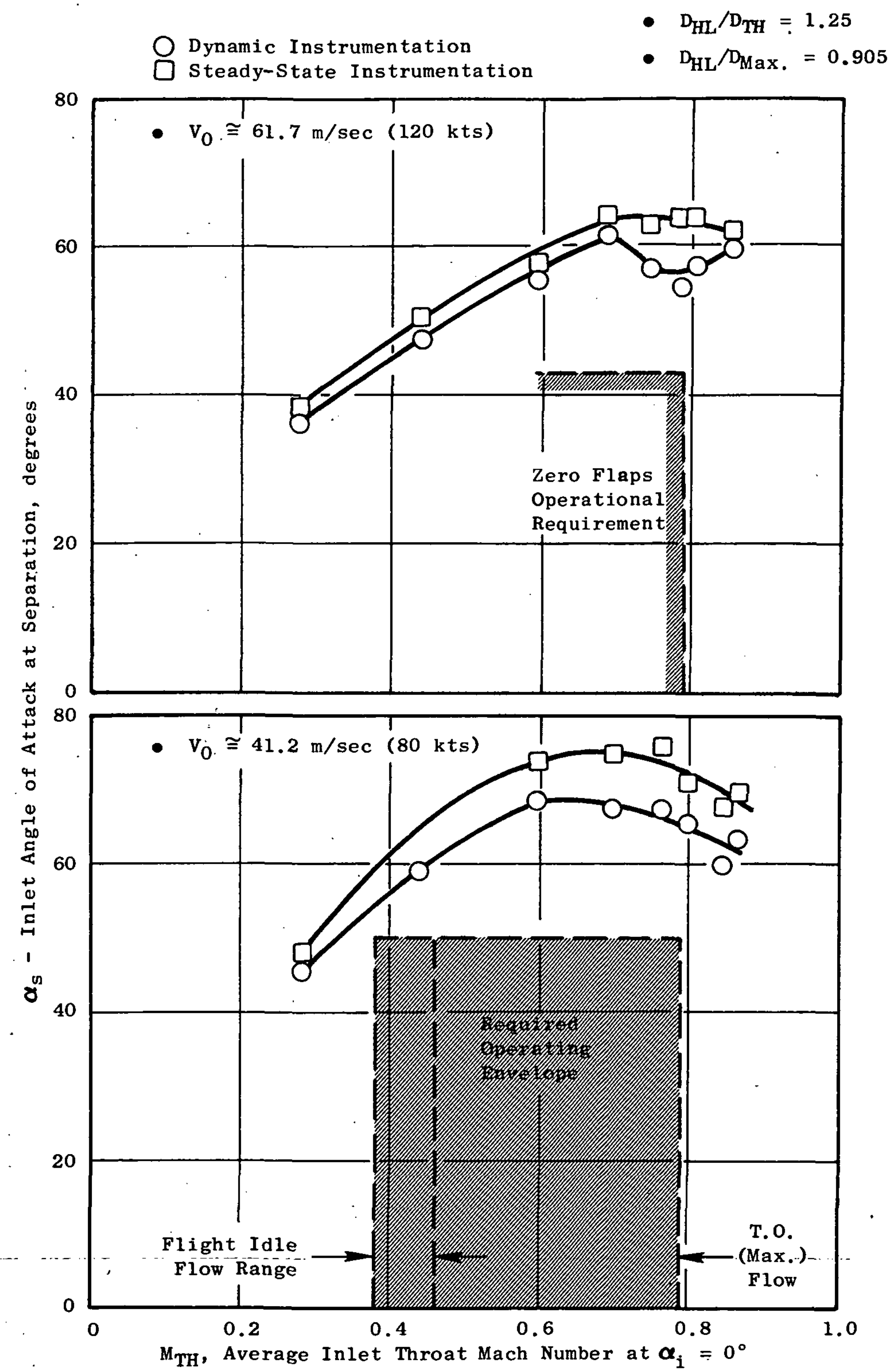

Figure 14. Inlet Separation Boundaries at Angle of Attack, Inlet No. 3.

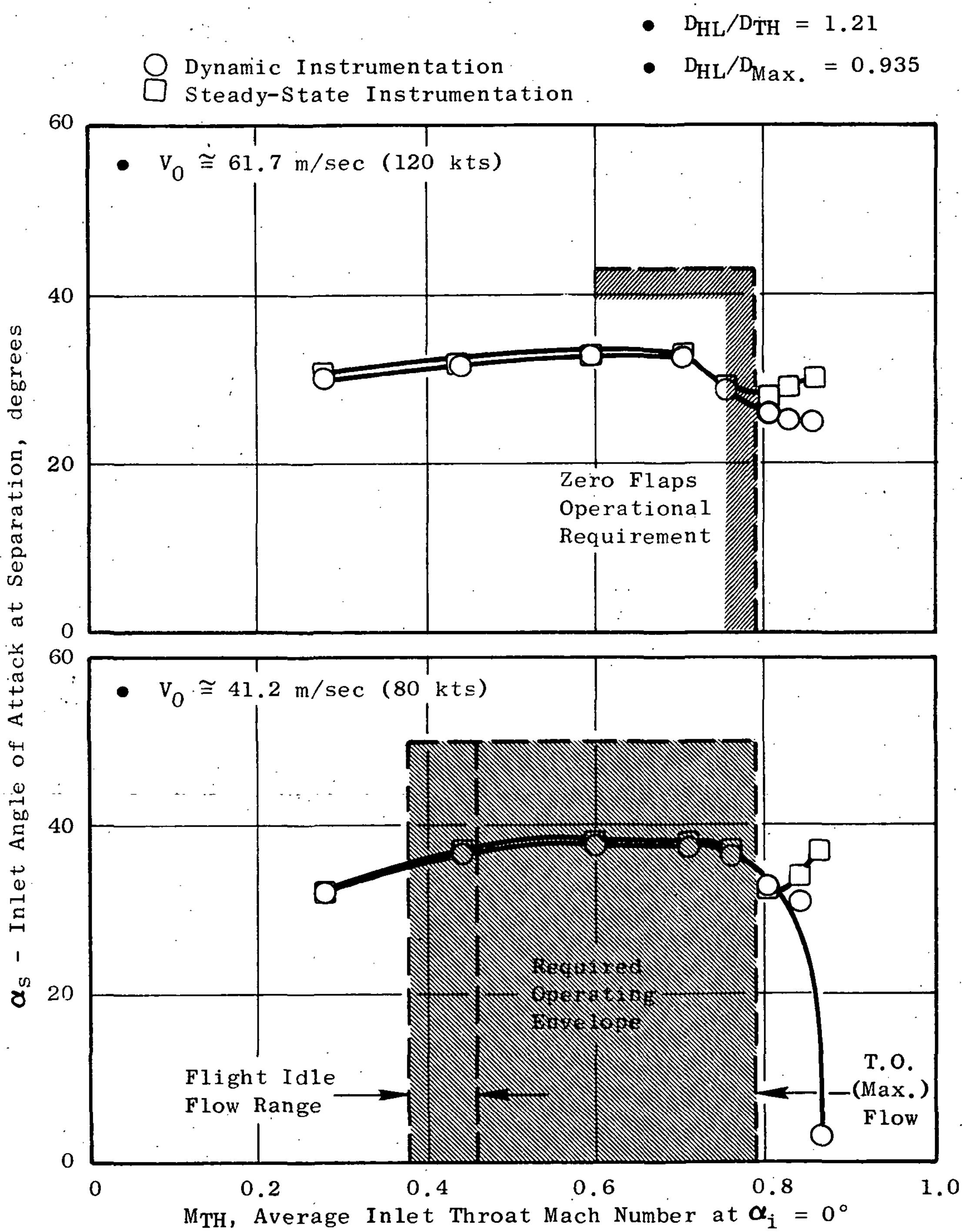

Figure 15. Inlet Separation Boundaries at Angle of Attack, Inlet No. 4.

Figures 12-15 show that the agreement between steady-state and dynamic separation indicators lessens as the internal lip contraction is increased, with the dynamic instrumentation always indicating separation first. The latter trend seems logical, but the variation with internal lip design is not understood.

The average throat Mach number at zero angle of attack has been used, in Figures 12-15 and elsewhere in the report, as a meaningful indicator of diffuser exit corrected flow for all angles of attack. This is because a constant $\Delta P/P$ was maintained, resulting in an approximately constant value of corrected weight flow as incidence angle was increased. Since the engine operates at constant corrected flow, the above method is appropriate.

Having examined the operating capability of each inlet, the inlet performance differences are the next concern. Figure 16 and 17 show steady-state total pressure recovery and distortion for all four inlets as a function of angle of attack at comparable, near-design throat Mach numbers and nominal flight speeds of 41.2 and 61.7 m/sec (80 and 120 kts). Again, the configurations pair off similarly to their operating capability trends. Inlet No. 3 is the best performer, with inlet No. 2 slightly worse. Inlet No. 4 is next, until separation occurs, beyond which inlet No. 1 becomes superior to inlet No. 4. These data show the beneficial effect of increasing internal lip contraction, even for unseparated flow operation, and also the importance of external lip design, as did the operating capability trends first seen in Figures 12-15. They also indicate that relatively efficient performance is attainable over the required angle-of-attack spectrum with either inlet No. 2 or No. 3. Inlet recovery is above 98% and distortion is below the target limit of 20%, even at the most stringent operating condition, 61.7 m/sec (120 kts) and 43°. (The 20% distortion limit is a typical General Electric preliminary design value established in lieu of demonstrated QCSEE capability at this early stage of the fan development program.)

Further perspective of the impact of internal lip design on distortion is given by the contour plots of Figures 18 and 19, which compare distorted areas and levels for inlets No. 1, 2 and 3 at flight speeds of 41.2 and 61.7 m/sec (80 and 120 kts), respectively. Each inlet is shown at zero angle of attack and near the maximum required angle of attack for comparable corrected flow demand. (In these two figures only, the actual throat Mach number calculated at angle of attack is shown, but an approximately constant corrected flow demand is represented for each inlet, except as noted for inlet No. 1 at 61.7 m/sec (120 kts), between zero and the higher angle of attack, so the zero angle-of-attack M_{TH} value in the top row is indicative of corrected airflow demand.) These plots show a dramatic change in extent of the distorted region as internal lip diameter ratio is changed, and further confirm the unacceptability of inlet No. 1. While the QCSEE fan stability margin allocation had not been finalized at the time of inlet selection, it is felt that inlet No. 2's most extreme distortion characteristics at 61.7 m/sec (120 kts), 43°, should be compatible with unstalled engine operation.

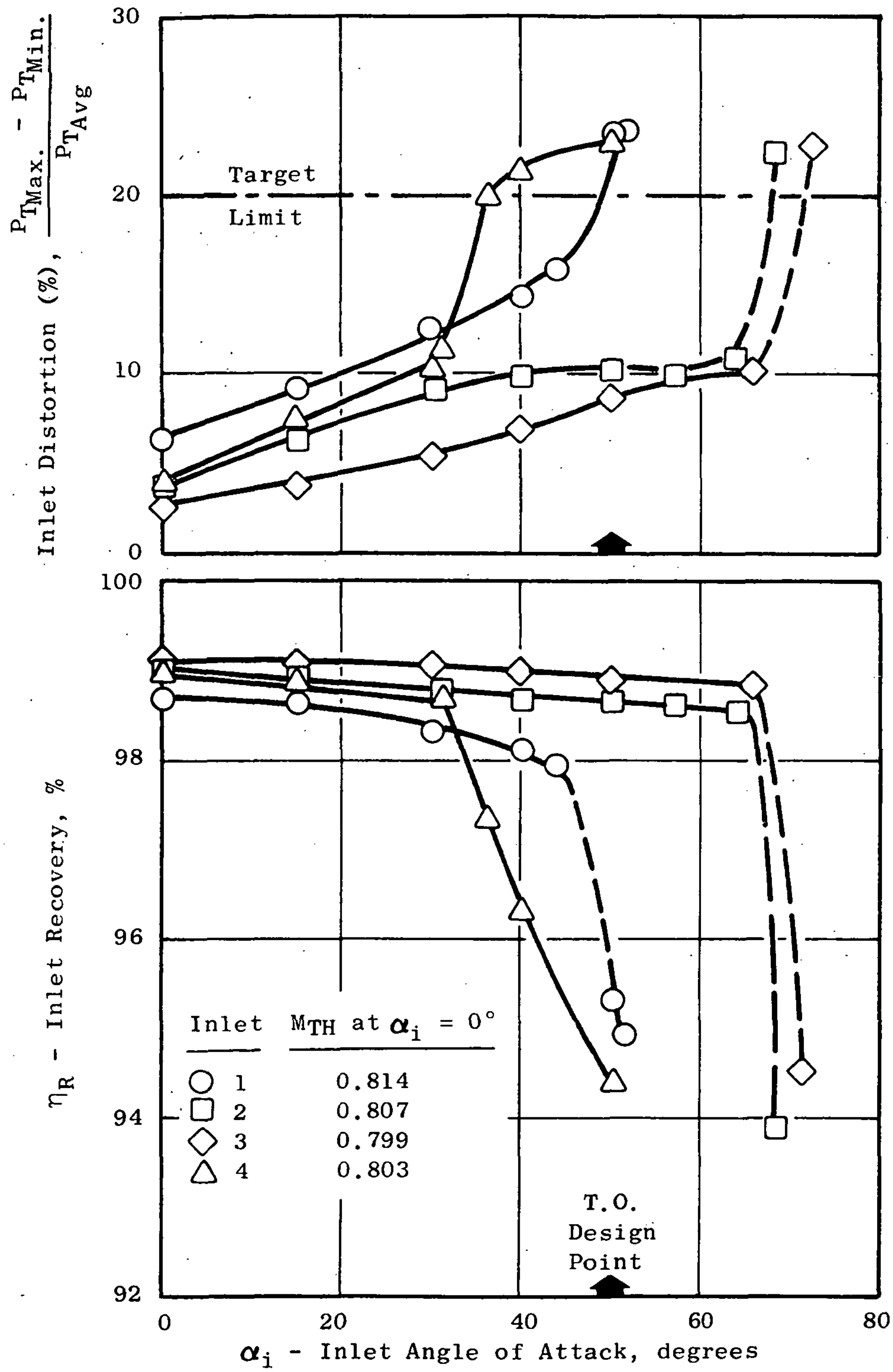

Figure 16. Inlet Performance Comparison at Angle of Attack, $V_0 \cong 41.2$ m/sec (80 kts).

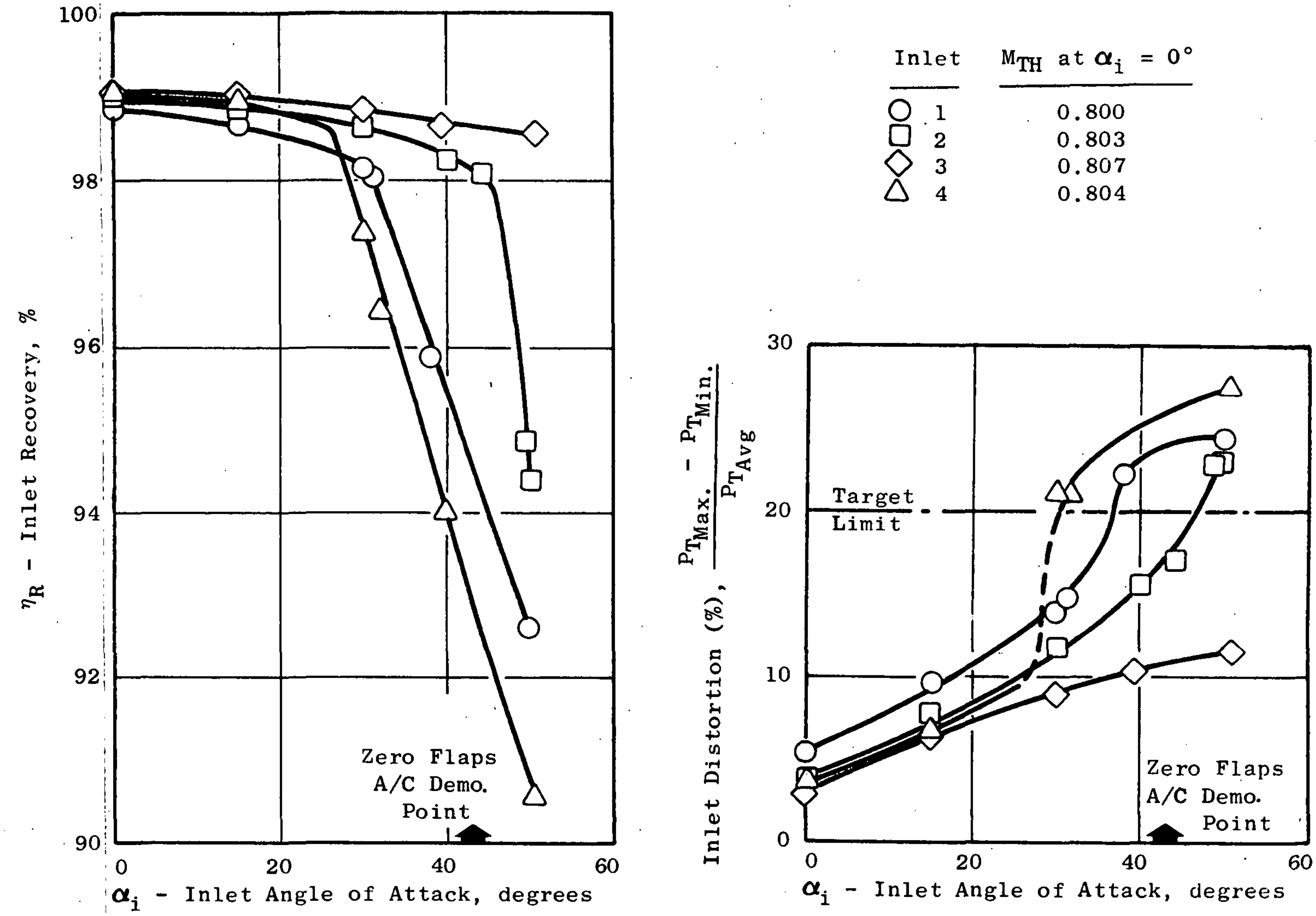

Figure 17. Inlet Performance Comparison at Angle of Attack, $V_0 \cong 61.7$ m/sec (120 kts).

- $\Delta P/P$ is Distortion Parameter
- Contour Values are P_T/P_{T_O}

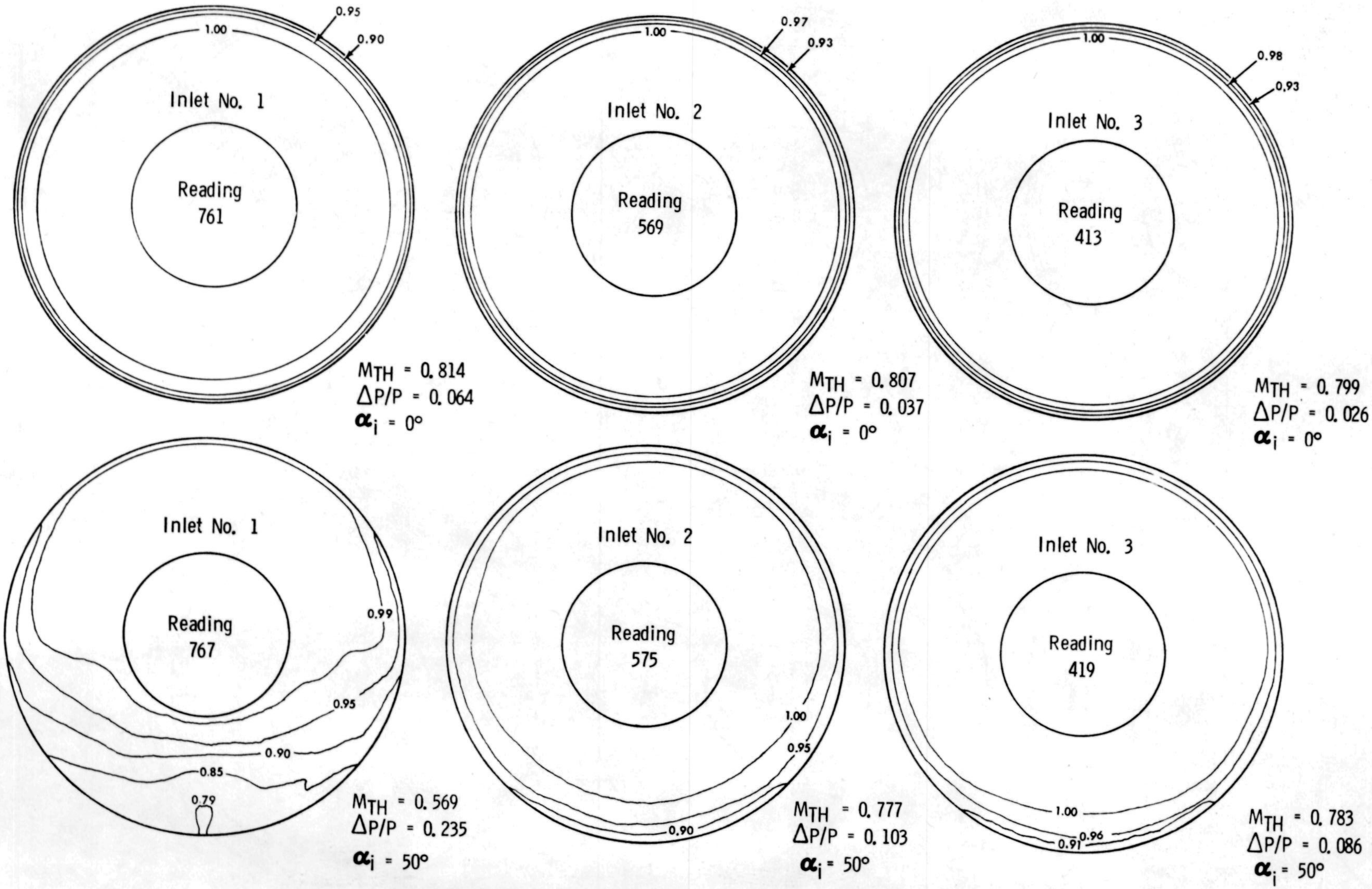

Figure 18. Fan Face Distortion Contour Comparison, $V_o \cong 41.2$ m/sec (80 kts).

- Contour Values are P_T/P_{T_O}
- $\Delta P/P$ is Distortion Parameter

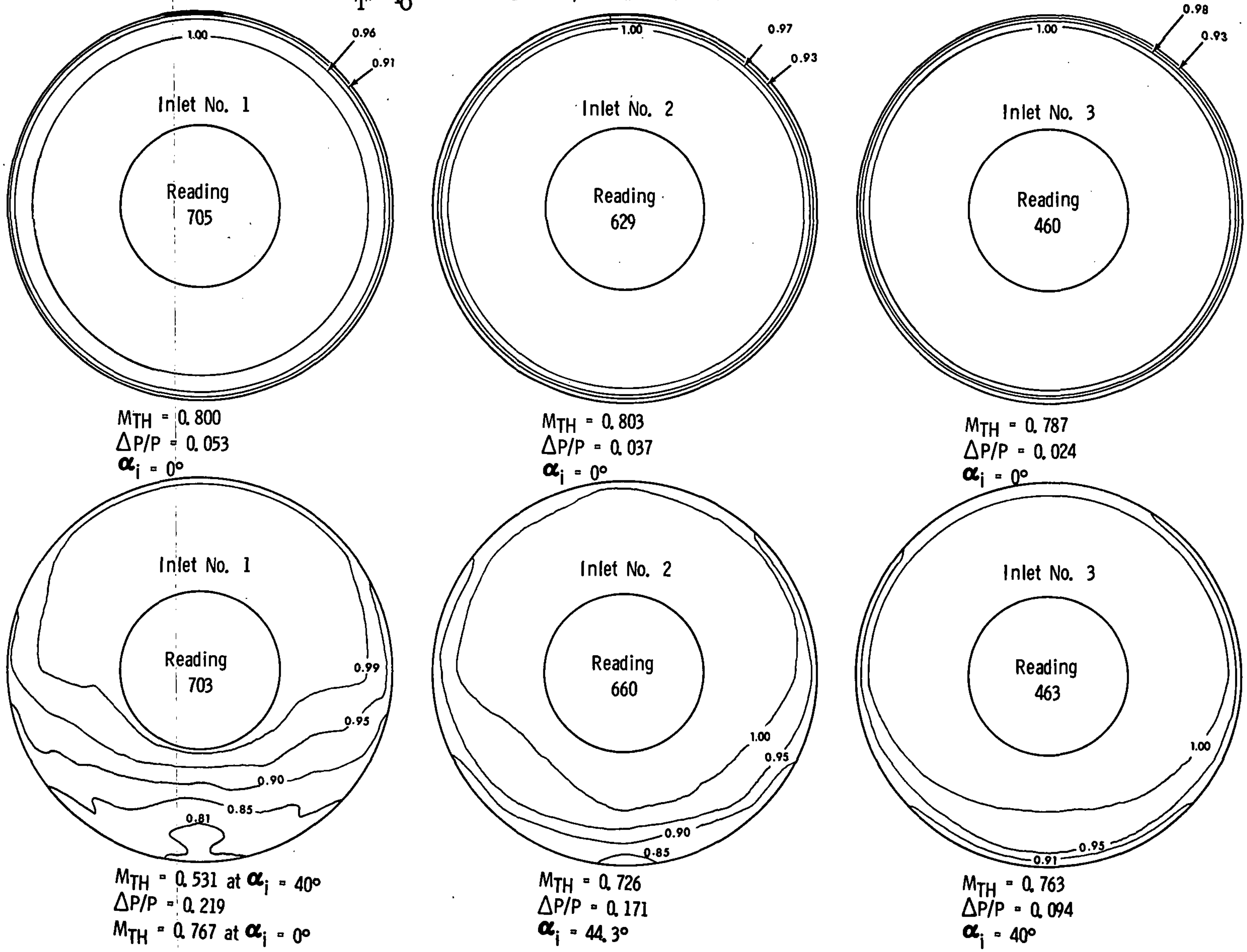

Figure 19. Fan Face Distortion Contour Comparison, $V_o \cong 61.7$ m/sec (120 kts).

Distortion characteristics measured at the middiffuser Kulite rake station are compared in Figures 20-23 to some of the diffuser exit data of Figures 16 and 17. Both steady-state and dynamic distortion trends are shown for the Kulite measurements; the latter characteristics were obtained by filtering the data at an actual frequency of 500 Hz, or the scaled equivalent of about 60-75% of fan rotor frequency for the QCSEE engines. These plots show that the middiffuser and diffuser exit steady-state distortion levels are comparable, with the former a bit higher at high angles of attack. Slight difference in probe immersion depths (Figures 7 and 9), as well as rake axial location, is believed responsible. Dynamic distortion levels are generally 1-1/2 to 2 times as great as steady-state distortions, except for low steady-state values, which is consistent with results of other test programs representing a variety of intake systems. Steady-state distortion for inlet No. 1 at 41.2 m/sec (80 kts), Figure 20, is slightly in excess of the 20% target limit; distortion at 61.7 m/sec (120 kts) (not shown here) is prohibitively high, especially when the extent of the low pressure region (shown in Figures 18 and 19) is considered. Comparable data for inlet No. 2 at both 41.2 m/sec (80 kts), Figure 21, and 61.7 m/sec (120 kts), Figure 22, are within the 20% target limit. Performance of inlet No. 3, again achieved at the expense of a larger nacelle, is even better, as shown in Figure 23 for 41.2 m/sec (80 kts).

After evaluation of the foregoing results, the lip design of inlet No. 2 (1.21 D_{HL}/D_{TH}, 0.905 $D_{HL}/D_{Max.}$) was selected for the bottom contour for future QCSEE inlet evaluation programs. Basis for this decision was its satisfaction of all design constraints within the smallest possible inlet diameter. If a future modification appears warranted, for some presently unforeseen reason, acquisition of the inlet No. 3 data will allow such a change to be made with confidence.

7.2 SELECTION OF SIDE INLET CONTOUR

Since an internal lip diameter ratio, D_{HL}/D_{TH}, of 1.17 was tentatively selected for the QCSEE preliminary design nacelle, this discussion will be restricted to inlets No. 1 and No. 2. Figure 24 presents a performance comparison of these two designs operating in a 18.0 m/sec (35 kts), 90° crosswind; recovery and distortion are shown as a function of throat Mach number at zero inlet incidence, as discussed in Section 7.1. Both inlets experienced flow separation at low power settings near ground idle, a phenomenon that has been noted previously for other inlets of lower internal lip contraction ratio and at reduced crosswind velocities. However, as evidenced by the abrupt improvements in performance, this low throat Mach separation clears at a much lower power setting for inlet No. 2 than for inlet No. 1, due to the fuller nose curvature of the former. In addition, the performance of inlet No. 1 slightly above the 0.79 design throat Mach number deteriorates rapidly, relative to that of inlet No. 2. These two factors, together with the superior performance of inlet No. 2 over a broad power setting range, suggest that the side inlet internal diameter ratio should be increased from its preliminary value of 1.17. Comparison of distortion contours in Figure 25

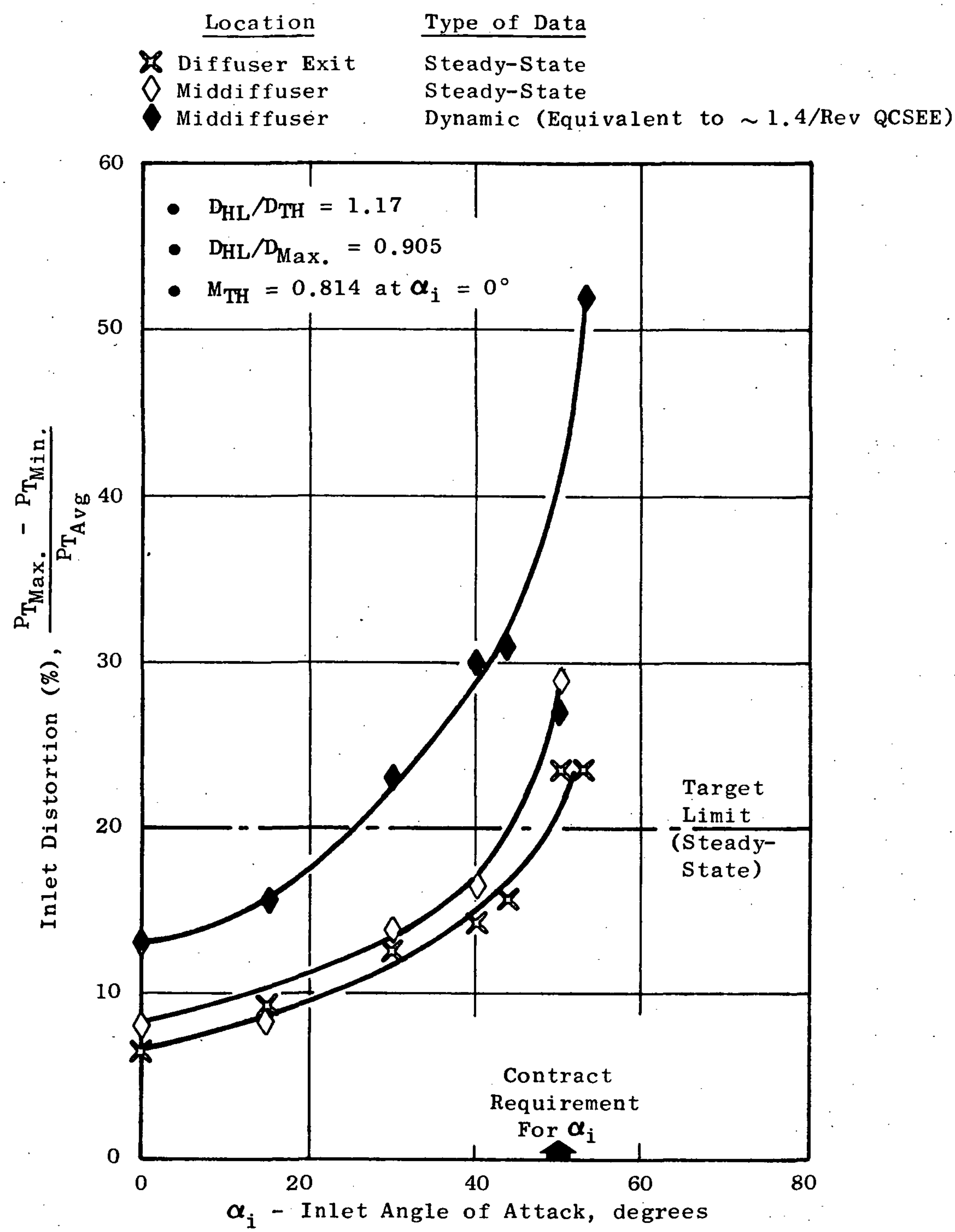

Figure 20. Comparison of Steady-State and Dynamic Distortion Levels, Inlet No. 1, $V_0 \cong 41.2$ m/sec (80 kts).

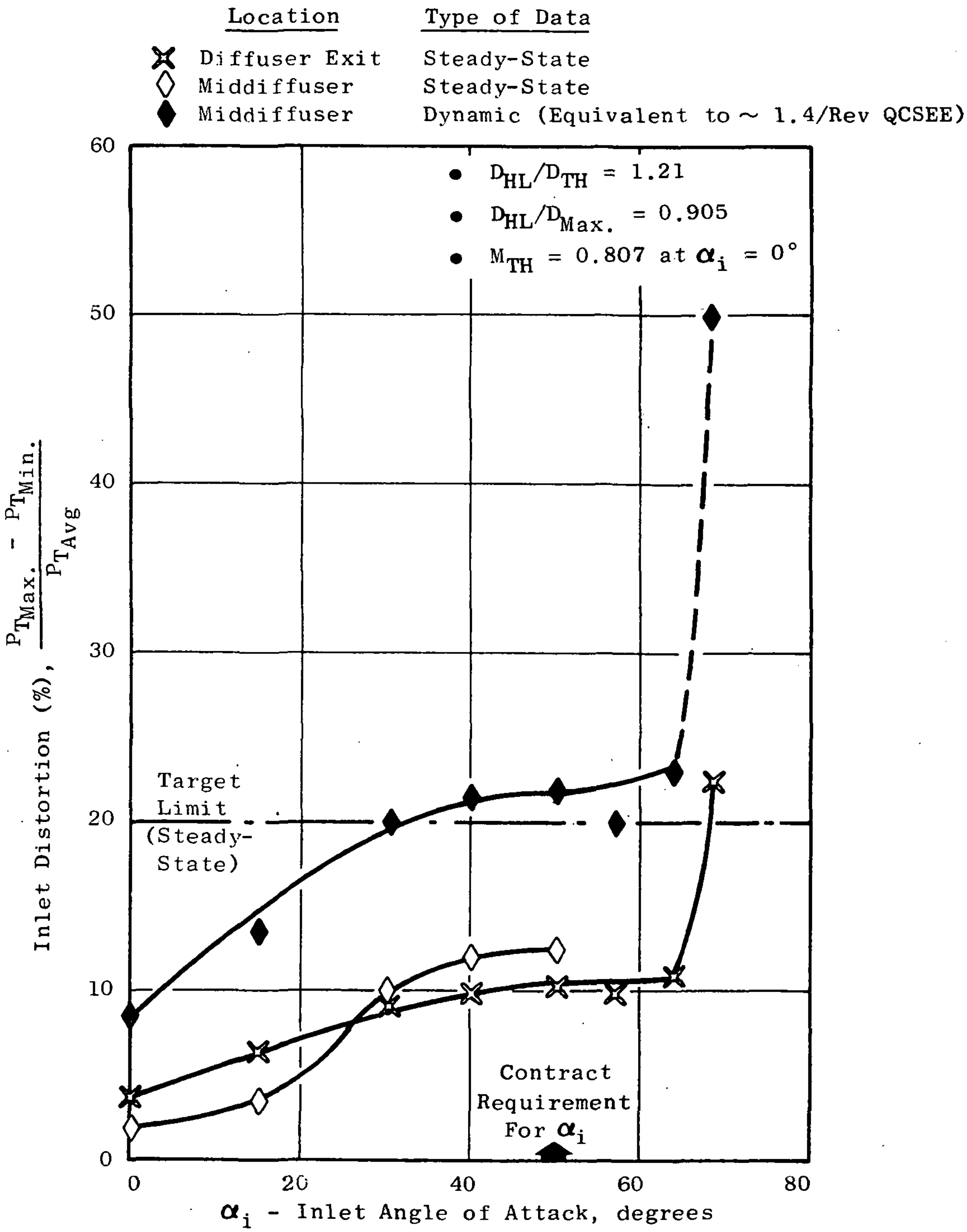

Figure 21. Comparison of Steady-State and Dynamic Distortion Levels, Inlet No. 2, $V_0 \cong 41.2$ m/sec (80 kts).

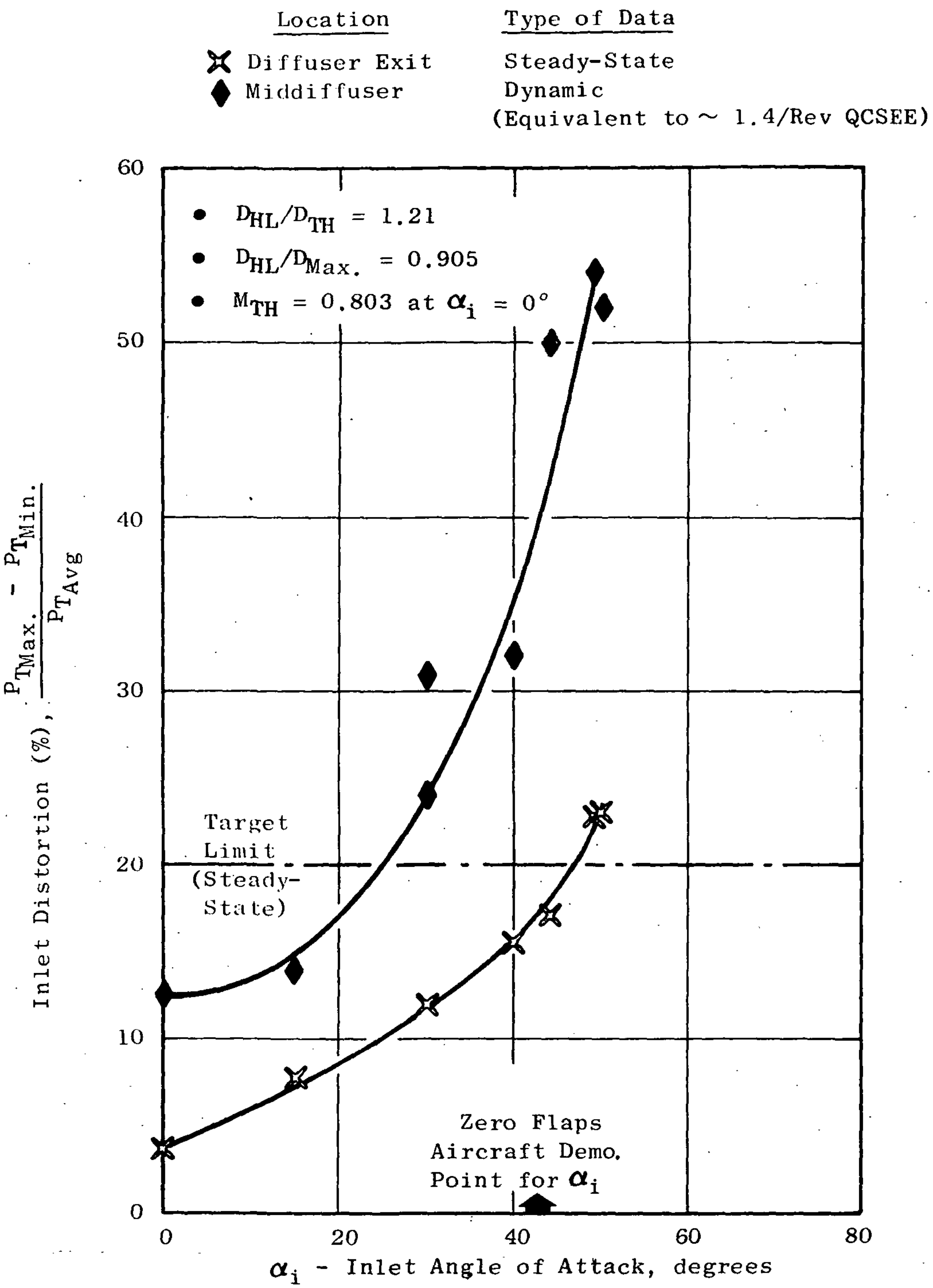

Figure 22. Comparison of Steady-State and Dynamic Distortion Levels, Inlet No. 2, $V_0 \cong 61.7$ m/sec (120 kts).

- $D_{HL}/D_{TH} = 1.25$
- $D_{HL}/D_{Max.} = 0.905$
- $M_{TH} = 0.799$ at $\alpha_i = 0°$

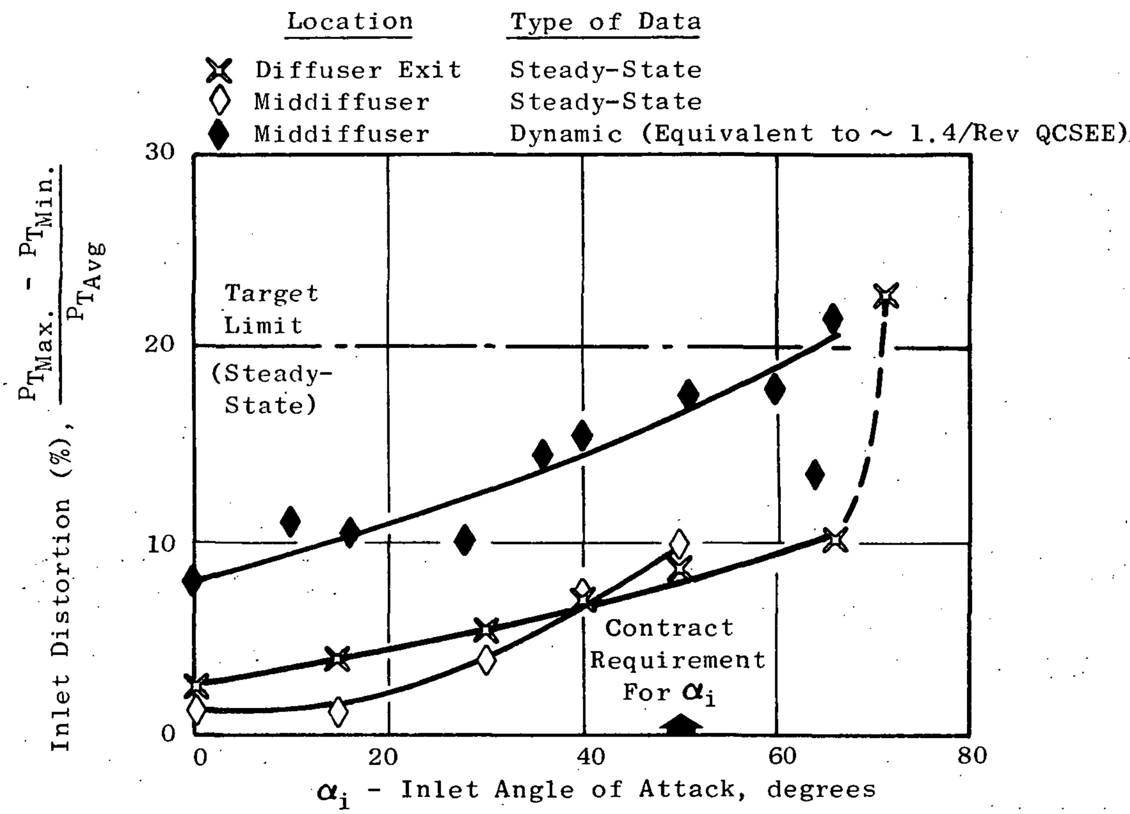

Figure 23. Comparison of Steady-State and Dynamic Distortion Levels, Inlet No. 3, $V_0 \cong 41.2$ m/sec (80 kts).

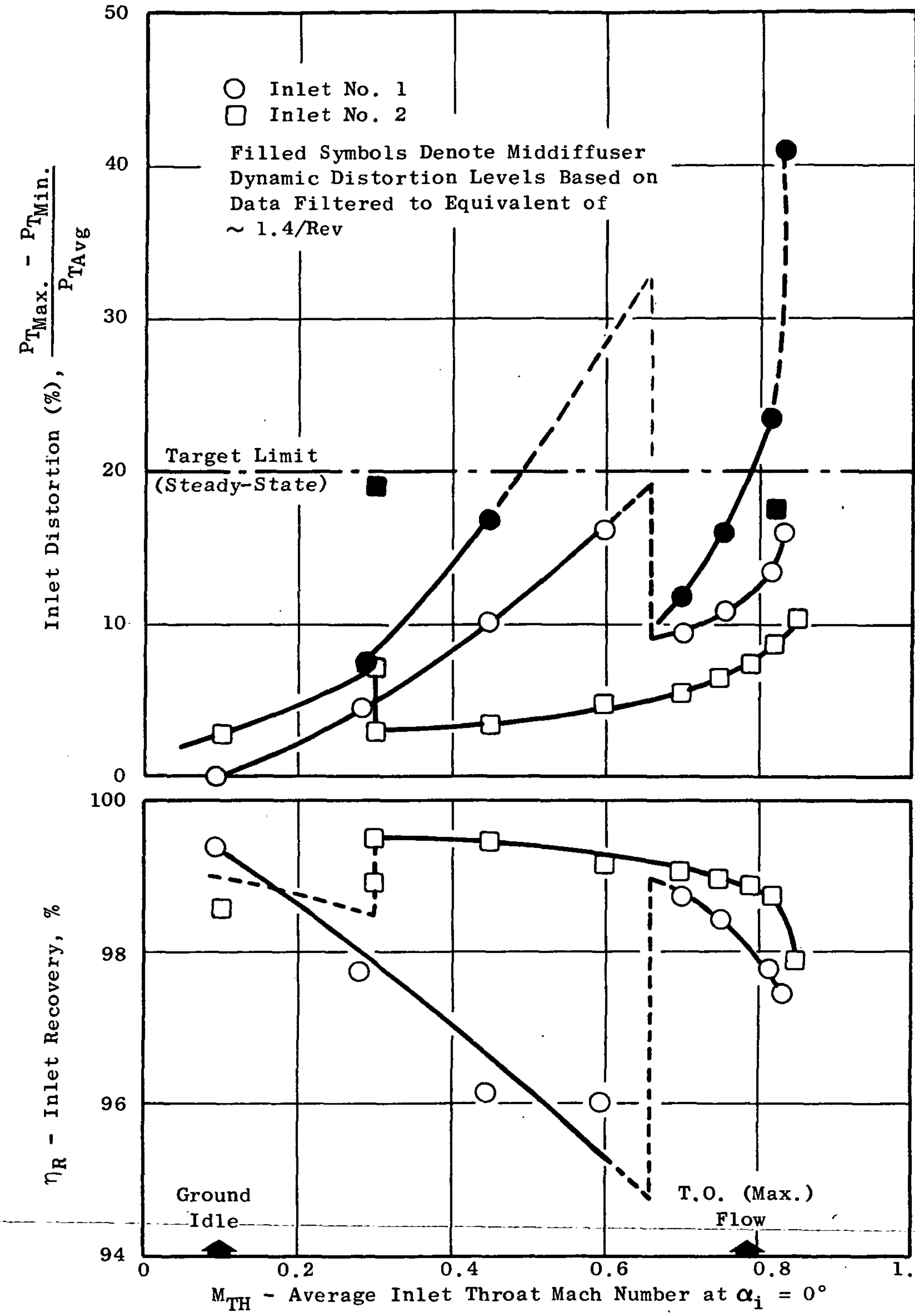

Figure 24. Inlet Performance Comparison in 90°, 18.0 m/sec (35 kts) Crosswind.

- $\Delta P/P$ is Distortion Parameter
- Contour Values are P_T/P_{T_O}

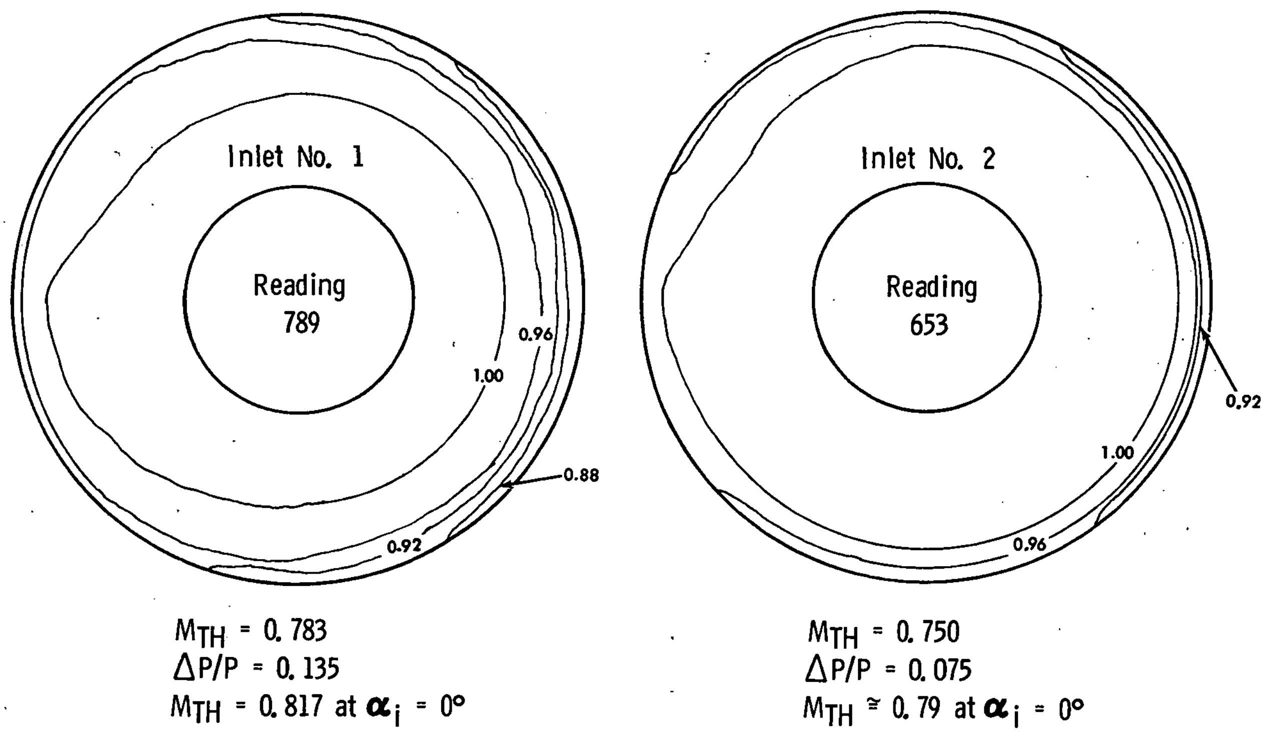

Figure 25. Fan Face Distortion Comparison, 18.0 m/sec (35 kts), 90° Crosswind.

supports this view, as inlet No. 1 is seen to suffer a larger area of low pressure than inlet No. 2 at comparable crosswind operating conditions.

It might be contended that a D_{HL}/D_{TH} intermediate between the 1.17 and 1.21 designs tested would suffice. However, it is felt that, with flow separation an inherently discontinuous phenomenon, such a selection could not be made with the desired confidence. In any event, the savings in nacelle size would be minor. Consequently, the 1.21 D_{HL}/D_{TH}, 0.905 $D_{HL}/D_{Max.}$ design was also selected for the side contour.

7.3 SELECTION OF TOP INLET CONTOUR

The only operating situation that might conceivably produce a flow incidence pattern impacting the top inlet contour selection is climb with an engine out. This would produce a very low mass-flow ratio for that inlet, resulting in extreme prediffusion of the "captured" streamtube and high local incidence near the top of the inlet. Depending upon the specific aircraft characteristics, this might necessitate a lower external diameter ratio, $D_{HL}/D_{Max.}$, to prevent local flow separation and minimize nacelle drag to improve aircraft performance in this demanding situation. The increased external cowl "thickness", $R_{Max.}/R_{HL}$, would demand a corresponding reduction in internal lip diameter ratio, relative to a symmetric 1.21 design. While such a design is feasible, since an internal lip diameter ratio of 1.12-1.13 has been found adequate for high throat Mach number CTOL designs such as current wide-body aircraft, it would necessitate a more complex and expensive asymmetric inlet.

McDonnell-Douglas evaluated this situation for the YC-15 configuration and concluded that a symmetric inlet, of the proportions selected for the bottom and side contours, would be adequate.

Since the top inlet forebody contour also affects cruise drag, McDonnell-Douglas estimated the excess cruise drag associated with an axisymmetric inlet configuration and found it to be small.

In view of these results, and also because the complexity required to vary lip design over only the top half of the inlet did not seem to justify the modest local envelope reductions possible, a circumferentially uniform inlet lip was selected. This decision also was consistent with consideration of relative acoustic performance measurements that were made (Reference 2).

7.4 ADDITIONAL INLET PERFORMANCE CHARACTERISTICS

Adoption of a symmetric inlet lip, like that of inlet No. 2, allows presentation of additional data representative of the future QCSEE inlet, except for effects of a minor change in diffuser design and a different spinner design, as mentioned in Section 4.2. Included are measured wall Mach number gradients that were employed to select the approximate axial location of the static pressure tap for the throat Mach number control.

Additional performance trends are shown in Figures 26-28. Figure 26 presents inlet recovery as a function of angle of attack for 41.2 m/sec (80 kts) and three throat Mach numbers, ranging from approximately flight idle to well beyond the 0.79 design value. Excellent performance is apparent in all cases, with recoveries in excess of 98% even at 50° angle of attack and near-choking airflow. Figure 27 shows static inlet recovery for simulated QCSEE fan blade passing frequencies (5kHz for OTW, 8kHz for UTW) investigated. Figure 28 gives recovery and distortion at 41.2 m/sec (80 kts) for 0° and 50° angles of attack. While they also demonstrate the excellent performance trends, these plots illustrate the precipitous degradation that occurs as the limiting flow is reached, somewhat beyond the design point and practical operating range. In addition, a decrease in calculated throat Mach number with increasing flow demand is exhibited at this point. Such double-valued behavior would preclude satisfactory control operation in this region. However, experience indicates that the limiting average throat Mach number can be expected to increase with inlet scale, due to relatively thinner throat boundary layer blockage and correspondingly higher throat flow coefficient. This trait will be examined in the upcoming 50.8 centimeter (20 inch) diameter inlet test at NASA-Lewis and eventually on the QCSEE engine.

The sensitivity of inlet acoustic suppression resulting from flow acceleration to inlet throat Mach number, or corrected flow, and the desire to avoid inlet instability and/or choking at above-design throat Mach numbers necessitate an accurate engine flow control. The variable area fan nozzle of the QCSEE engines requires a positive, closed-loop control system to accomplish this task. Accordingly, an active inlet throat Mach number control scheme has been devised that will sense an inlet wall static pressure and the freestream stagnation pressure and relate their ratio to average throat Mach number via data to be acquired in the 50.8 centimeter (20 inch) diameter inlet test. It is anticipated that desired throat Mach number settings from 0.50 to somewhat beyond the 0.79 design value will be available with this system.

Information pertaining to design of the throat Mach number control is shown in Figures 29-34, which contain measured axial wall Mach number gradients for a variety of flight conditions. Figures 29-31 are for level flight at 41.2 m/sec (80 kts) and a range of throat Mach numbers, to show the wall Mach number sensitivity at various axial positions. Inviscid analytical flowfield predictions obtained from the Streamtube Curvature computer program (Reference 6) were made for the design point throat Mach number of 0.79 and are shown to be in substantial agreement with the corresponding test results in Figure 30. Figures 32-34 show similar data for several high incidence situations. Data for both top and bottom contours are presented, to illustrate the relatively short length required for the flow to redistribute and become circumferentially uniform. Consideration of these data has resulted in a tentative static pressure location at X/L between 0.30 and 0.40 on the side contours of the inlet, subject to 50.8 centimeter (20 inch) inlet test results. Such a location is felt to balance the conflicting desires for sensitivity to flow changes (more forward location) and insensitivity to flow incidence (more aft location).

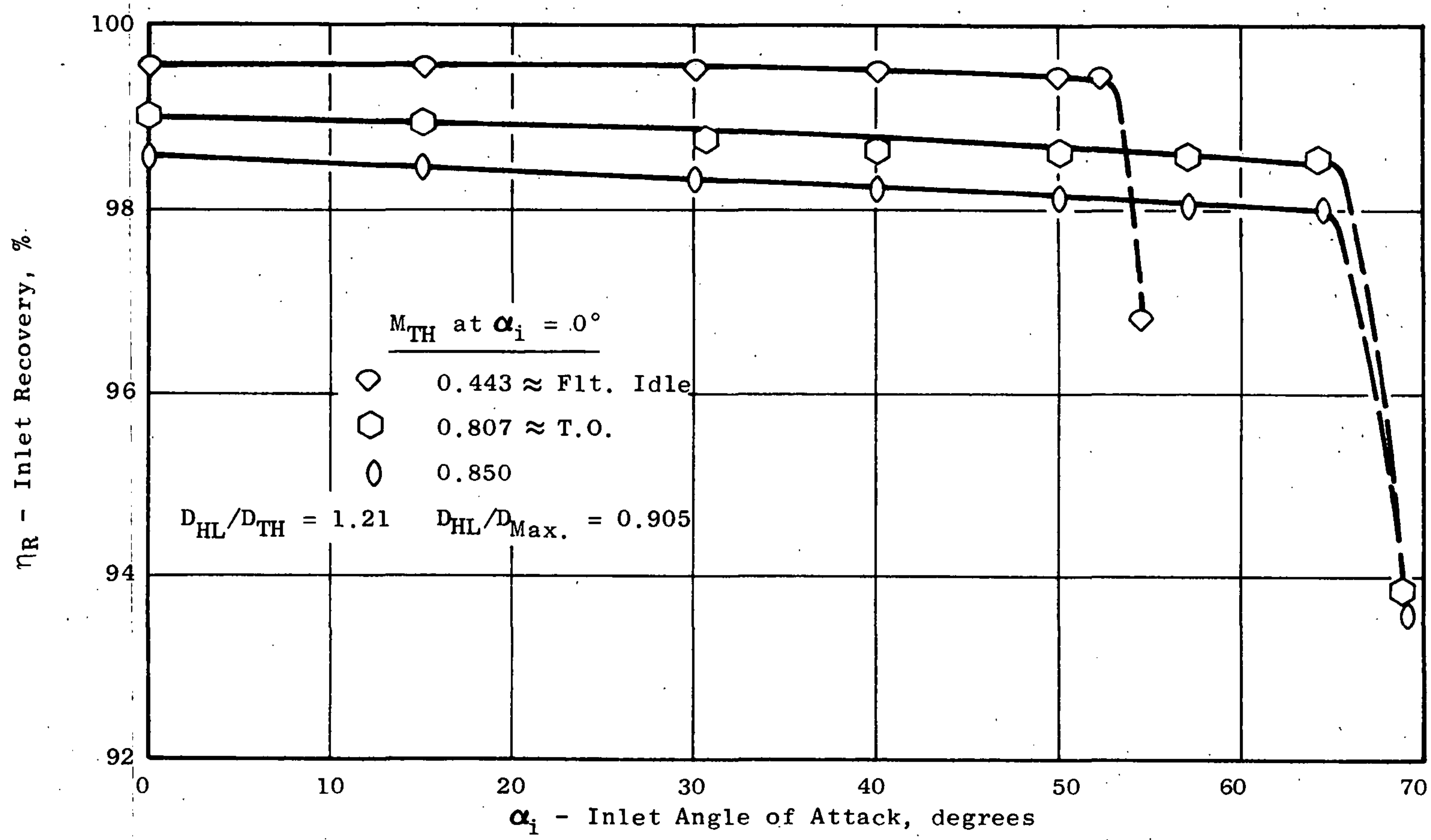

Figure 26. Inlet Recovery - Angle of Attack Characteristics, Inlet No. 2, $V_0 \cong 41.2$ m/sec (80 kts).

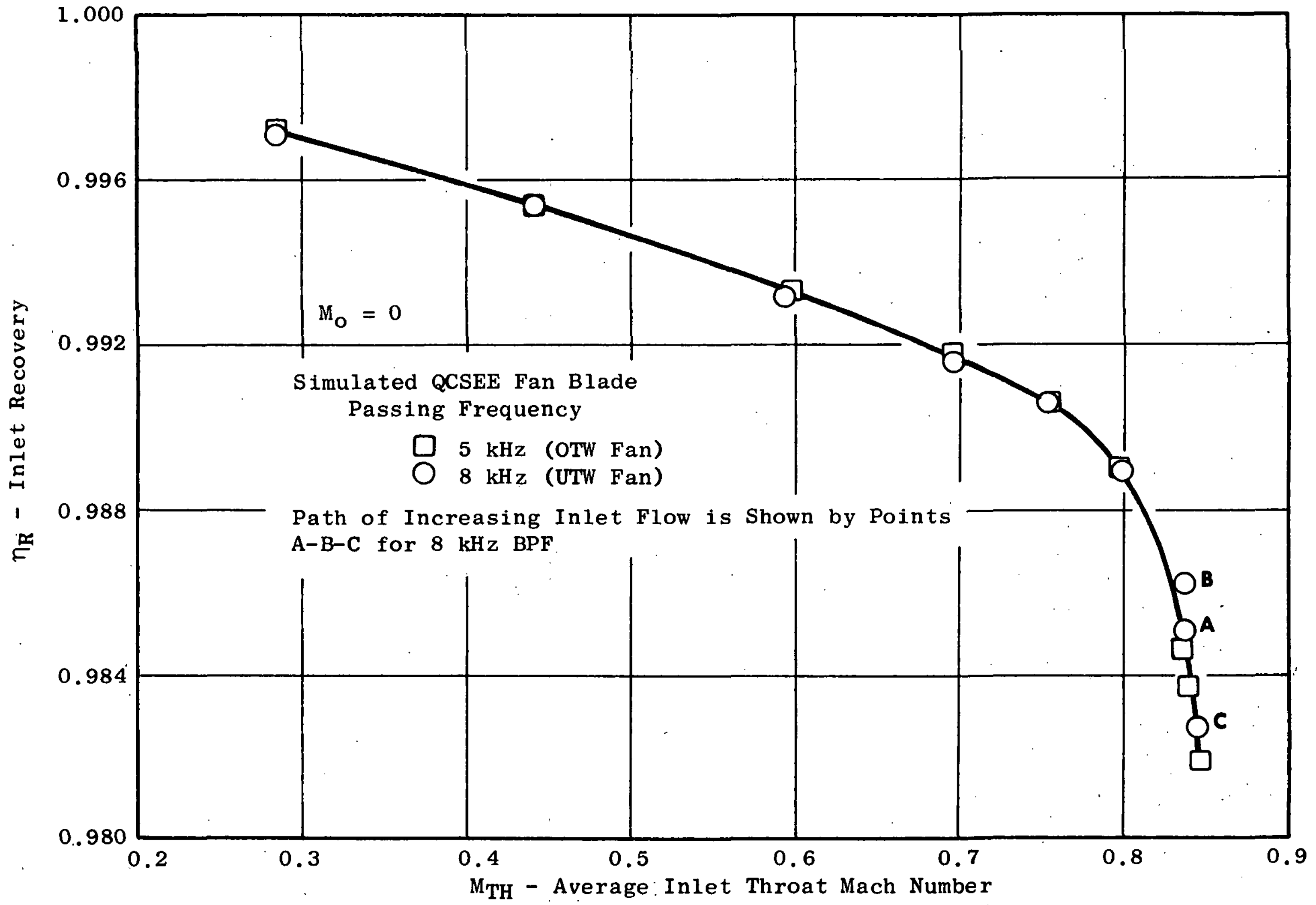

Figure 27. Static Inlet Recovery Characteristics, Inlet No. 2.

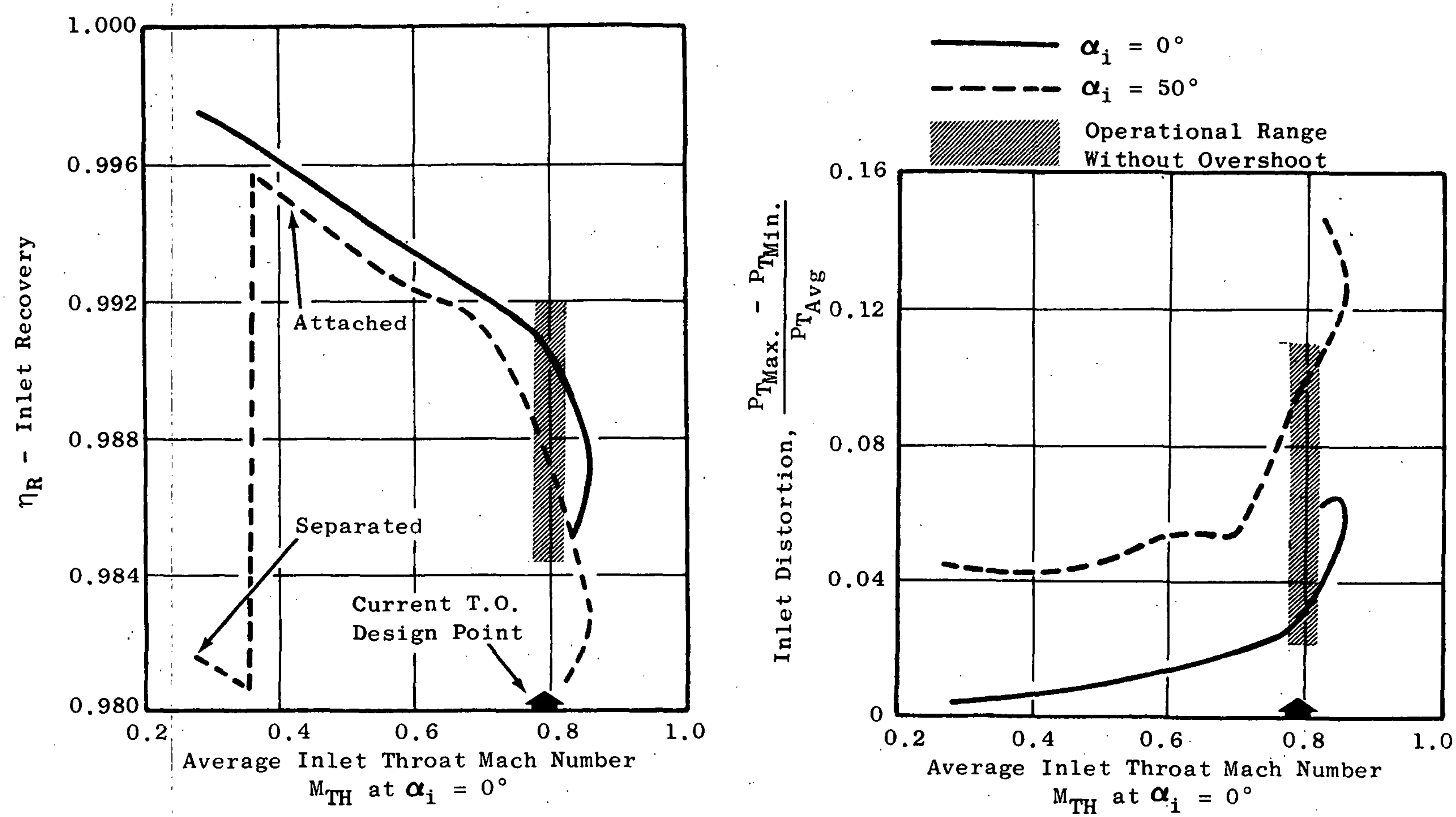

Figure 28. Inlet No. 2 Performance at $V_0 \cong 41.2$ m/sec (80 kts).

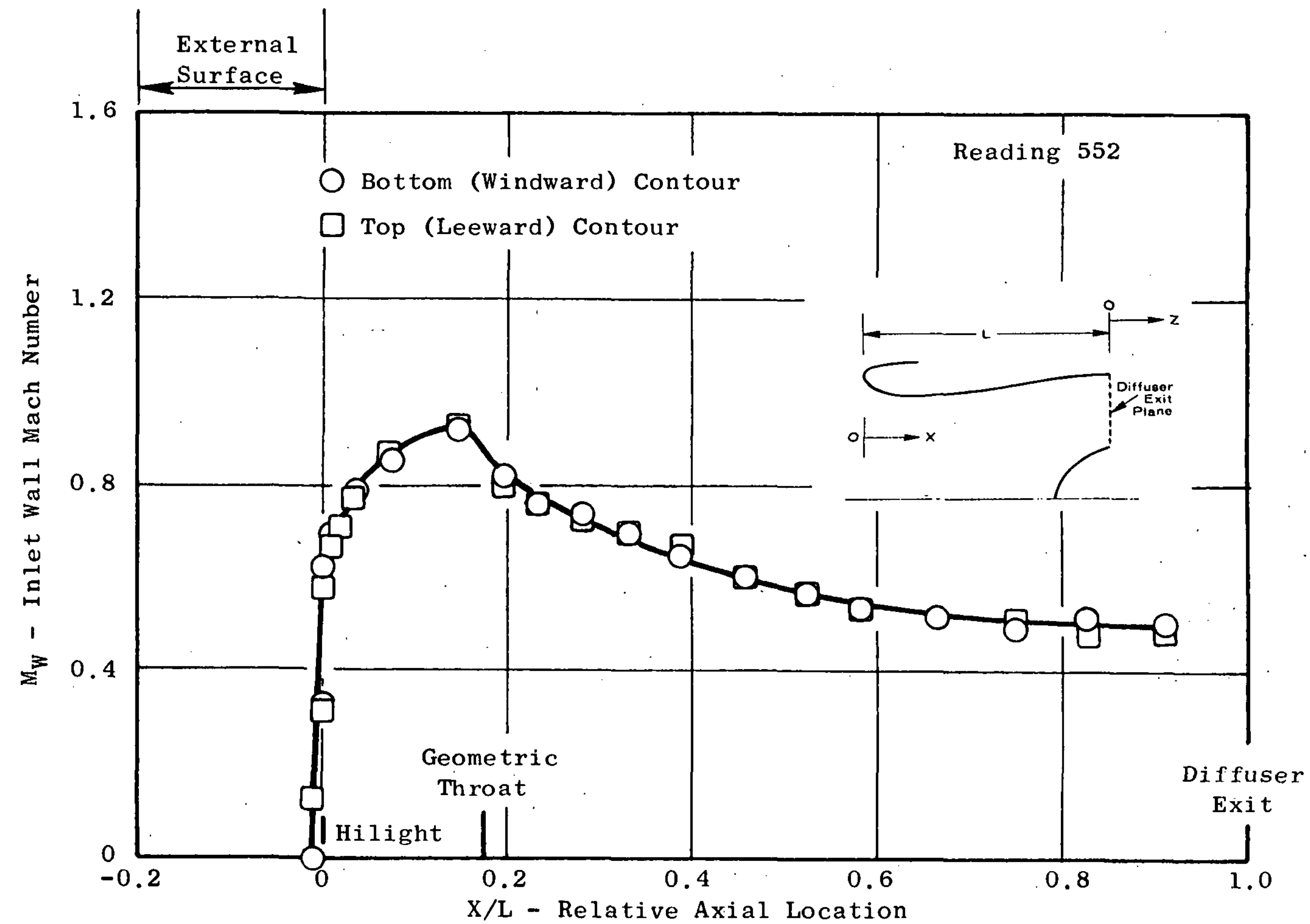

Figure 29. Wall Mach Number Axial Gradient, Inlet No. 2, $V_0 \cong 41.2$ m/sec (80 kts), $\alpha_i = 0°$, $M_{TH} = 0.709$.

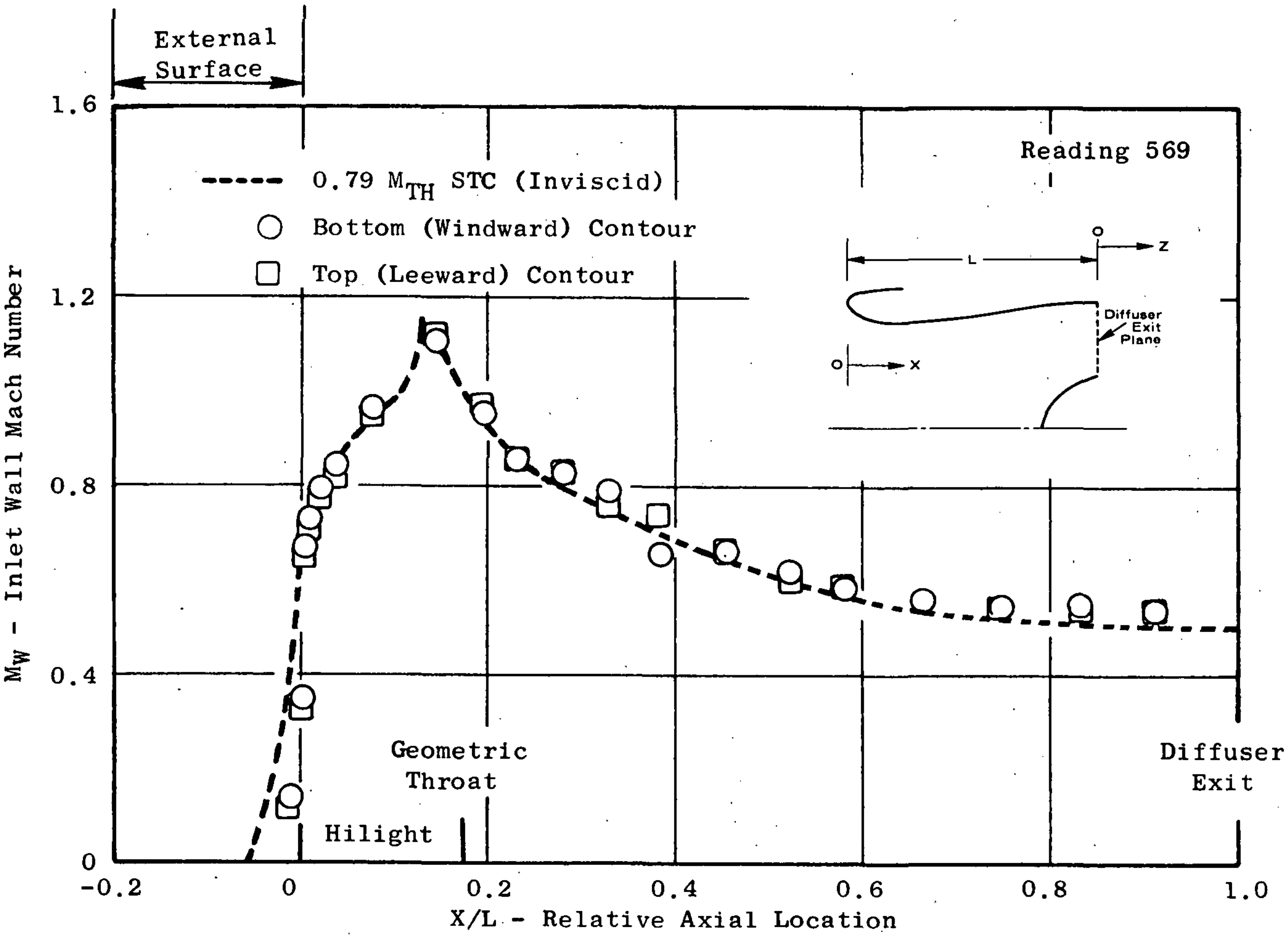

Figure 30. Wall Mach Number Axial Gradient, Inlet No. 2, $V_0 \cong 41.2$ m/sec (80 kts), $\alpha_i = 0°$, $M_{TH} = 0.807$.

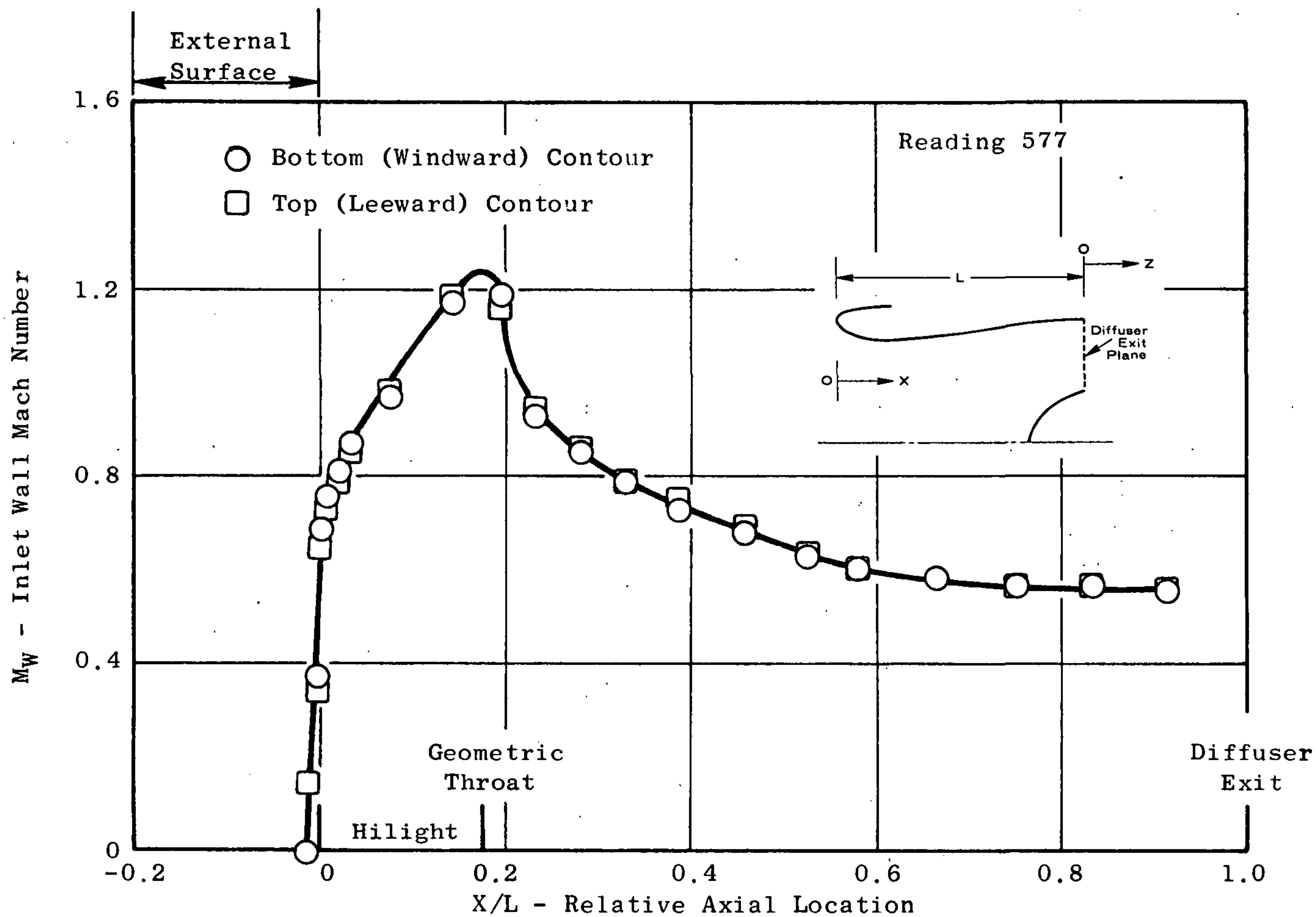

Figure 31. Wall Mach Number Axial Gradient, Inlet No. 2, $V_0 \cong 41.2$ m/sec (80 kts), $\alpha_i = 0°$, $M_{TH} = 0.857$.

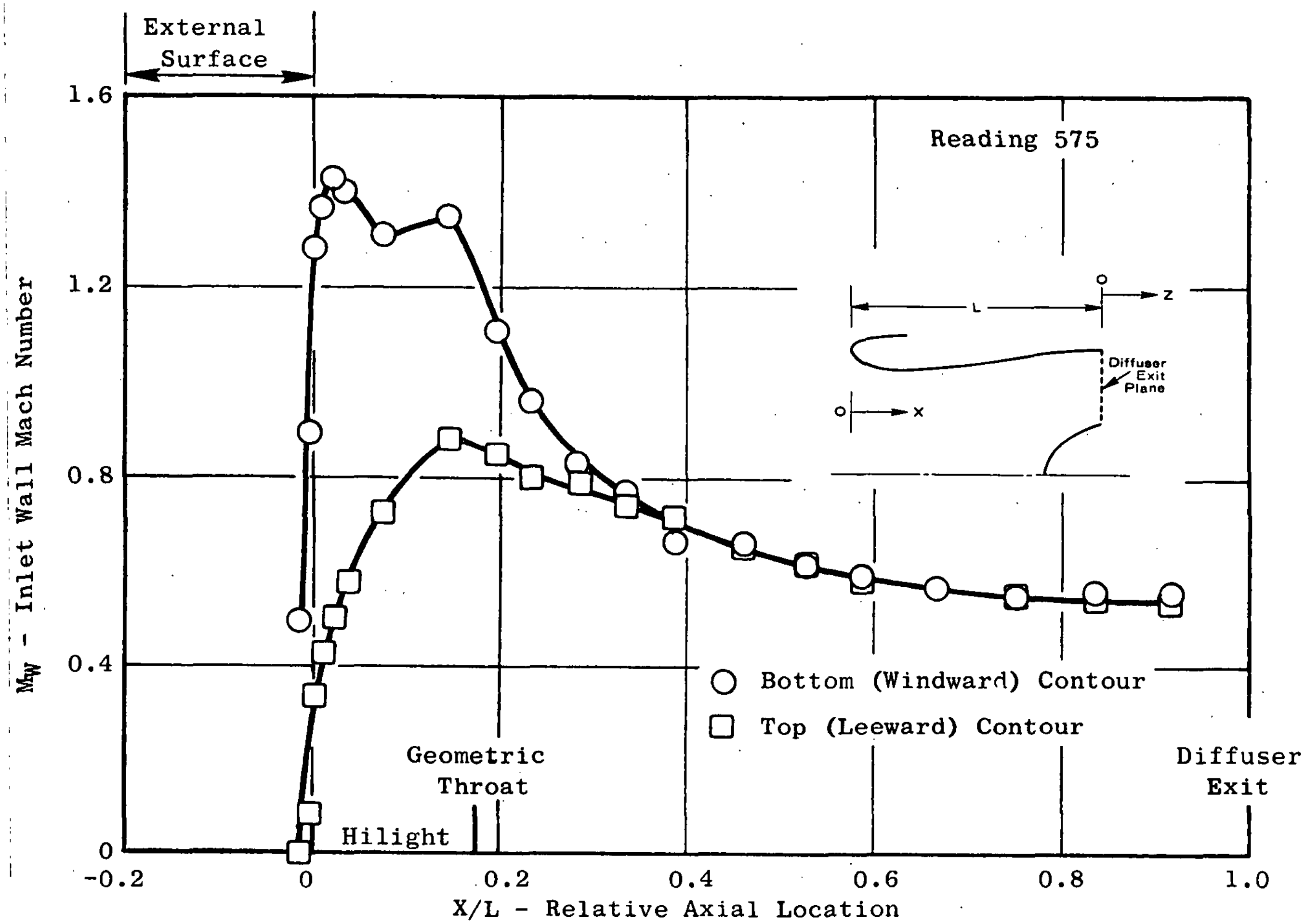

Figure 32. Wall Mach Number Axial Gradient, Inlet No. 2, $V_0 \cong 41.2$ m/sec (80 kts), $\alpha_i = 50.1°$, $M_{TH} = 0.807$ at $\alpha_i = 0°$.

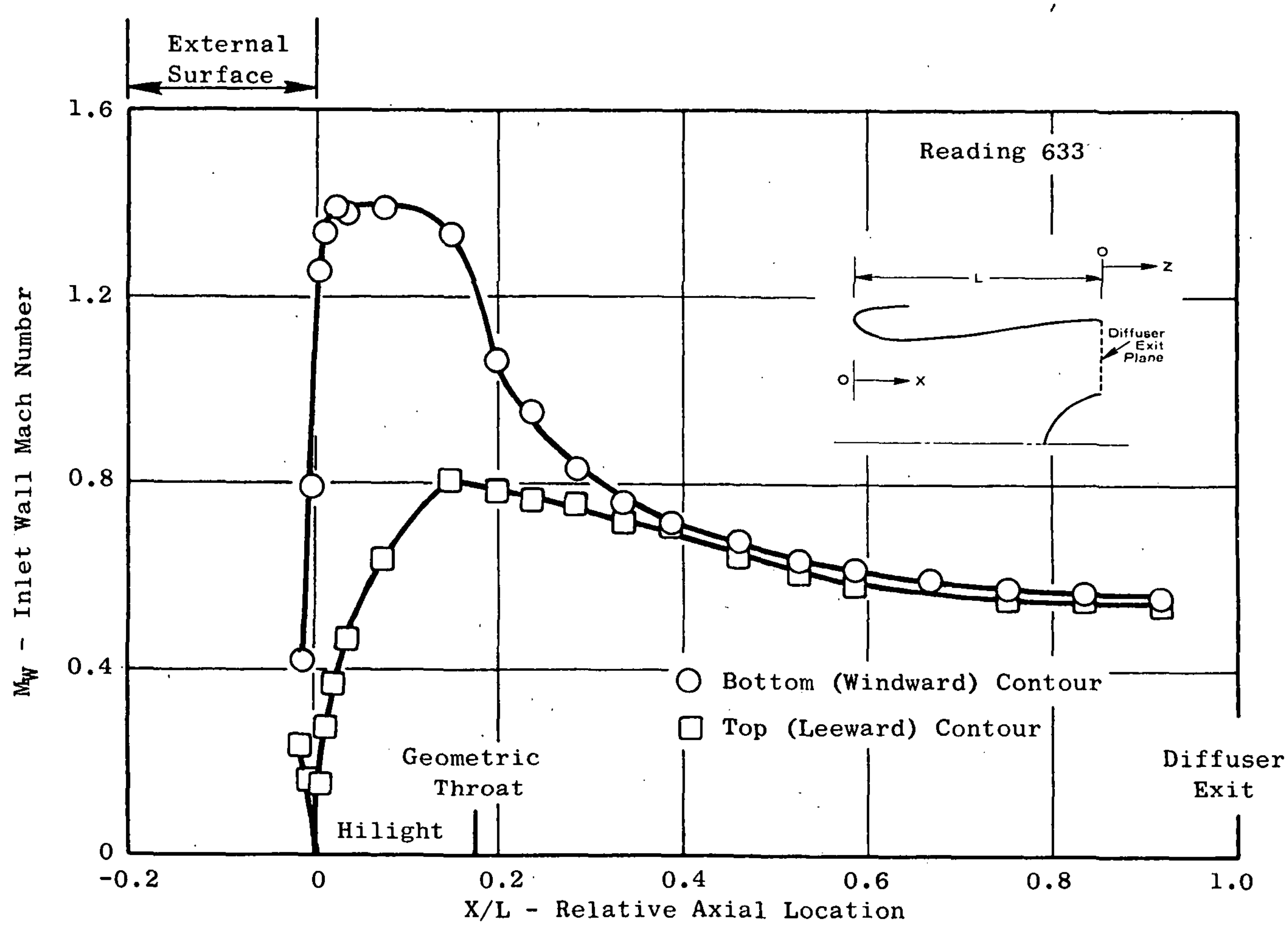

Figure 33. Wall Mach Number Axial Gradient, Inlet No. 2, $V_0 \cong 61.7$ m/sec (120 kts), $\alpha_i = 40.1°$, $M_{TH} = 0.803$ at $\alpha_i = 0°$.

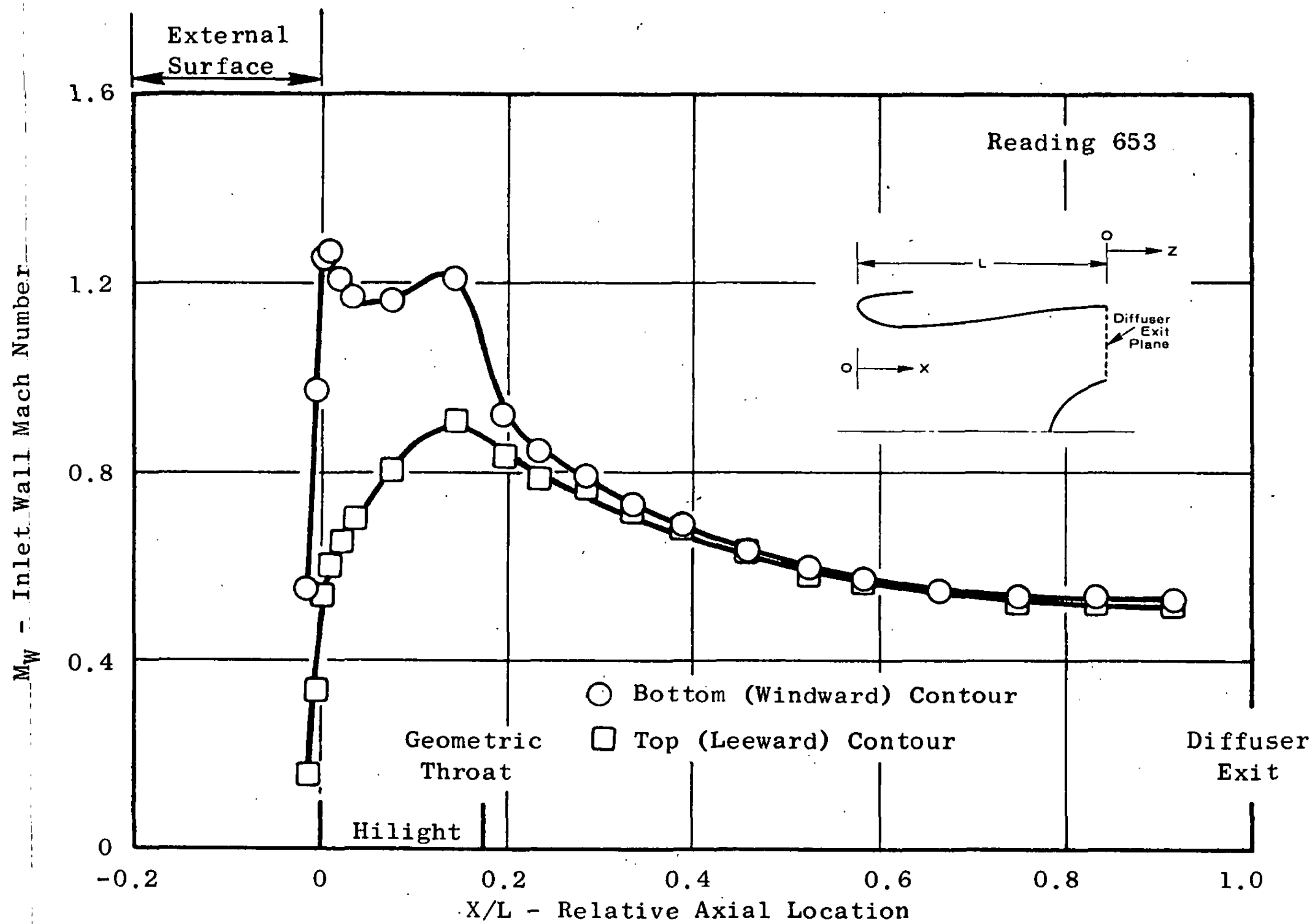

Figure 34. Wall Mach Number Axial Gradient, Inlet No. 2, $V_0 \cong 18$ m/sec (35 kts), $\alpha_i = 90°$, $M_{TH} \sim 0.79$ at $\alpha_i = 0°$.

Additional perspective on the amount of circumferential flow nonuniformity that is sustained at angle of attack is afforded by Figure 35. Maximum circumferential Mach number gradient measured by 8 taps is shown as a function of angle of attack for each of two axial locations, one just aft of the geometric throat and the other near the diffuser exit. In the high velocity region near the throat, increasing nonuniformity is seen as angle of attack increases, until inlet separation is encountered and lip flow breakdown results in nearly uniform conditions, as at zero angle of attack. (The zero angle-of-attack Mach number gradient should theoretically be zero, and should be regarded as the baseline value. It is presumed that the nonzero value is caused by burrs or similar irregularities in the static pressure orifices. This is supported by the fact that the residual zero angle of attack value is much smaller for the lower velocity, aft ring of taps.) Near 50° angle of attack, a Mach number differential of 0.35 is seen at the forward location. By contrast, no increase in aft diffuser flow nonuniformity occurs with angle of attack increases, until the inlet separates, when a moderate increase is noted. This trend is consistent with the data of Figures 32-34.

The amount of variation in throat Mach number due to inlet recovery change with increasing angle of attack is shown in Figure 36 for inlet No. 2 at nominal freestream velocities of 41.2 and 61.7 m/sec (80 and 120 kts). In each case, data are for an approximately constant corrected flow setting; the relatively small amount of flow variation actually present is indicated by the simulated fan face Mach number calculated from the diffuser exit pressure survey. At 41.2 m/sec (80 kts) and 50° angle of attack, throat Mach number is 0.026 below its zero angle of attack value, while at 61.7 m/sec (120 kts) and 43°, the corresponding value is 0.069 (although some of this is attributable to variation in inlet flow). These data point up the need to size the inlet for level flight conditions, rather than at angle of attack, in order to preclude excessive throat Mach number demand, and possibly inlet choking, at the former condition.

Evaluation of two boundary layer separation predictors is made in Appendix C, based on posttest analysis of data from this test program.

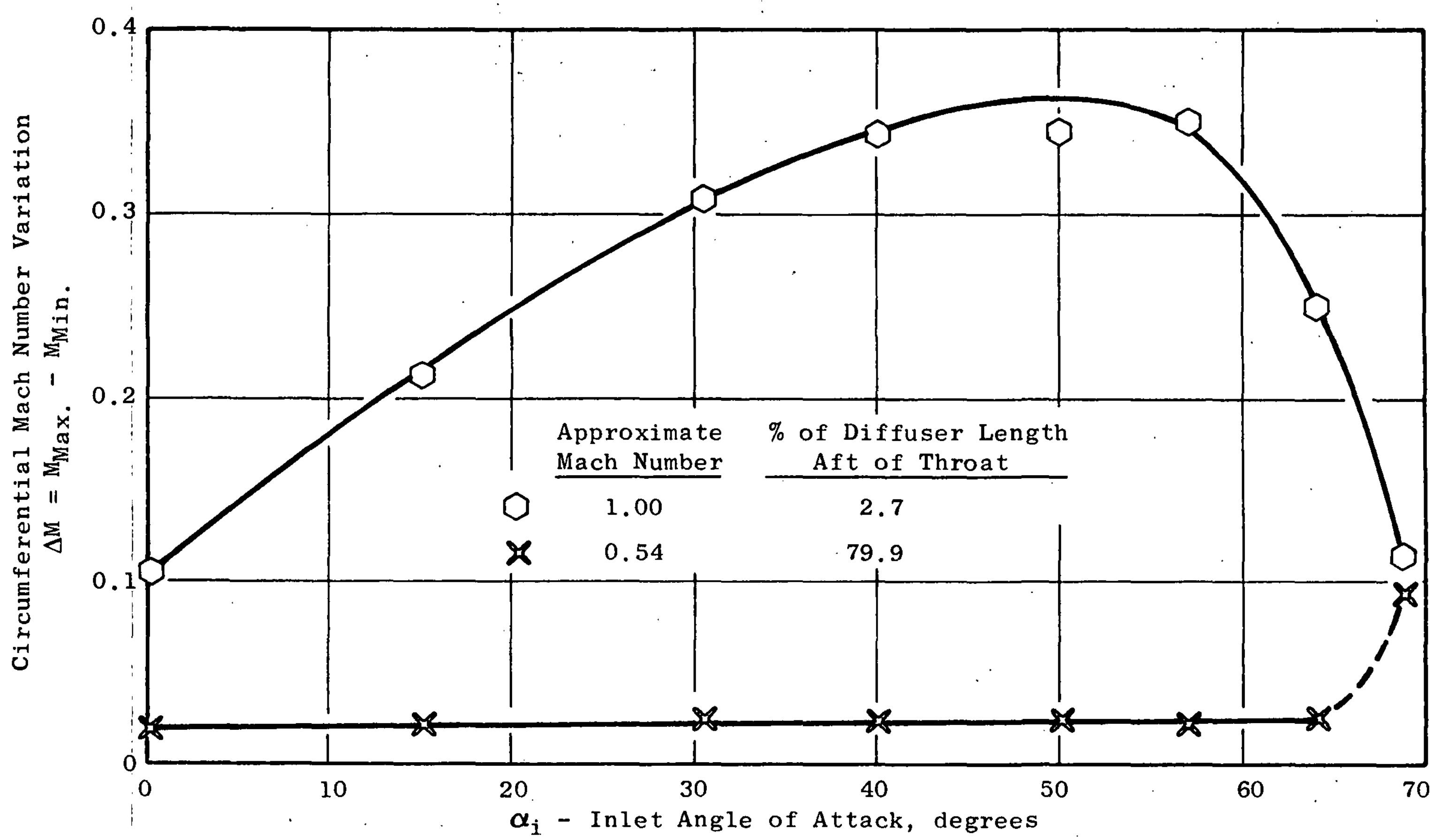

Figure 35. Circumferential Variation in Inlet Wall Mach Number, Inlet No. 2, $V_0 \cong 41.2$ m/sec (80 kts), $M_{TH} = 0.807$ at $\alpha_i = 0°$.

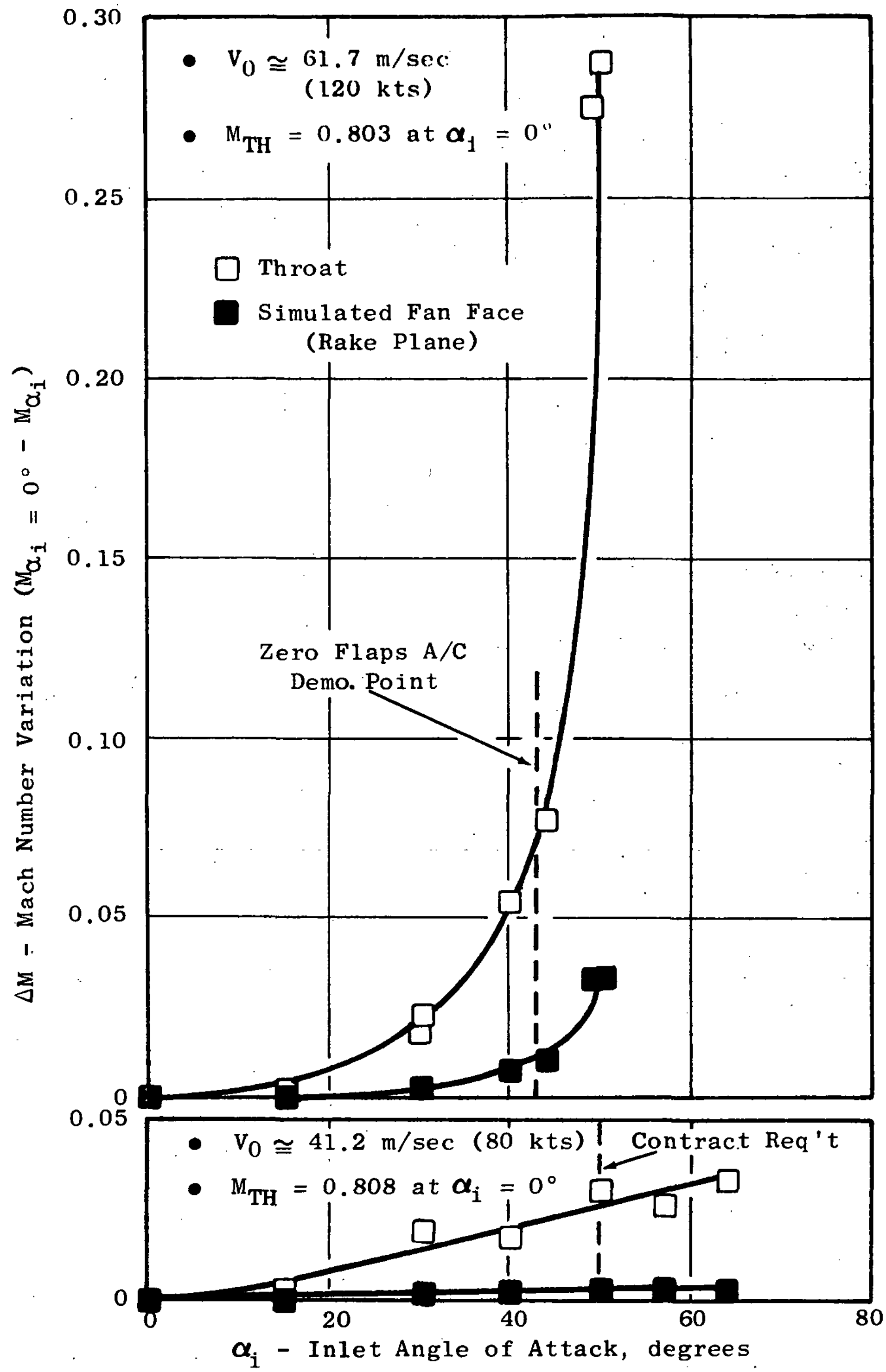

Figure 36. Inlet Throat and Exit Mach Number Variation with Angle of Attack, Inlet No. 2.

SECTION 8.0

CONCLUSIONS

- The high throat Mach number inlet concept has been shown to be feasible for a STOL aircraft that places high angle-of-attack requirements upon the induction system. QCSEE angle-of-attack and static crosswind conditions were met with stable, highly efficient operation up to and beyond the design throat Mach number range.

- Internal lip contraction ratio has a strong impact upon tolerance to inlet flow incidence and performance, as expected. An inlet hilight diameter to throat diameter ratio of 1.21 is required to operate with attached flow at 41.2 m/sec (80 kts) 50° angle of attack and 61.7 m/sec (120 kts) 43° angle of attack, while a value between 1.17 and 1.21 is similarly needed for operation in a 18.0 m/sec (35 kts) static crosswind.

- External cowl design in the region of nose curvature was shown to be important to low speed inlet performance and stability. Careful consideration must be given to the juncture of internal and external lip contours, especially for the relatively high contraction internal lips demanded by a QCSEE-type application.

- Diffuser design guidelines previously established for separation-free performance at high angles of attack and moderate (0.60) throat Mach number were successfully employed at higher throat Mach number (0.79) for the single design of this investigation.

- Various on-line separation detectors derived from both steady-state and dynamic pressure measurements were found to agree, within about 7° at worst, on the onset of separation angle of attack. Separations were indicated almost simultaneously by inlet lip and diffuser exit detectors, suggesting that separation initiated on the high velocity lip and then rapidly propagated down the diffuser.

- Dynamic to steady-state distortion level ratios were about 1.5-2.0, for moderate to high steady-state levels, which is consistent with previous observations of other intake systems.

- Analytical flowfield predictions for operation at zero inlet angle of attack were in good agreement with test data, especially when the absence of viscous effects in the former is considered. This represents yet another confirmation of the Streamtube Curvature computer program's ability to calculate highly compressible, axisymmetric internal flow fields.

- Static pressure taps located on the inlet side contours at approximately 30% to 40% of the (internal) inlet length from the nose will be adequately responsive to flow changes, yet insensitive enough to angle of attack and crosswind effects, to serve as part of the key QCSEE throat Mach number control.

- The adequacy of the General Electric AERO and SABBL (Stratford and Beavers Boundary Layer) programs as analytical tools for boundary layer separation prediction was confirmed by processing wall pressure data for one of the inlets tested.

APPENDIX A

TEST LOGS

The test logs contained in this appendix were copied from the originals which recorded the tunnel "Q" in English units. Equivalent values for Q are given here to assist the reader in interpreting the test logs.

lb/ft^2	N/m^2	kts	m/sec
4.0	191.5	35	18.0
21.0	1005.5	80	41.2
46.0	2202.5	120	61.7
52.0	2489.8	128	65.8

STATIC TEST MATRIX

Date: 6/21 Test Configuration: GE1 Test Engineer: BAM, DLP

Comments: None

Set Point (Nominal M_{TH})	Flow Setting Parameter $\left[\frac{\Delta P}{P}\right]_f$	Blade Passing Frequency, KHz			
		0 ↓	5 ↓	8 ↓	9.6 ↓
No Flow	0	814			
0.10*					
0.30	3.83			807	
0.45	8.34			808	
0.60	13.20			809	
0.70	16.40			810	
0.75	18.45			811	
0.79	20.50			812	
0.82**	21.50			813	
ΔdB Limit					
$\frac{W\sqrt{\theta}}{\delta}$ Limit					

* Ground Idle
** Flow Limit

35 KNOTS TEST MATRIX

Date: 6/21 Test Configuration: GE1 Test Engineer: BAM, DLP

Comments: Siren Hz = 8000; Q $\approx$ 4.0 psf; Reading 805 run at $\Delta P/P \approx 21$. This configuration would not acoustically choke at $\alpha = 0°$.

$\alpha = 0$ Set Point (Nominal M_{TH})	$\left[\frac{\Delta P}{P}\right]_f$	Reading Number		
		α_i → 0°	α_i → 90°	α_i ↓ 90°
No Flow (Hz = 0)	≈ 0	782		
0.10*	0.55	791	792	783
0.30	3.85	794	793	784
0.45	8.32	795	796	785
0.60	13.27	797	798	786
0.70	16.30	799	800	787
0.75	18.22	801	802	788
0.79	20.00	803	804	789
0.82 **	20.50	805	806	790
ΔdB Limit				
$\frac{W\sqrt{\theta}}{\delta}$ Limit				

* Ground Idle
** Flow Limit

BASIC DATA MATRIX

Date: 6/21 Test Configuration: GE1 Test Engineer: BAM, DLP

Comments: Siren Hz = 8000; Q = 21 psf (80 kts)

$\alpha = 0$ Set Point (Nominal M_{TH})	$\left[\frac{\Delta P}{P}\right]_f$	Sweep $\alpha_i \downarrow \alpha_s$	Reading Number							
			α_s $-\epsilon$	α_s $+\epsilon$	$\overrightarrow{\alpha_i}$ 0°	$\overrightarrow{\alpha_i}$ 15°	$\overrightarrow{\alpha_i}$ 30°	$\overrightarrow{\alpha_i}$ 40°	$\overrightarrow{\alpha_i}$ 50°	α_i >50°
No Flow (Hz = 0)	≈ 0				726					
0.10 *										
0.30	3.95		728	729	727	730	731	732		
0.45	8.40		734	735	733	736	737	738	739	
0.60	13.30		741	742	740	743	744	745	746	
0.70	16.44		748	749	747	750	751	752	753	
0.75	18.00		755	756	754	757	758	759	760	
0.79	19.15		762	763	761	764	765	766	767	
0.82	20.67		769	770	768	771	772	773	774	
ΔdB Limit	21.30		776	777	775	778	779	780	781	
$\frac{W\sqrt{\theta}}{\delta}$ Limit										

* Ground Idle

BASIC DATA MATRIX

Date: 6/21 Test Configuration: GE1 Test Engineer: BAM, DLP

Comments: Siren Hz = 8000; Q = 46 psf (120 kts)

$\alpha = 0$ Set Point (Nominal M_{TH})	$\left[\frac{\Delta P}{P}\right]_f$	Sweep $\alpha_i \downarrow \alpha_s$	Reading Number							
			α_s $-\epsilon$	α_s $+\epsilon$	α_i 0°	α_i 15°	α_i 30°	α_i 40°	α_i 50°	α_i >50°
No Flow (Hz = 0)	≈ 0				672					
0.10*										
0.30	4.0		674		673	675	676	677		
0.45	8.47		679	680	678	681	682	683		
0.60	13.35		685	686	684	687	688	689	690	
0.70	16.62		692	693	691	694	695	696	697	
0.75	18.16		699	700	698	701	702	703	704	
0.79	19.28		706	707	705	708	709	710	711	
0.82	20.50		713	714	712	715	716	717	718	
ΔdB Limit	21.00		720	721	719	722	723	724	725	
$\frac{W\sqrt{\theta}}{\delta}$ Limit										

* Ground Idle

STATIC TEST MATRIX

Date: 6/19 Test Configuration: GE2 Test Engineer:

Comments: None

Set Point (Nominal M_{TH})	$\left[\frac{\Delta P}{P}\right]_f$	Blade Passing Frequency, KHz			
		0 ↓	5 ↓	8 ↓	9.6 ↓
No Flow	0	551	540	529	
0.10 *	0.54		541	530	
0.30	3.83		542	531	
0.45	8.23		543	532	
0.60	13.25		544	533	
0.70	16.25		545	534	
0.75	17.80		546	535	
0.79	19.80		547	536	
0.82	20.20		548	537	
Split Suppression	20.4		549	538	
$\frac{W\sqrt{\theta}}{\delta}$ Limit	20.7		550	539	

* Ground Idle

35 KNOTS TEST MATRIX

Date: ~~6/19~~ 6/20 Test Configuration: GE2 Test Engineer: HLW, DLP

Comments: Siren Hz = 8000; Q ≈ 4.0 psf; No acoustic data on Readings 646, 649; Reading 647 - No noise (siren).

$\alpha = 0$ Set Point (Nominal M_{TH})	$\left[\frac{\Delta P}{P}\right]_f$	Reading Number $\alpha_i \rightarrow$ 0°	$\alpha_i \rightarrow$ 90°	$\alpha_i \downarrow$ 90°
No Flow (Hz = 0)	≈ 0	645		
0.10*	235			646
0.30				647 648
0.45				649
0.60				650
0.70				651
0.75				652
0.79				653
0.82				654
ΔdB Limit				
$\frac{W\sqrt{\theta}}{\delta}$ Limit				655

* Ground Idle

BASIC DATA MATRIX

Date: 6/19 6/20 Test Configuration: GE2 Test Engineer: HLW, DLP

Comments: Siren Hz = 8000; Q = 21 psf (80 kts); Reading 504, Q = 52, W = 0, Hz = 0 at request of BB and N; Bad readings: 589, 593; Reading 528, Q shift during record (α_i = 0, 0.75 M_{th}); $\Delta P/P$ not held above α_s.

$\alpha = 0$ Set Point (Nominal M_{TH})	$\left[\frac{\Delta P}{P}\right]_f$	Sweep $\alpha_i \downarrow \alpha_s$	Reading Number							
			α_s $-\epsilon$	α_s $+\epsilon$	$\alpha_i \rightarrow$ 0°	$\alpha_i \rightarrow$ 15°	$\alpha_i \rightarrow$ 30°	$\alpha_i \rightarrow$ 40°	$\alpha_i \rightarrow$ 50°	α_i >50°
No Flow (Hz = 0)	≈ 0				496					
0.30	3.88	44°	498	499	497	500	501	502	503	
0.45	8.28	57°	506	507	505	508	509	510	511	
0.60	13.28	72°	513	514	512	515	516	517	518	60° 519
0.70	16.38	87°	521	522	520	523	524	525	526	65° 627
0.70	16.50	91°	553 555	554	552	556	557	558	559	65° 560
0.75	18.00	75°	562	563	561	564	565	566	567	60° 568
0.79	18.95	70°	570	571	569	572	573	574	575	57° 576
0.82	19.95	69°	578	579	577	580	581	582	583	57° 584
Split Suppression	20.37	69°	586	587	585	588	590 589	591	592	57° 593 594
$\frac{W\sqrt{\theta}}{\delta}$ Limit	20.50	69°	596	597	595	598	599	600	601	57° 602

BASIC DATA MATRIX

6/19
Date: 6/20   Test Configuration: GE2   Test Engineer: HLW, DLP

Comments: Siren Hz = 8000; Q = 46 psf (120 kts); No noise recorded for $\alpha_s - \epsilon$ and $\alpha_s + \epsilon$

$\alpha = 0$ Set Point (Nominal M_{TH})	$\left[\frac{\Delta P}{P}\right]_f$	Sweep $\alpha_i \downarrow \alpha_s$	Reading Number							
			α_s $-\epsilon$	α_s $+\epsilon$	$\alpha_i \rightarrow$ 0°	$\alpha_i \rightarrow$ 15°	$\alpha_i \rightarrow$ 30°	$\alpha_i \rightarrow$ 40°	$\alpha_i \rightarrow$ 50°	α_i >50°
No Flow (Hz = 0)	≈ 0				603					
0.10 *										
0.30	3.90	36°	670	671	604	605	606	607	608	
0.45	8.34	44°	668	669	609	610	611	612	613	
0.60	13.40	46°	666	667	614	615	616	617	618	
0.70	16.50	50°	664	665	619	620	621	622	623	
0.75	18.05	47°	662	663	624	625	626	627	628	
0.79	18.94	47°	660	661	629	630	631 632	633	634	
0.82	20.00	46°	658	659	635	636	637	638	639	
ΔdB Limit										
$\frac{W\sqrt{\theta}}{\delta}$ Limit	26.75	~40° ?	656	657	640	641	642	643	644	

* Ground Idle

STATIC TEST MATRIX

Date: 6/12 6/13 Test Configuration: GE3 Test Engineer: BAM, DLP

Comments: Reading 375 - Postrun calibration: Zeros

Set Point (Nominal M_{TH})	$\left[\frac{\Delta P}{P}\right]_f$	Blade Passing Frequency, KHz			
		0 ↓	5 ↓	8 ↓	9.6 ↓
No Flow	0	376 375			
0.10 *	0.51	357		366	
0.30	3.84	358		367	
0.45	8.30	359		368	
0.60	13.29	360		369	
0.70	16.40	361		370	
0.75	17.90	362		371	
0.79	18.95	363		372	
0.82	19.70	364		373	
ΔdB Limit					
$\frac{W\sqrt{\theta}}{\delta}$ Limit	20.50	365		374	

* Ground Idle

35 KNOTS TEST MATRIX

Date: 6/13 Test Configuration: GE3 Test Engineer: HLW, DLP

Comments: Siren Hz = 8000; Q $\approx$ 4.0 psf; Reading 495: zero flow, zero fan.

$\alpha = 0$ Set Point (Nominal M_{TH})	$\left[\frac{\Delta P}{P}\right]_f$	Reading Number		
		α_i → 0°	α_i → 90°	α_i ↓ 90°
No Flow (Hz = 0)	≈ 0	475		
0.10*	0.52		494	476
0.30	3.75		493	477
0.45	8.15		492	478
0.60	13.01		491	479
0.70	16.10		490	480
0.75	17.50		489	481
0.79	18.40		488	482
0.82	19.02	486	487	483
ΔdB Limit				
$\frac{W\sqrt{\theta}}{\delta}$ Limit	21.50		485	484

* Ground Idle

BASIC DATA MATRIX

Date: 6/13 Test Configuration: GE3 Test Engineer: HLW, DLP

Comments: Siren Hz = 8000; Q = 21 psf (80 kts)

$\alpha = 0$ Set Point (Nominal M_{TH})	$\left[\frac{\Delta P}{P}\right]_f$	Sweep $\alpha_i \downarrow \alpha_s$	Reading Number							
			α_s $-\epsilon$	α_s $+\epsilon$	$\overrightarrow{\alpha_i}$ 0°	$\overrightarrow{\alpha_i}$ 15°	$\overrightarrow{\alpha_i}$ 30°	$\overrightarrow{\alpha_i}$ 40°	$\overrightarrow{\alpha_i}$ 50°	α_i >50°
No Flow (Hz = 0)	≈ 0				377					
0.10*										
0.30	3.86	48°	379	380	378	381	382	383	384	
0.45	8.30	57°	386	387	385	388	389	390	391	
0.60	13.20	68°	393	394	392	395	396	397	398	
0.70	16.35	68°	400	401	399	402	403	404	405	
0.75	17.85	69°	407	408	406	409	410	411	412	
0.79	18.75	66°	414	415	413	416	417	418	419	
0.82	19.50	68°	421	422	420	423	424	425	426	
ΔdB Limit										
$\frac{W\sqrt{\theta}}{\delta}$ Limit	2120	67°	428	429	427	430	431	432	433	

* Ground Idle

BASIC DATA MATRIX

Date: 6/13 Test Configuration: GE3 Test Engineer: HLW, DLP

Comments: Siren Hz = 8000; Q = 46 psf (120 kts)

$\alpha = 0$ Set Point (Nominal M_{TH})	$\left[\frac{\Delta P}{P}\right]_f$	Sweep $\alpha_i \downarrow \alpha_s$	Reading Number							
			α_s $-\epsilon$	α_s $+\epsilon$	$\overrightarrow{\alpha_i}$ 0°	$\overrightarrow{\alpha_i}$ 15°	$\overrightarrow{\alpha_i}$ 30°	$\overrightarrow{\alpha_i}$ 40°	$\overrightarrow{\alpha_i}$ 50°	α_i >50°
No Flow (Hz = 0)	≈ 0				434					
0.10 *										
0.30	3.75	40°			435	436	437	438	439	
0.45	8.15	50°			440	441	442	443	444	
0.60	13.02	58°			445	446	447	448	449	
0.70	16.12	65°			450	451	452	453	454	
0.75	17.57	63°			455	456	457	458	459	
0.79	18.47	64°			460	461	462	463	464	
0.82	19.10	63°			465	466	467	468	469	
ΔdB Limit										
$\frac{W\sqrt{\theta}}{\delta}$ Limit	21.00	62°			470	471	472	473	474	

* Ground Idle

STATIC TEST MATRIX

Date: 6/25 Test Configuration: GE4 Test Engineer: HLW, DLP

Comments: Siren off on Reading 930

Set Point (Nominal M_{TH})	$\left[\frac{\Delta P}{P}\right]_f$	Blade Passing Frequency, KHz			
		0 ↓	5 ↓	8 ↓	9.6 ↓
No Flow	0	929			
0.10*	0.46			939	
0.30	3.86			938	
0.45	8.44			937	
0.60	13.76			936	
0.70	16.95			935	
0.75	18.45			934	
0.79	19.50			933	
0.82	21.60			932	
ΔdB Limit					
$\frac{W\sqrt{\theta}}{\delta}$ Limit	23.90			930 931	

* Ground Idle

35 KNOTS TEST MATRIX

Date: 6/25 Test Configuration: GE4 Test Engineer: HLW, DLP

Comments: Siren Hz = 8000; Q $\approx$ 4.0 psf; Reading 916 $\Delta P/P$ = 18.9; No acoustics on readings 922, 925, 926.

$\alpha = 0$ Set Point (Nominal M_{TH})	$\left[\frac{\Delta P}{P}\right]_f$	Reading Number $\alpha_i \rightarrow$ 0°	$\alpha_i \rightarrow$ 90°	$\alpha_i \downarrow$ 90°
No Flow (Hz = 0)	$\approx$ 0	915		
0.10 *	0.45			924
0.30	3.77			923
0.45	8.41			922
0.60	13.62	925	926	921
0.70	17.00			920
0.75	18.40			919
0.79	19.60	927	928	918
0.82	20.80			917
ΔdB Limit				
$\frac{W\sqrt{\theta}}{\delta}$ Limit	25.80			916

* Ground Idle

BASIC DATA MATRIX

Date: 6/25 Test Configuration: GE4 Test Engineer: HLW, DLP

Comments: Siren Hz = 8000; Q = 21 psf (80 kts); Speed counter did not work; used analyzer to set speed.

$\alpha = 0$ Set Point (Nominal M_{TH})	$\left[\frac{\Delta P}{P}\right]_f$	Sweep $\alpha_i \downarrow \alpha_s$	Reading Number							
			α_s $-\epsilon$	α_s $+\epsilon$	$\overrightarrow{\alpha_i}$ 0°	$\overrightarrow{\alpha_i}$ 15°	$\overrightarrow{\alpha_i}$ 30°	$\overrightarrow{\alpha_i}$ 40°	$\overrightarrow{\alpha_i}$ 50°	α_i >50°
No Flow (Hz = 0)	≈ 0				815					
0.10 *										
0.30	3.81	32°	817	818	816	819	820	821	822	
0.45	8.35	37°	824	825	823	826	827	828	829	
0.60	13.45	38°	831	832	830	833	834	832	835	
0.70	16.65	38°	837	838	836	839	840	838	841	
0.75	18.10	37°	843	844	842	845	846	847	848	
0.79	19.15	33°	850	851	849	852	853	854	855	
0.82	20.10	34°	857	858	856	859	860	861	862	
ΔdB Limit										
$\frac{W\sqrt{\theta}}{\delta}$ Limit	22.50	~40° ±5° ?	864	865	863	866	867	868	869	

* Ground Idle

BASIC DATA MATRIX

Date: 6/25 Test Configuration: GE4 Test Engineer: HLW, DLP

Comments: Siren Hz = 8000; Q = 46 psf (120 kts); No acoustics on readings 886, 887.

$\alpha = 0$ Set Point (Nominal M_{TH})	$\left[\frac{\Delta P}{P}\right]_f$	Sweep $\alpha_i \downarrow \alpha_s$	Reading Number							
			α_s $-\epsilon$	α_s $+\epsilon$	α_i 0°	α_i 15°	α_i 30°	α_i 40°	α_i 50°	α_i >50°
No Flow (Hz = 0)	≈ 0				870					
0.10*										
0.30	3.80	~30°			871	872	873	874	875	
0.45	8.29	~32°			876	877	878	879	880	
0.60	13.39	~33°			881	882	883	884	892	
0.70	16.51	~33°	886	887	885	888	889	890	891	
0.75	18.05	~29°		896	893	894	895	897	898	
0.79	19.02	~30°		902	899	900	901	903	904	
0.82	20.00				905	906	907	908	909	
ΔdB Limit										
$\frac{W\sqrt{\theta}}{\delta}$ Limit	21.30	~15°			910	911	912	913	914	

* Ground Idle

APPENDIX B

TABULATION OF KEY INLET PERFORMANCE PARAMETERS

Config.	Rdg	V_o/V^*	M_o	α_i ~ Degrees	η_R	$(\Delta P/P)$ Distortion	M_{TH}
1	672	222.37	0.1930	0.546	0.99891	0.0025694	0
	673	211.02	0.18399	0.560	0.99755	0.0041761	0.27176
	674	212.92	0.18582	29.198	0.98249	0.068713	0.26749
	675	211.62	0.18476	15.146	0.99774	0.0090137	0.27238
	676	211.27	0.18452	30.059	0.98060	0.073338	0.26724
	677	210.38	0.18375	40.135	0.96575	0.097930	0.26279
	678	208.37	0.18211	0.122	0.99574	0.0080337	0.44574
	679	208.19	0.18197	34.165	0.99455	0.044549	0.44210
	680	208.14	0.18190	39.105	0.96640	0.10311	0.27558
	681	209.94	0.18344	15.107	0.99554	0.20134	0.44700
	682	209.76	0.18328	29.954	1.0172	1.0062	0.37643
	683	269.34	0.23598	101.660	1.0775	-0.66409	0
	684	213.87	0.18697	0.077	0.99353	0.016175	0.59892
	685	211.96	0.18528	38.532	0.99233	0.076054	0.59008
	686	210.83	0.18423	43.329	0.94998	0.16406	0.36207
	687	210.76	0.18414	15.003	0.99349	0.027200	0.59936
	688	310.99	0.18445	30.072	0.99253	0.049182	0.59671
	689	210.59	0.18410	40.200	0.99132	0.084867	0.59115
	690	209.58	0.18319	50.016	0.94009	0.16236	0.31333
	691	210.59	0.18405	0.104	0.99166	0.023258	0.71130
	692	210.96	0.18439	33.708	0.98840	0.10156	0.69090
	693	211.26	0.18470	39.692	0.95252	0.20181	0.48249
	694	217.62	0.19027	15.055	0.99130	0.044103	0.70175
	695	211.66	0.18499	30.241	0.98992	0.091050	0.69889
	696	211.17	0.18450	39.991	0.95178	0.19909	0.48117
	697	213.34	0.18632	50.068	0.93085	0.20984	0.38401
	698	213.96	0.18675	0.156	0.99030	0.034217	0.76651
	699	213.37	0.18639	33.721	0.98360	0.13689	0.72138
	700	212.15	0.18537	38.844	0.95496	0.21174	0.53376
	701	213.46	0.18648	15.146	0.98934	0.073489	0.76326
	702	214.15	0.18710	30.059	0.98516	0.12082	0.73640
	703	213.45	0.18657	40.057	0.95208	0.21924	0.53124
	704	211.89	0.18521	49.990	0.92827	0.22774	0.41764
	705	212.81	0.18596	0.104	0.98844	0.052734	0.79958
	706	213.49	0.18656	31.310	0.98030	0.14843	0.74332
	707	212.43	0.18570	37.984	0.95881	0.22199	0.60361
	708	213.42	0.18652	15.107	0.98654	0.095765	0.79665
	709	211.92	0.18516	30.098	0.98156	0.13976	0.75688
	710	275.29	0.24112	102.180	0.82520	2.8581	1.000
	711	210.81	0.18428	50.016	0.92612	0.24420	0.43294
	712	212.93	0.18612	0.156	0.98432	0.073266	0.85514
	713	211.68	0.18497	32.105	0.97442	0.18633	0.74249
	714	211.92	0.18517	36.224	0.96248	0.21604	0.66917
	715	213.37	0.18639	15.159	0.98272	0.11336	0.82929
	716	212.06	0.18532	30.033	0.97667	0.16106	0.78560
	717	211.16	0.18457	40.083	0.95092	0.23326	0.60094
	718	211.27	0.18463	50.042	0.92269	0.25520	0.45550

Config.	Rdg	V_o/V^*	M_o	α_i ∿ Degrees	η_R	$(\Delta P/P)$ Distortion	M_{TH}
1	719	213.30	0.18638	0.038	0.98009	0.081337	0.84388
	720	212.26	0.18544	31.857	0.97249	0.19423	0.76664
	721	212.06	0.18523	37.371	0.95678	0.22736	0.63320
	722	212.77	0.18591	15.120	0.97981	0.12780	0.83584
	723	211.09	0.18445	30.046	0.97375	0.18033	0.77336
	724	212.31	0.18551	40.083	0.94984	0.24539	0.60041
	725	211.08	0.18441	50.029	0.91925	0.26815	0.46998
	726	143.31	0.12561	0.260	0.99918	0.0010732	0
	727	144.04	0.12631	0.260	0.99710	0.0044420	0.28706
	728	142.52	0.12497	36.159	0.99682	0.023593	0.28481
	729	143.32	0.12567	39.913	0.98352	0.47252	0.17928
	730	144.86	0.12708	15.146	0.99714	0.0079265	0.28709
	731	143.85	0.12620	29.993	0.99707	0.017626	0.28484
	732	141.67	0.12428	40.096	0.98326	0.047231	0.18328
	733	145.81	0.12791	0.273	0.99540	0.0095496	0.44821
	734	143.25	0.12565	44.619	0.99422	0.045608	0.44034
	735	141.85	0.12445	49.351	0.96609	0.10302	0.27618
	736	143.04	0.12550	15.133	0.99559	0.015002	0.44626
	737	143.97	0.12629	30.059	0.99523	0.027216	0.44156
	738	143.01	0.12546	40.044	0.99468	0.037211	0.44190
	739	142.21	0.12474	49.963	0.96593	0.10222	0.27352
	740	143.88	0.12626	0.195	0.99309	0.016905	0.60726
	741	142.31	0.12487	47.774	0.96400	0.16351	0.43784
	742	140.73	0.12345	52.140	0.95502	0.16828	0.39282
	743	143.97	0.12629	15.146	0.99306	0.024669	0.60426
	744	143.12	0.12559	30.124	0.99301	0.036043	0.60658
	745	143.50	0.12593	40.187	0.99240	0.059096	0.60202
	746	142.98	0.12546	50.146	0.95880	0.16345	0.41944
	747	144.80	0.12703	0.169	0.99161	0.026176	0.70857
	748	142.57	0.12514	48.399	0.98714	0.12265	0.68383
	749	141.80	0.12445	52.166	0.95448	0.20212	0.49322
	750	144.88	0.12712	15.133	0.99148	0.36853	0.70922
	751	143.02	0.12548	30.019	0.99043	0.070239	0.70252
	752	143.54	0.12593	40.005	0.98891	0.10169	0.69665
	753	141.93	0.12458	50.055	0.98626	0.12626	0.67842
	754	145.02	0.12727	0.064	0.99008	0.040936	0.77646
	755	142.63	0.12516	46.613	0.98306	0.13922	0.72337
	756	142.95	0.12542	51.241	0.95338	0.21686	0.53629
	757	143.06	0.12557	15.159	0.98914	0.077747	0.75930
	758	142.40	0.12498	30.150	0.98689	0.10863	0.74513
	759	142.48	0.12504	40.005	0.98469	0.12631	0.73534
	760	142.45	0.12500	50.042	0.95500	0.21778	0.54863
	761	144.5]	0.o2680	0.122	0.98709	0.063877	0.81359
	762	142.63	0.12518	43.954	0.97963	0.15816	0.74655
	763	144.38	0.12671	51.515	0.94915	0.23620	0.55577
	764	145.60	0.12776	15.094	0.98628	0.092024	0.80122
	765	145.74	0.12787	30.124	0.98312	0.12648	0.77921

Config.	Rdg	V_o/V^*	M_o	α_i ~ Degrees	η_R	($\Delta P/P$) Distortion	M_{TH}
1	766	144.41	0.12677	40.070	0.98108	0.14343	0.76559
	767	143.60	0.12605	50.068	0.95314	0.23487	0.56897
	768	146.76	0.12878	0.090	0.98080	0.079751	0.83929
	769	143.96	0.12637	41.777	0.97422	0.18428	0.78780
	770	143.65	0.12609	49.325	0.96022	0.22049	0.65961
	771	147.30	0.12926	15.133	0.97965	0.10367	0.84682
	772	144.99	0.12722	30.111	0.97753	0.16073	0.80851
	773	144.98	0.12727	40.031	0.97484	0.16709	0.77823
	774	144.75	0.12707	50.042	0.95888	0.23667	0.63714
	775	146.17	0.12828	0.247	0.97596	0.088386	0.85862
	776	144.75	0.12708	42.690	0.97092	0.19398	0.76753
	777	144.68	0.12701	49.038	0.95900	0.23594	0.66932
	778	146.05	0.12819	15.107	0.97579	0.10459	0.84012
	779	145.31	0.12752	30.046	0.97371	0.16831	0.81306
	780	143.76	0.12614	39.991	0.97177	0.18618	0.78008
	781	143.92	0.12635	50.003	0.95518	0.24526	0.66119
	782	61.270	0.054065	0.143	0.99903	0.00057886	0.013375
	783	61.263	0.054065	89.995	0.99397	0.0018717	0
	784	61.049	0.53888	89.930	0.97759	0.045178	0.12924
	785	61.079	0.53932	89.930	0.96145	0.10187	0.25137
	786	60.420	0.53355	89.943	0.96038	0.16241	0.43859
	787	61.032	0.053888	89.930	0.98760	0.93703	0.68373
	788	60.283	0.53220	89.930	0.98429	0.13541	0.78279
	790	59.536	0.52589	89.930	0.97430	0.15985	0.78672
	791	62.797	0.055458	0.090	0.99875	0.0019362	0.091573
	792	60.475	0.053399	88.639	0.99394	0.0030019	0.0041298
	793	59.524	0.052589	90.607	0.97737	0.046502	0.13171
	794	63.265	0.055886	-0.744	0.99727	0.0053583	0.28218
	795	62.893	0.055544	-0.744	0.99531	0.011737	0.44601
	796	59.714	0.052771	89.708	0.99374	0.041858	0.43912
	797	62.670	0.055372	0.573	0.99313	0.019579	0.59920
	798	59.629	0.052680	89.695	0.99013	0.074411	0.59210
	799	61.900	0.054679	-0.529	0.99120	0.029774	0.70091
	800	60.518	0.053489	89.565	1.0068	-0.061635	0
	801	64.108	0.056649	0.104	0.97785	0.54351	0.75749
	802	60.931	0.053844	90.516	0.98398	0.11153	0.74176
	803	62.869	0.055544	0.351	0.98124	0.075148	0.81749
	804	59.437	0.052544	90.542	0.97770	0.13892	0.78171
	805	63.477	0.056099	0.899	0.97640	0.76734	0.83168
	806	60.625	0.053578	89.773	0.97282	0.15273	0.79338
	807	0	0	0.195	0.99715	0.015415	0.28236
	808	0	0	0.195	0.99498	0.020062	0.44234
	809	0	0	0.195	0.99285	0.026240	0.59932
	810	0	0	0.195	0.99027	0.058034	0.70841
	811	0	0	0.195	0.98605	0.081682	0.76503
	812	0	0	0.195	0.97516	0.11356	0.80830
	813	0	0	0.182	0.97486	0.095172	0.81802
	814	0	0	0.195	0.99902	0.00057535	0.013406

Config.	Rdg	V_o/V^*	M_o	α_i ∿ Degrees	η_R	($\Delta P/P$) Distortion	M_{TH}
2	496	144.46	0.12727	0.090	0.99978	0.0013894	0.016311
	497	142.26	0.12514	0.090	0.99752	0.0042646	0.28195
	498	144.29	0.12686	40.995	0.99683	0.022890	0.27867
	499	143.61	0.12622	46.131	0.98298	0.045368	0.17316
	500	144.30	0.12720	15.120	0.99752	0.0070697	0.28522
	501	144.22	0.12710	30.059	0.99728	0.13479	0.28175
	502	141.68	0.12485	40.044	0.99696	0.022457	0.28091
	503	141.52	0.12476	49.990	0.98145	0.045181	0.15812
	504	222.08	0.19496	0.090	0.99892	0.0024044	0.018856
	505	143.79	0.12652	0.104	0.99571	0.0071849	0.44258
	506	142.91	0.12569	52.284	0.99438	0.045631	0.43596
	507	143.23	0.12599	54.461	0.96844	0.10070	0.28216
	508	146.02	0.12839	15.159	0.99559	0.011295	0.44037
	509	145.00	0.12744	30.072	0.99544	0.022069	0.43700
	510	143.78	0.12637	40.044	0.99517	0.031504	0.43774
	511	143.48	0.12609	49.977	0.99453	0.043091	0.43620
	512	144.37	0.12678	0.090	0.99365	0.014400	0.59791
	513	142.74	0.12531	67.444	0.99090	0.081391	0.58468
	514	142.54	0.12516	71.159	0.94316	0.16292	0.32594
	515	146.04	0.12819	15.094	0.99353	0.018899	0.59888
	516	145.59	0.12774	29.993	0.99343	0.027220	0.59885
	517	142.85	0.12531	40.018	0.99305	0.38308	0.59656
	518	143.70	0.12612	50.615	0.99241	0.053804	0.59369
	519	141.30	0.12397	60.196	0.99187	0.071456	0.58970
	520	145.62	0.12770	0.130	0.99200	0.021055	0.70451
	521	142.87	0.12544	81.418	0.98837	0.10280	0.67894
	522	142.10	0.12479	83.594	0.90956	0.24041	0.35697
	523	145.03	0.12744	15.042	0.99889	0.027135	0.69959
	524	145.02	0.12738	30.072	0.99173	0.038521	0.69855
	525	145.25	0.12759	40.304	0.99177	0.045099	0.69706
	526	145.00	0.12737	50.276	0.99142	0.054884	0.69853
	527	144.08	0.12661	65.032	0.99045	0.071529	0.69242
	528	83.613	0.073826	0.051	0.99108	0.029614	0.75354
	529	0	0	0.090	0.99887	0.0010038	0.0095933
	530	0	0	0.090	0.99867	0.0025319	0.094807
	531	0	0	0.090	0.99712	0.010263	0.28276
	532	0	0	0.090	0.99542	0.022146	0.43966
	533	0	0	0.090	0.99317	0.025605	0.59346
	534	0	0	0.090	0.99161	0.040994	0.69543
	535	0	0	0.090	0.99060	0.044841	0.75151
	536	0	0	0.104	0.98887	0.059023	0.79759
	537	0	0	0.104	0.98503	0.090265	0.83494
	538	0	0	0.090	0.98615	0.081220	0.83573
	539	0	0	0.090	0.98271	0.088632	0.84300
	540	0	0	0.090	0.9903	0.0012999	0.13676
	541	0	0	0.104	0.99870	0.0021211	0.095427
	542	0	0	0.090	0.99720	0.010141	0.28256
	543	0	0	0.090	0.99538	0.015661	0.43934

Config.	Rdg	V_o/V^*	M_o	α_i ~ Degrees	η_R	($\Delta P/P$) Distortion	M_{TH}
2	544	0	0	0.090	0.99327	0.026283	0.59731
	545	0	0	0.090	0.99184	0.031352	0.69442
	546	0	0	0.090	0.99058	0.053052	0.75421
	547	0	0	0.090	0.98897	0.048760	0.79555
	548	0	0	0.090	0.98460	0.088516	0.83405
	549	0	0	0.090	0.98369	0.083013	0.83690
	550	0	0	0.090	0.98193	0.083360	0.84495
	551	0	0	0.090	0.99897	0.0008629	0.016348
	552	140.04	0.12318	0.143	0.99201	0.022108	0.70880
	553	140.69	0.12372	82.930	0.91243	0.22614	0.33752
	554	141.08	0.12399	84.742	0.91144	0.22798	0.33656
	555	141.06	0.12389	78.654	0.98890	0.097739	0.69051
	556	143.87	0.12639	15.107	0.99214	0.030862	0.71322
	557	143.95	0.12645	30.254	0.99122	0.041814	0.70642
	558	143.52	0.02603	40.018	0.99158	0.049184	0.70352
	559	142.51	0.12510	50.029	0.99116	0.055551	0.70042
	560	142.33	0.12493	65.163	0.99051	0.070696	0.69953
	561	143.42	0.12582	0.156	0.99125	0.024515	0.77148
	562	144.34	0.12648	68.734	0.98785	0.10205	0.74424
	563	144.61	0.12663	73.023	0.93111	0.22030	0.43281
	564	147.10	0.12882	15.081	0.99074	0.041411	0.75080
	565	146.28	0.12807	30.033	0.99011	0.067203	0.75259
	566	146.69	0.12845	40.578	0.98920	0.083937	0.75304
	567	146.45	0.12824	50.146	0.98866	0.085863	0.75081
	568	145.04	0.12697	60.027	0.98818	0.090713	0.74986
	569	146.94	0.12864	0.182	0.99016	0.036788	0.80745
	570	146.47	0.12837	64.133	0.98552	0.10945	0.77472
	571	144.44	0.12658	68.721	0.93867	0.22502	0.53800
	572	148.31	0.12996	15.094	0.98961	0.064286	0.80500
	573	146.28	0.12817	30.554	0.98790	0.091931	0.78849
	574	146.39	0.12828	40.096	0.98704	0.098681	0.79009
	575	146.46	0.12841	50.081	0.98654	0.o0254	0.77728
	576	144.61	0.12678	57.055	0.98611	0.098754	0.78120
	577	146.11	0.12796	0.077	0.98749	0.058339	0.85679
	578	143.97	0.12609	63.207	0.98196	0.13104	0.79378
	579	144.28	0.12643	69.621	0.93908	0.24000	0.52331
	580	144.64	0.12669	15.094	0.98683	0.076763	0.82602
	581	145.44	0.12738	29.980	0.98491	0.10695	0.82097
	582	144.58	0.12663	40.109	0.98415	0.12067	0.80972
	583	144.70	0.12673	50.029	0.98320	0.12322	0.80517
	584	144.30	0.12645	57.016	0.98293	0.12770	0.80034
	585	145.11	0.12712	0.143	0.98597	0.064900	0.84964
	586	144.85	0.12688	64.420	0.98007	0.14535	0.80697
	587	145.90	0.12791	69.099	0.93588	0.24551	0.51260
	588	148.96	0.13062	15.081	0.98502	0.083116	0.84982
	589	149.17	0.13084	30.202	0.98325	0.11641	0.82299
	590	142.76	0.12531	30.111	0.98374	0.11721	0.83725

Config.	Rdg	V_o/V^*	M_o	α_i ∿ Degrees	η_R	($\Delta P/P$) Distortion	M_{TH}
2	591	142.78	0.12546	40.031	0.98271	0.12790	0.82230
	592	142.14	0.12493	50.016	0.98168	0.13674	0.80950
	593	143.69	0.12629	57.042	0.98083	0.14517	0.80568
	594	143.78	0.12637	57.042	0.98087	0.14430	0.80697
	595	145.53	0.12794	0.077	0.98515	0.063694	0.82655
	596	144.29	0.12693	63.885	0.97863	0.16443	0.80147
	597	144.46	0.12710	68.695	0.97335	2.6306	0.53975
	598	144.86	0.12746	15.146	0.98471	0.088334	0.85332
	599	142.22	0.12519	30.176	0.98307	0.11258	0.83696
	600	141.41	0.12447	40.044	0.98217	0.13565	0.82555
	601	142.27	0.12521	50.107	0.98106	0.13649	0.81624
	602	142.52	0.12542	57.029	0.98001	0.15427	0.80416
	603	210.28	0.18492	0.130	0.99884	0.0014634	0
	604	212.58	0.18683	0.130	0.99746	0.0037904	0.28345
	605	212.19	0.18638	15.120	0.99729	0.0088572	0.28181
	606	212.02	0.18618	30.033	0.99695	0.19875	0.27876
	607	213.56	0.18746	40.044	0.98022	0.045585	0.14863
	608	216.29	0.18983	49.950	0.97172	0.043084	0.78276
	609	208.32	0.18282	0.064	0.99565	0.0083852	0.44280
	610	207.10	0.18168	15.029	0.99571	0.013015	0.44250
	611	207.94	0.18237	30.189	0.99500	0.029163	0.43828
	612	206.12	0.18065	40.018	0.99450	0.043564	0.43774
	613	212.65	0.18647	50.107	0.95932	0.099314	0.22883
	614	211.96	0.18580	0.117	0.99380	0.013774	0.60347
	615	212.78	0.18648	15.081	0.99344	0.021524	0.60246
	616	211.88	0.18570	30.046	0.99303	0.039551	0.59683
	617	212.19	0.18591	39.952	0.99268	0.54223	0.59678
	618	210.99	0.18484	49.977	0.94920	0.16703	0.36985
	619	212.17	0.18603	0.051	0.99193	0.019565	0.70771
	620	210.64	0.18474	15.068	0.99192	0.033592	0.70341
	621	212.89	0.18667	29.954	0.99128	0.059688	0.70005
	622	211.99	0.18584	40.239	0.98967	0.093494	0.69179
	623	213.11	0.18676	50.003	0.94677	0.19991	0.45797
	624	214.11	0.18753	0.051	0.99122	0.024855	0.77392
	625	213.15	0.18670	15.094	0.99042	0.058743	0.76149
	626	210.38	0.18424	30.019	0.98860	0.091129	0.75775
	627	208.65	0.18274	40.031	0.98598	0.12445	0.73932
	628	211.74	0.18541	50.029	0.94529	0.21820	0.50423
	629	212.34	0.18594	0.143	0.99008	0.036703	0.80323
	630	211.04	0.18479	15.120	0.98884	0.077468	0.80070
	631	211.70	0.18534	30.241	0.98647	0.11752	0.78013
	632	210.41	0.18427	30.098	0.98616	0.11922	0.78566
	633	217.51	0.19047	40.070	0.98236	0.15489	0.74875
	634	216.14	0.18943	50.198	0.94410	0.23043	0.51610
	635	221.60	0.19431	0.077	0.98703	0.056721	0.87141
	636	211.96	0.18592	15.068	0.98585	0.094715	0.84547
	637	212.15	0.18614	30.137	0.98244	0.13641	0.81083
	638	211.19	0.18532	40.005	0.97831	0.16867	0.77197

Config.	Rdg	V_o/V^*	M_o	$\alpha_1 \sim$ Degrees	η_R	($\Delta P/P$) Distortion	M_{TH}
2	639	212.72	0.18670	50.081	0.94965	0.23861	0.56157
	640	214.46	0.18835	0.090	0.94183	0.16561	0.86785
	641	211.52	0.18574	15.042	0.94350	0.19878	0.87323
	642	209.58	0.18399	30.072	0.94520	0.25938	0.84555
	643	211.47	0.18566	40.044	0.94839	0.27825	0.84346
	644	209.61	0.18401	50.081	0.93460	0.31724	0.70106
	645	60.866	0.53800	0.077	0.99887	0.0010458	0.009312
	646	60.320	0.053355	90.034	0.98545	0.027192	0.091647
	647	61.180	0.054109	90.034	0.98924	0.070725	0.28794
	648	62.284	0.055113	90.034	0.99513	0.29644	0.37026
	649	60.352	0.053399	90.021	0.99465	0.034878	0.42556
	650	61.206	0.054153	90.034	0.99180	0.046856	0.57665
	651	61.313	0.054285	90.021	0.99063	0.054790	0.6723
	652	61.511	0.054460	90.021	0.98969	0.065224	0.71927
	653	62.061	0.054940	90.008	0.98888	0.074758	0.74964
	654	62.206	0.055070	90.021	0.98739	0.086596	0.77755
	655	60.904	0.053932	90.021	0.97875	0.10339	0.84293
	656	211.82	0.18612	33.304	0.94690	0.26702	0.86089
	657	211.71	0.18600	42.507	0.95016	0.28444	0.81207
	658	210.86	0.18526	43.433	0.97624	0.19336	0.73942
	659	210.26	0.18468	51.749	0.94321	0.24456	0.53675
	660	211.25	0.18535	44.345	0.98075	0.17059	0.72564
	661	211.73	0.18584	49.364	0.94896	0.22762	0.52751
	662	211.12	0.18506	44.371	0.98446	0.14392	0.72303
	663	211.63	0.18547	48.960	0.94777	0.22383	0.52286
	664	210.53	0.18449	46.535	0.98748	0.12466	0.67909
	665	210.05	0.18393	51.476	0.94450	0.20750	0.45967
	666	212.33	0.18578	41.790	0.99222	0.065323	0.59825
	667	212.12	0.18536	48.217	0.95256	0.17050	0.39271
	668	211.61	0.18526	40.539	0.99463	0.046747	0.43577
	669	210.88	0.18463	44.502	0.96535	0.10439	0.27791
	670	211.50	0.18510	33.761	0.99696	0.022132	0.28020
	671	211.85	0.18541	33.774	0.98546	0.47219	0.19068
3	356	0	0	0.182	0.99896	0.00057057	0.023403
	357	0	0	0.208	0.99869	0.0020176	0.090800
	358	0	0	0.195	0.99744	0.011271	0.28240
	359	0	0	0.195	0.99549	0.023096	0.44183
	360	0	0	0.195	0.99376	0.042802	0.59987
	361	0	0	0.195	0.99239	0.050879	0.70464
	362	0	0	0.208	0.99093	0.076707	0.76042
	363	0	0	0.208	0.99022	0.065114	0.80696
	364	0	0	0.195	0.98985	0.053761	0.83825
	365	0	0	0.208	0.98515	0.11970	0.86574
	366	0	0	0.208	0.99872	0.0016891	0.091458
	367	0	0	0.208	0.99728	0.010260	0.28304
	368	0	0	0.208	0.99559	0.023381	0.44096

Config.	Rdg	V_o/V^*	M_o	$\alpha_i \sim$ Degrees	η_R	($\Delta P/P$) Distortion	M_{TH}
3	369	0	0	0.195	0.99333	0.044044	0.59925
	370	0	0	0.208	0.99250	0.038527	0.70049
	371	0	0	0.195	0.99150	0.034820	0.76199
	372	0	0	0.195	0.99034	0.065872	0.80188
	373	0	0	0.208	0.98766	0.10727	0.84922
	374	0	0	0.195	0.98690	0.081037	0.86913
	375	0	0	0.208	0.99901	0.00056972	0.023409
	376	0	0	0.182	0.99897	0.00042223	0.0000237
	377	144.41	0.12677	0.117	0.99898	0.0016777	0.021217
	378	144.37	0.12673	0.117	0.99747	0.0043522	0.28133
	379	141.73	0.12447	42.559	0.99703	0.021331	0.26962
	380	141.29	0.12407	46.418	0.98463	0.044103	0.17623
	381	147.87	0.12983	15.055	0.99749	0.0056417	0.27319
	382	146.42	0.12860	30.046	0.99745	0.012364	0.2742
	383	146.71	0.12897	40.174	0.99698	0.020054	0.27090
	384	146.35	0.12869	50.042	0.98200	0.044235	0.15195
	385	149.20	0.13126	0.025	0.99577	0.0069505	0.43904
	386	143.31	0.12620	57.211	0.99455	0.046657	0.43597
	387	143.27	0.12616	62.060	0.96415	0.10013	0.25472
	388	145.66	0.12822	15.133	0.99575	0.10147	0.43895
	389	144.21	0.12705	30.124	0.99557	0.017318	0.43977
	390	143.07	0.12605	40.005	0.99529	0.27505	0.43992
	391	144.18	0.12703	50.016	0.99481	0.039655	0.43839
	392	145.80	0.12843	0.116	0.99369	0.012163	0.59705
	393	144.45	0.12733	68.213	0.99166	0.074257	0.58818
	394	143.22	0.12622	72.384	0.94534	0.16271	0.34065
	395	146.60	0.12917	15.120	0.99376	0.016650	0.58950
	396	145.41	0.12811	30.072	0.99352	0.021977	0.59602
	397	144.26	0.12710	40.018	0.99327	0.030689	0.59399
	398	145.42	0.12822	50.068	0.99322	0.044688	0.59290
	399	145.85	0.12858	0.143	0.99238	0.018084	0.69887
	400	143.62	0.12660	68.356	0.99058	0.079390	0.69006
	401	143.18	0.12620	74.366	0.93958	0.20289	0.41148
	402	146.44	0.12911	15.146	0.99230	0.023421	0.69273
	403	145.5	0.12802	30.033	0.99221	0.029932	0.70112
	404	143.36	0.12641	40.018	0.99194	0.036150	0.69985
	405	144.72	0.12761	50.016	0.99171	0.44488	0.69527
	406	144.26	0.12723	0.090	0.99152	0.021500	0.76363
	407	141.59	0.12481	69.125	0.98924	0.095938	0.74280
	408	141.15	0.12447	74.326	0.94052	0.22084	0.46084
	409	142.89	0.12605	15.029	0.99137	0.027131	0.75933
	410	143.31	0.12645	29.993	0.99128	0.038330	0.76772
	411	141.64	0.12497	40.083	0.99086	0.054287	0.75937
	412	141.13	0.12451	50.094	0.99038	0.064601	0.75032
	413	142.01	0.12537	0.156	0.99093	0.025618	0.79927
	414	140.76	0.12428	65.971	0.98822	0.10085	0.77844
	415	139.91	0.12355	71.302	0.94503	0.22665	0.50671
	416	143.68	0.12684	15.029	0.99078	0.037773	0.78371

Config.	Rdg	V_o/V^*	M_o	α_i ~ Degrees	η_R	$(\Delta P/P)$ Distortion	M_{TH}
3	417	144.05	0.12727	30.085	0.99030	0.054358	0.78426
	418	141.53	0.12504	40.044	0.98981	0.069238	0.78515
	419	141.93	0.12538	50.029	0.98887	0.086471	0.78334
	420	143.77	0.12697	0.012	0.98997	0.032873	0.84622
	421	141.67	0.12491	68.421	0.97585	0.18790	0.80315
	422	141.35	0.12455	72.762	0.94268	0.23294	0.52371
	423	145.25	0.12787	15.094	0.98974	0.053406	0.82460
	424	144.43	0.12703	30.137	0.98889	0.074583	0.80520
	425	144.18	0.12684	40.083	0.98819	0.091833	0.80567
	426	144.68	0.12716	50.081	0.98708	0.098878	0.80008
	427	142.87	0.12563	0.051	0.98275	0.074815	0.86824
	428	140.94	0.12408	66.805	0.97476	0.19118	0.77041
	429	139.70	0.12300	77.520	0.93352	0.25935	0.52250
	430	142.35	0.12535	15.003	0.98259	0.84704	0.86329
	431	143.02	0.12599	30.019	0.98206	0.096329	0.87066
	432	141.87	0.12504	39.978	0.98162	0.12302	0.85081
	433	144.52	0.12735	50.016	0.98101	0.13288	0.83690
	434	211.66	0.18639	-0.118	0.99913	0.0024055	0.00927
	435	210.37	0.18501	-0.118	0.99751	0.0036960	0.27515
	436	209.68	0.18399	15.094	0.99575	0.0062862	0.27521
	437	209.95	0.18397	30.124	0.99718	0.016795	0.27534
	438	206.97	0.18123	40.096	0.98334	0.043390	0.16337
	439	203.70	0.17839	50.016	0.97726	0.041992	0.11047
	440	200.29	0.17533	0.077	0.99589	0.0056167	0.43781
	441	191.11	0.16715	15.107	0.99585	0.010727	0.43546
	442	192.01	0.16790	30.085	0.99557	0.023530	0.43218
	443	188.10	0.16437	40.083	0.99508	0.035603	0.43232
	444	206.08	0.17995	50.003	0.96387	0.099071	0.24726
	445	203.27	0.17727	0.064	0.99392	0.011787	0.59112
	446	203.18	0.17713	15.003	0.99365	0.020749	0.58619
	447	206.29	0.17998	29.902	0.99383	0.034654	0.58329
	448	211.70	0.18494	40.070	0.99292	0.049327	0.58614
	449	215.73	0.18852	50.055	0.99196	0.071044	0.57721
	450	214.76	0.18793	0.156	0.99252	0.016016	0.68847
	451	212.28	0.18603	15.042	0.99235	0.028088	0.68568
	452	214.40	0.18799	30.019	0.99217	0.041522	0.68515
	453	208.64	0.18312	39.978	0.99186	0.053008	0.68530
	454	207.10	0.18186	50.211	0.99138	0.066218	0.68230
	455	208.52	0.18319	0.038	0.99171	0.022135	0.74448
	456	208.63	0.18345	15.172	1.0139	0.98953	0.57870
	457	207.33	0.18240	29.941	0.99121	0.052440	0.73949
	458	206.63	0.18187	40.083	0.99040	0.067309	0.73684
	459	207.45	0.18276	50.055	0.98965	0.079574	0.73340
	460	208.89	0.18388	0.117	0.99104	0.023807	0.78690
	461	208.22	0.18310	15.042	0.99110	0.040915	0.77756
	462	208.94	0.18369	30.137	0.98971	0.076213	0.76916
	463	208.73	0.18347	39.926	0.98855	0.093982	0.76331
	464	208.42	0.18322	50.068	0.98762	0.10004	0.75590

Config.	Rdg	V_o/V^*	M_o	α_i ∿ Degrees	η_R	($\Delta P/P$) Distortion	M_{TH}
3	465	211.89	0.18632	-0.014	0.99038	0.029123	0.80723
	466	210.99	0.18543	15.133	0.99010	0.063126	0.80294
	467	211.40	0.18574	30.033	0.98847	0.087695	0.79111
	468	212.03	0.18635	39.653	0.98672	0.10332	0.77869
	469	209.60	0.18413	50.524	0.98544	0.11522	0.77192
	470	209.77	0.18418	0.077	0.98382	0.077419	0.85741
	471	211.22	0.18555	15.094	0.98303	0.10288	0.85695
	472	209.80	0.18455	29.889	0.98164	0.12040	0.84886
	473	209.65	0.18445	40.070	0.98001	0.13867	0.82867
	474	207.87	0.18292	49.911	0.97869	0.16080	0.80800
	475	59.490	0.052544	0.064	0.99879	0.0016175	0.00000592
	476	59.929	0.052951	89.969	0.99418	0.0062709	0.013311
	477	59.901	0.052951	89.969	0.98105	0.044451	0.15103
	478	60.003	0.053041	89.982	0.99440	0.03176	0.43394
	479	59.404	0.052499	89.969	0.99219	0.041421	0.58740
	480	58.013	0.051258	89.982	0.99075	0.046183	0.68004
	481	58.172	0.051397	89.969	0.98997	0.056261	0.73394
	482	57.981	0.051258	89.969	0.98935	0.065099	0.76886
	483	57.978	0.051258	89.956	0.98856	0.060238	0.79559
	484	58.992	0.052134	89.969	0.97990	0.10190	0.86389
	485	58.565	0.051721	89.786	0.97893	0.11842	0.86366
	486	61.876	0.054679	0.117	0.99022	0.041566	0.80361
	487	59.772	0.052816	89.760	0.98844	0.063595	0.79909
	488	59.757	0.052771	89.239	0.98923	0.052338	0.76420
	489	58.534	0.051721	90.086	0.99020	0.046156	0.73416
	490	58.656	0.051813	89.982	0.99076	0.042767	0.68217
	491	59.557	0.052589	90.203	0.99236	0.041109	0.58243
	492	56.574	0.049939	91.455	0.99455	0.030528	0.43134
	493	61.399	0.054241	91.481	0.98368	0.044495	0.17471
	494	20.082	0.017740	89.656	0.99643	0.010414	0.089108
	495	0	0	-0.809	0.99897	0.00058055	0.01893
4	815	143.84	0.12680	0.077	0.99889	0.00088208	0.018935
	816	145.40	0.12802	0.077	0.99753	0.0042465	0.28080
	817	143.94	0.12669	30.358	0.99701	0.020208	0.27861
	818	143.84	0.12665	35.038	0.98502	0.046249	0.18322
	819	145.83	0.12837	15.068	0.99727	0.0063428	0.28006
	820	145.07	0.12766	30.319	0.99696	0.019405	0.27811
	821	143.41	0.12620	40.330	0.98200	0.044556	0.15584
	822	142.53	0.12544	50.042	0.97680	0.044212	0.11781
	823	144.16	0.12705	0.012	0.99580	0.0074221	0.44210
	824	143.34	0.12639	34.660	0.99458	0.043358	0.43634
	825	141.18	0.12451	38.518	0.97148	0.099182	0.30236
	826	143.67	0.12673	15.003	0.99560	0.012912	0.44092
	827	143.55	0.12663	30.453	0.99502	0.035082	0.43673
	828	142.40	0.12571	39.692	0.96964	0.10055	0.29382
	829	141.40	0.12489	49.755	0.95957	0.098195	0.23048
	830	143.73	0.12695	0.012	0.99348	0.015633	0.59994

Config.	Rdg	V_o/V^*	M_o	α_i ~ Degrees	η_R	$(\Delta P/P)$ Distortion	M_{TH}
4	831	143.28	0.12658	36.863	0.99141	0.074129	0.58826
	832	141.94	0.12540	39.548	0.96563	0.15749	0.44901
	833	143.95	0.12720	15.081	0.99305	0.036763	0.59813
	834	142.66	0.12618	29.694	0.99231	0.054368	0.59272
	835	140.86	0.12458	49.833	0.94701	0.18044	0.41866
	836	142.88	0.12628	0.025	0.99198	0.020736	0.71016
	837	142.68	0.12611	35.320	0.98961	0.085496	0.69460
	838	142.34	0.12576	39.170	0.97046	0.18446	0.57596
	839	144.11	0.12727	15.055	0.99126	0.046544	0.70682
	840	143.72	0.12688	29.759	0.99032	0.069292	0.69477
	841	141.54	0.12491	50.211	0.94956	0.19945	0.46273
	842	144.47	0.12746	0.104	0.99099	0.026382	0.76193
	843	142.63	0.12590	35.299	0.98798	0.097403	0.74280
	844	143.19	0.12637	38.049	0.96895	0.19714	0.60755
	845	144.12	0.12716	15.081	0.99018	0.057453	0.75864
	846	142.96	0.12609	29.798	0.98902	0.084713	0.74495
	847	143.39	0.12648	39.835	0.96580	0.20158	0.58504
	848	142.32	0.12552	49.898	0.94633	0.21664	0.49295
	849	144.75	0.12765	0.064	0.98961	0.040163	0.80263
	850	144.04	0.12697	31.232	0.98668	0.11364	0.78331
	851	143.85	0.12675	36.433	0.97316	0.19974	0.67322
	852	144.28	0.12714	15.016	0.98869	0.074239	0.80880
	853	143.18	0.12612	30.163	0.98688	0.10430	0.78055
	854	144.00	0.12682	40.109	0.96298	0.21363	0.59725
	855	143.29	0.12620	50.289	0.94366	0.22944	0.51165
	856	145.07	0.12776	0.064	0.98746	0.053651	0.84077
	857	143.89	0.12663	31.884	0.98051	0.14527	0.77765
	858	143.65	0.12646	38.545	0.96505	0.22137	0.64925
	859	143.97	0.12677	15.081	0.98605	0.080308	0.82852
	860	144.61	0.12729	30.111	0.98348	0.13688	0.81435
	861	142.99	0.12584	40.917	0.95998	0.22973	0.61346
	862	142.52	0.12542	50.185	0.94272	0.24273	0.53227
	863	144.92	0.12757	0.090	0.97322	0.10662	0.86686
	864	143.58	0.12656	33.461	0.96958	0.22645	0.77396
	865	142.27	0.12544	42.572	0.95532	0.25506	0.66887
	866	145.22	0.12809	15.198	0.97479	0.15980	0.86825
	867	143.37	0.12648	30.059	0.97290	0.20944	0.81349
	868	142.51	0.12580	39.809	0.96157	0.25263	0.69103
	869	143.03	0.12633	50.081	0.94558	0.26255	0.61045
	870	209.26	0.18457	0.117	0.99888	0.0014693	0.018883
	871	208.85	0.18410	0.130	0.99738	0.0034739	0.27776
	872	208.10	0.18339	15.042	0.99749	0.0072769	0.27829
	873	208.37	0.18361	30.358	0.99631	0.042065	0.26605
	874	208.25	0.18344	40.617	0.97817	0.043686	0.12465
	875	208.31	0.18345	50.459	0.97165	0.041555	0.070246
	876	210.39	0.18519	0.064	0.99575	0.0060331	0.43777
	877	209.74	0.18468	15.081	0.99565	0.012401	0
	878	208.57	0.18360	29.720	0.99489	0.042547	0.43409

Config.	Rdg	V_o/V^*	M_o	α_i ∿ Degrees	η_R	$(\Delta P/P)$ Distortion	M_{TH}
4	879	208.36	0.18336	40.005	0.96298	0.097942	0.24408
	880	208.26	0.18326	49.768	0.94285	0.12297	0.21976
	881	209.64	0.18440	0.038	0.99377	0.012233	0.59740
	882	210.23	0.18484	15.042	0.99367	0.020072	0.59640
	883	209.42	0.18410	30.033	0.99220	0.063308	0.58786
	884	209.43	0.18422	40.383	0.94797	0.16238	0.35158
	885	208.35	0.18315	0.022	0.99221	0.019018	0.70488
	886	210.55	0.18498	31.427	0.98987	0.085146	0.68709
	887	209.41	0.18389	40.800	0.94025	0.20180	0.41491
	888	209.33	0.18375	15.120	0.99192	0.031699	0.69645
	889	210.35	0.18468	30.137	0.99020	0.081040	0.69164
	890	209.11	0.18362	40.005	0.94100	0.20022	0.41686
	891	209.15	0.18383	49.677	0.92084	0.21027	0.34078
	892	209.20	0.18396	50.250	0.91922	0.21166	0.34041
	893	210.96	0.18557	0.117	0.99127	0.023356	0.75619
	894	211.46	0.18605	14.925	0.99099	0.046572	0.75125
	895	210.77	0.18562	29.993	0.97901	0.18115	0.74564
	896	210.38	0.18529	32.157	0.96512	0.20047	0.57111
	897	209.80	0.18480	40.565	0.94084	0.21660	0.46856
	898	210.18	0.18516	50.172	0.91561	0.22941	0.36074
	899	210.95	0.18603	0.104	0.99023	0.036061	0.80403
	900	210.64	0.18579	15.081	0.98947	0.067490	0.79527
	901	210.59	0.18575	30.202	0.97369	0.21136	0.69092
	902	209.76	0.18502	32.014	0.96433	0.21100	0.60400
	903	209.91	0.18516	39.952	0.94014	0.23197	0.48825
	904	207.93	0.18336	50.498	0.90549	0.27490	0.42093
	905	211.01	0.18605	0.051	0.98801	0.048899	0.83027
	906	210.88	0.18580	15.042	0.98712	0.076725	0.83762
	907	211.91	0.18669	30.124	0.97222	0.19633	0.70172
	908	210.47	0.18534	40.643	0.93722	0.24158	0.49676
	909	209.96	0.18481	50.772	0.90478	0.27855	0.42022
	910	211.21	0.18594	0.416	0.98181	0.068299	0.86010
	911	211.78	0.18639	15.198	0.98172	0.10532	0.85607
	912	211.00	0.18568	30.124	0.96905	0.22165	0.71420
	913	210.19	0.18493	41.178	0.93309	0.26012	0.51303
	914	209.58	0.18435	50.602	0.90537	0.27893	0.42095
	915	61.619	0.054373	0.143	0.99899	0.00050179	0.021294
	916	60.423	0.053355	90.269	0.97295	0.19905	0.75222
	917	59.280	0.052362	90.269	0.97431	0.19638	0.74632
	918	59.110	0.052226	90.269	0.97751	0.18069	0.73387
	919	61.289	0.054197	90.256	0.98005	0.15836	0.70666
	920	60.402	0.053444	0.983	0.13445	0.66989	
	921	60.182	0.053265	90.269	0.98603	0.10666	0.57121
	922	58.518	0.051813	90.269	0.96371	0.097541	0.27640
	923	60.748	0.05380	90.269	0.97869	0.043643	0.13191
	924	58.856	0.05218	90.269	0.99455	0.00084181	0.010174
	925	63.360	0.056184	0.130	0.99193	0.030315	0.60506
	926	59.767	0.052996	90.842	0.98462	0.11511	0.60123

Config.	Rdg	V_o/V^*	M_o	α_i ~ Degrees	η_R	($\Delta P/P$) Distortion	M_{TH}
4	927	62.576	0.055501	0.143	0.98597	0.068403	0.81454
	928	60.477	0.053578	89.565	0.96854	0.22696	0.76567
	929	0	0	0.038	0.99897	0.00056403	0.021307
	930	0	0	0.051	0.96340	0.17876	0.85557
	931	0	0	0.051	0.97552	0.13054	0.83978
	932	0	0	0.051	0.97649	0.13154	0.84754
	933	0	0	0.051	0.98527	0.099580	0.80506
	934	0	0	0.077	0.98620	0.087450	0.75219
	935	0	0	0.064	0.98758	0.099329	0.70259
	936	0	0	0.077	0,99079	0.063951	0.60229
	937	0	0	0.077	0.99392	0.043347	0.44172
	938	0	0	0.090	0.99671	0.018092	0.27915
	939	0	0	0.077	0.99870	0.0022592	0.085217

APPENDIX C - EVALUATION OF THE AERO AND SABBL BOUNDARY LAYER SEPARATION PREDICTOR

Wall static pressure measurements from inlet No. 2 were used to exercise the AERO (Reference 7) and SABBL (Stratford and Beavers Boundary Layer, Reference 6) computer programs in order to evaluate their sensitivity to increasingly adverse internal flow pressure gradients. In this manner, their "goodness" in predicting proximity to separation could be determined since the actual separation points were observed during the test, as described in Section 6.

Data points at V_o = 41.2 and 61.7 m/sec (80 and 120 kts), $M_{TH} \simeq 0.6$ and 0.8, and angles of attack ranging from zero tc the attached flow point nearest separation were processed. The value of each method's separation indicator (friction coefficient C_f for AERO and the "F" parameter for SABBL) closest to the critical (i.e., separation) value was then recorded. These extreme values are plotted, in Figure 37, as a function of angle of attack. A consistent trend toward the critical indicator value with increasing angle is noted, except for one SABBL case where the critical value was exceeded prematurely (i.e., prior to separation). A more revealing characterization is to plot the same values of separation indicator against the actual proximity to observed separation, i.e., $(\alpha_s - \alpha_i)$; this was done in Figure 38. (The separation point indicated by steady-state instrumentation was used, since that type of data is being evaluated.) It is apparent that most of the curves, if extrapolated, would reach their critical value at approximately the point of separation.

These trends indicate that both methods are responsive to increasingly adverse pressure distributions and give generally reliable indications of separation, with the AERO technique slightly superior. These results were also desired from a pragmatic sense; for use, in conjunction with level flight STC flow analyses, in evaluating the probable angle-of-attack capability of several candidate inlets for the 50.8 centimeter (20 inch) QCSEE program.

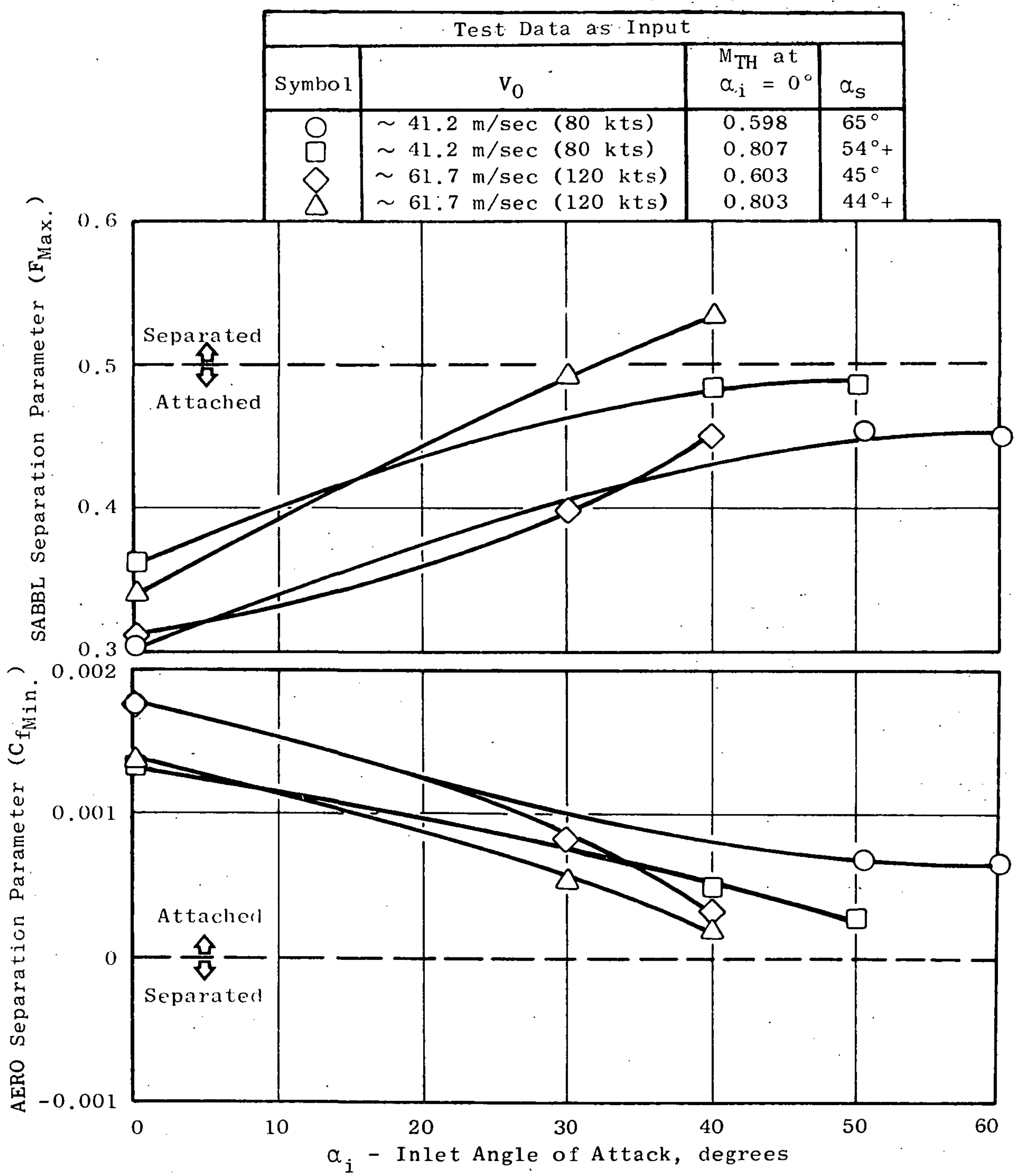

Figure 37. SABBL and AERO Boundary Layer Separation Predictors Vs. Inlet Angle of Attack, Inlet No. 2.

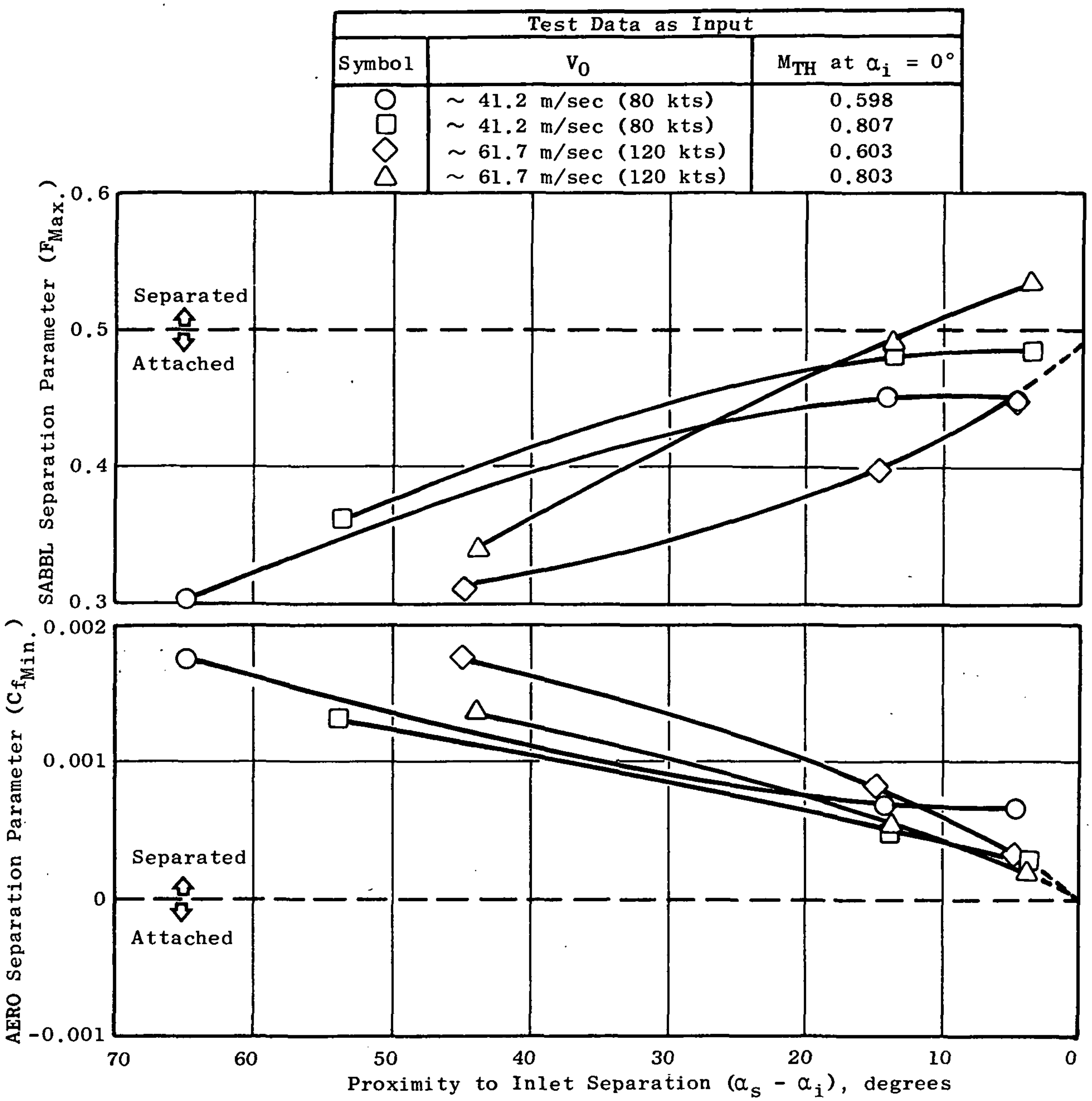

Figure 38. SABBL and AERO Boundary Layer Separation Predictors Vs. Proximity to Separation, Inlet No. 2.

SECTION 10.0

NOMENCLATURE

Symbol	Description
A	Area
a	Ellipse semimajor axis
BPF	Blade passing frequency
b	Ellipse semiminor axis
C_f	Friction coefficient
D	Diameter
F	Stratford and Beavers boundary layer separation parameter
h	Total pressure probe immersion depth
L	Inlet internal length, from leading edge to diffuser exit
L*	Reference length, defined as 2.54 cm.
M	Mach number
P	Pressure
Q	Wind tunnel dynamic head, $1/2\ \rho V^2$
R	Radius
V	Velocity
V*	Reference velocity, defined as 0.305 m/sec
X	Forebody length from leading edge to maximum diameter; also, axial location measured from leading edge
Z	Inlet axial station referenced to diffuser exit
α	Angle of attack
$\Delta P/P$	Flow setting parameter; also, total pressure distortion defined as $(P_{T_{max.}} - P_{T_{min.}})/P_{T_{avg}}$

NOMENCLATURE (Continued)

Symbol	Description
ε	A small increment in angle of attack
η_R	Area-weighted average total pressure recovery, P_{T2}/P_{TO}
θ	Diffuser angle; also, circumferential location
ρ	Density

Subscripts

Avg	Average
EQ	Equivalent
EX	Diffuser Exit Plane
F	Fan rotor
HL	Hilight
i	Inlet
Max.	Maximum
Min.	Minimum
O	Freestream or tunnel conditions
S	Separation point; also, static
T	Total
TH	Throat plane
W	Wall
2	Diffuser exit plane

SECTION 11.0

REFERENCES

1. Yuska, J.A., Diedrich, J.H., and Clough, N., "Lewis 9- by 15-Foot V/STOL Wind Tunnel", TM X-2305, 1971, NASA, Cleveland, Ohio.

2. Miller, B.A., et.al., "Effect of Entry-lip Design on Aerodynamics and Acoustics of High-Throat-Mach-Number Inlets for the Quiet, Clean, Short-haul Experimental Engine", TM-X-3222, May 1975, NASA, Cleveland, Ohio.

3. Wesoky, H.L., and Steffen, F.W., "Wind Tunnel Tests of A 20 Inch Diameter 1.15 Pressure Ratio Fan Engine Model", AIAA Paper No. 73-1216, 1973, NASA, Cleveland, Ohio.

4. Albers, J.A., and Felderman, E.J., "Boundary-Layer Analysis of Subsonic Inlet Diffuser Geometries for Engine Nacelles", TN D-7520, March, 1974, NASA, Cleveland, Ohio.

5. Tripp, S.M., "Dynamic Data System For QCSEE 12" Inlet Test Program", EST 74-7, November 14, 1974, GE, Cincinnati, Ohio.

6. Keith, J.S., Ferguson, D.R., Merkle, C.L., Heck, P.H., and Lahti, D.J., "Analytical Method For Predicting the Pressure Distribution About A Nacelle At Transonic Speeds", NASA CR-2217, July, 1973, prepared by GE, Cincinnati, Ohio, for NASA Langley Research Center.

7. Ferguson, D.R., "BL - Program for the Analysis of Laminar and Turbulent Boundary Layers", R70AEG197, June, 1970, GE, Cincinnati, Ohio.

DISTRIBUTION LIST

AiResearch Division
Garret Corporation
F.B. Wallace
402 South 36 Street
Phoenix, Arizona 80434

American Airlines
Maintenance and Engineering Center
K. Grayson
Tulsa, Oklahoma 74151

Andrews Air Force Base
Lt. Col. G. Strand
AFSC Headquarters
Washington, D.C. 20334

AVCO/Lycoming
S. Deckert
550 S. Main Street
Stratford, Connecticut 06497

The Boeing Company
H. Higgins
P.O. Box 3999
Seattle, Washington 98124

The Boeing Company
Wichita Division
D. Torkelson
Wichita, Kansas 67210

Bolt, Beranek and Newman, Inc.
R. Hayden
50 Moulton Street
Cambridge, Massachusetts 02138

Curtiss-Wright Corporation
Power Systems Division
W. Johnson
One Passaic Street
Wood Ridge, New Jersey 07075

Department of Transportation
NASA/DOT Joint Office of Noise Abatement
C. Foster
Office of Secretary
Washington, D. C. 20590

Detroit Diesel Allison Division of General Motors
F. Walters
Suite 312
333 West First Street
Dayton, Ohio 45402

Douglas Aircraft Company
L. Malthan
3855 Lakewood Boulevard
Long Beach, California 90801

Enivronment Protection Agency
J. Schettino
1835 "K" Street, NW
Washington, D.C. 20460

Federal Aviation Administration
Noise Abatement Division
J. Woodall
Washington, D.C. 20590

General Dynamics Convair Division
G. Nicoloff
San Diego, California 92112

Grumman Aerospace Corporation
C. Hoeltzer
South Oyster Bay Road
Bethpage, New York 11714

Hamilton Standard
Division of United Aircraft
A. Jackson
Windsor Locks, Connecticut 06096

Lockheed Aircraft Corporation
T. Higgins
Burbank, California 91503

Lockheed Georgia Company
H.S. Sweet
Marietta, Georgia 30060

NASA Installations

NASA Headquarters
N.F. Rekos
Washington, D.C. 20546

NASA-Ames Research Center
L. Roberts
Moffett Field, California 94035

NASA-Flight Research Center
D.R. Scott
Edwards, California 93523

NASA-Langley Research Center
R. Kuhn
Hampton, Virginia 23665

NASA-Lewis Research Center
21000 Brookpark Road
Cleveland, Ohio 44135

E.F. Baehr
M.A. Beheim
D.N. Bowditch
L.J. Chelko
C.C. Ciepluch
E.W. Conrad
R.J. Denington
A. Ginsburg
M.J. Hartmann
R.H. Kemp
Lewis Library
R.W. Luidens
Report Control Office
L.W. Schopen
R.W. Schroeder
M.F. Valerino

NASA/Air Force Liaison
Wright Patterson Air Force Base
Dayton, Ohio 45433

L. Obery
C. Simpson
Col. C.E. Painter
G.K. Richey
G.P. Peterson

Pratt & Whitney Aircraft
Division of United Aircraft Corp.
J. Chew
20800 Center Ridge Road
Rocky River, Ohio 44116

Rohr Corporation
F. Hom
Box 878
Foot and H Street
Chula Vista, California 92012

Wyle Laboratories
L. Sutherland
128 Maryland Street
El Segundo, California 90245